STRUCTURE AND ENVIRONMENT

KIELCE UNIVERSITY OF TECHNOLOGY

Quarterly
Vol. 14, No. 4, 2022

ISSN 2081-1500
e-ISSN 2657-6902

• Architecture and urban planning • Civil engineering and transport • Environmental engineering, mining and energy

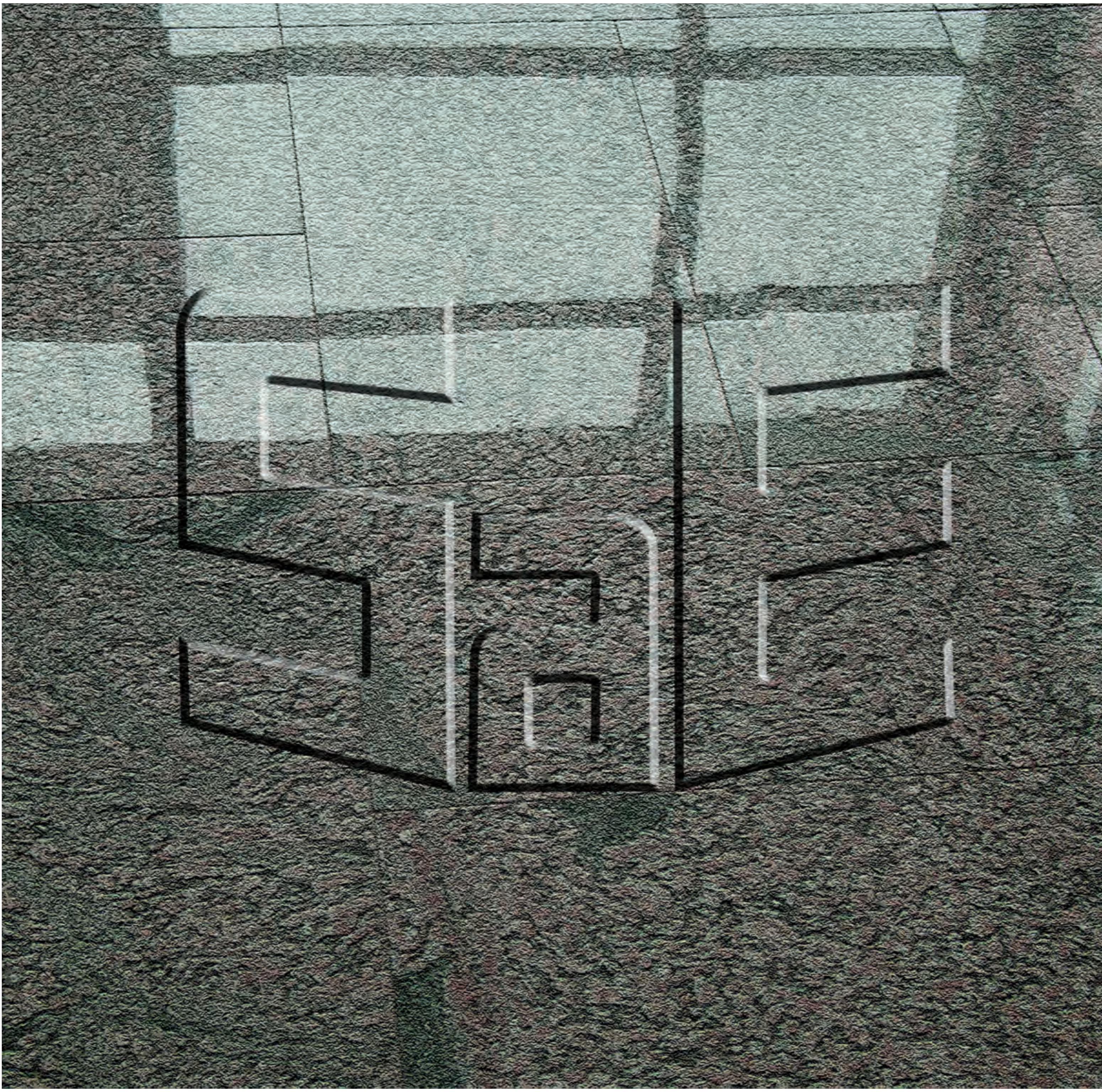

Available online at: https://sae.tu.kielce.pl

Contents

structure

environment

General data:

Format of the journal – electronic form

Frequency of publication – quarterly

The quarterly issues of Structure and Environment are their original version

The journal published by the Kielce University of Technology and De Gruyter Polska

e-ISSN 2657-6902

ISSN 2081-1500

DOI: 10.30540/sae/

Journal Metrics:

Index Copernicus Value (IVC) 2020 = 100

The Polish Ministry of Education and Science 2021 = 40 pkt

Kielce University of Technology 2022

INDEX COPERNICUS INTERNATIONAL

structure

structure

Edyta Spychał, Anna Kotwa
Structure and Environment 2022, vol. 14, (4), pp. 119-125, Article number: el 014
https://doi.org/10.30540/sae-2022-014

Structure and Environment
ISSN 2081-1500
e-ISSN 2657-6902
https://content.sciendo.com/sae
https://sae.tu.kielce.pl

sciendo

Kielce University of Technology

DOI: 10.30540/sae-2022-014

ASSESSMENT OF THE POSSIBILITY OF USING CHALCEDONITE POWDER AS A COMPONENT OF MORTARS

OCENA MOŻLIWOŚCI ZASTOSOWANIA MĄCZKI CHALCEDONITOWEJ JAKO SKŁADNIKA ZAPRAW BUDOWLANYCH

Edyta Spychał*, Anna Kotwa
Kielce University of Technology, Poland

Abstract

The article presents the results of the assessment of the possibility of using chalcedonite powder as a partial replacement for cement in mortars. Portland cement CEM I 42.5 R was used as a binder, which was replaced in the amount of 5%, 20%, 35% and 50% with chalcedonite powder. The experimental tests concerned the determination of the technological and mechanical properties of mortars: consistency, air content, compressive and bending strength, supplemented by X-ray diffraction analysis and calorimetric measurements of the pastes. The research results indicate that chalcedonite powder can be used in the production of mortars. The best mechanical properties of tested mortars were obtained in the case of replacing cement with the addition of powder in the amount of 5% and 20%.

Keywords: chalcedonite powder, cement mortar, additive, consistency, bending and compressive strength, calorimetrics measurements, XRD method

Streszczenie

W artykule dokonano oceny możliwości wykorzystania mączki chalcedonitowej jako częściowego zamiennika cementu w zaprawach budowlanych. Jako spoiwo zastosowano cement portlandzki CEM I 42,5 R, który zastępowano w ilości 5%, 20%, 35% oraz 50% mączką chalcedonitową. Badania doświadczalne dotyczyły określenia właściwości technologicznych i mechanicznych zapraw: konsystencji, zawartości powietrza, wytrzymałości na ściskanie i zginanie, uzupełnionych o rentgenowską analizę dyfrakcyjną oraz badania kalorymetryczne zaczynów. Wyniki badań wskazują, że mączka chalcedonitowa może być stosowana do produkcji zapraw budowlanych. Najlepsze właściwości mechaniczne badanych zapraw uzyskano w przypadku zastąpienia cementu dodatkiem mączki w ilości 5% i 20%.

Słowa kluczowe: mączka chalcedonitowa, zaprawa cementowa, dodatek, konsystencja, wytrzymałość na zginanie i ściskanie, pomiary kalorymetryczne, metoda XRD

1. INTRODUCTION

Chalcedonite is a sedimentary siliceous rock. It may be found in the deposits of Dęborzynek, Gapinin, Lubocz and Teofilów, in the region of Tomaszów Mazowiecki and Nowe Miasto. Chalcedonite, due to its very small area of occurrence, is one of the unique rocks in Poland and in Europe. The Teofilów deposit is the only one documented and currently exploited. The main component of the rock is chalcedony, other compounds are: quartz, opal, iron hydroxides, pyrite, manganese compounds and clay minerals. In chemical terms chalcedonite is a homogeneous material, consisting of silica in amount of about 94% by weight [1, 2]. Directions of use of chalcedonite in the form of sand

*Kielce University of Technology, Poland e-mail: espychal@tu.kielce.pl

and broken aggregate of fractions 0.8-2.0 mm and 16.0-32.0 mm have yet been varied. It has been classified, among others, as an aggregate for the foundation of road with small and very small traffic. It was used as a raw material for the production of powders for scrubbing and liquids for washing car chassis. Chalcedonite can be used as a sorbent in drinking water treatment [1, 3]. In the form of chalcedonite powder, this material was used in the alkali-silica reaction tests [4], as a partial replacement for fine aggregate in concrete [5], sand-lime products [6] or as a partial replacement for binder in lime mortars [7].

Carbon dioxide emissions accompannying production of cement clinker, the depletion of natural resources causes the search of alternative ingredients that may be a partial substitute for the basic raw materials used in the production of mortars and concretes. For both economical and ecological reasons as well as development of new technologies the need to look for a substitute for cement is constantly growing. Mineral addditives with pozzolanic properties used for the production of mortars and concretes are among others fly ash, silica fume, metakaolin, zeolites [8-11]. An alternative to commonly used mineral additives are stone powders, which are waste generated during the process of mechanical treatment or dedusting of mineral aggregates. Due to the fact that the chemical and mineral composition of these dusts is the same as the parent rock, they can be used in the production of construction products, being a partial substitute for a binder or fine aggregate [5, 6, 11-16]. The research carried out so far concentrated on the use of basalt [12-14, 17], marble [11, 18, 19], granite dust [13-15], melaphyre powder [20]. A commonly used material is limestone dust [12, 14, 20]. On the basis of the reserach to date, it has been found that these waste materials contribute to the improvement of rheological and mechanical properties, can increase durability of mortar and concrete. The possibilities of using stone dust in the production of mortars and concretes are wide, but varied, which is influenced by the grain size of material, its origin or the method of processing (drying, grinding) [12, 14].

The aim of the research presented in the article was to rate the possibility of using chalcedonite powder as the component of mortar by partially changing cement with waste material. The assessment was carried out on the basis of the technological and mechanical properties of the mortars, supplemented with calorimetric measurements and XRD X-ray diffraction pastes. This article is a continuation of the issues raised by the authors in the publication [21].

2. MATERIALS AND METHODS

Four series of mortars and pastes were prepared, in which Portland cement was substituted with chalcedonite powder in the amounts of 5% (CH5), 20% (CH20), 35% (CH35) and 50% (CH50) and reference sample – without additive (CH0). The industrial ordinary Portland cement CEM I 42.5 R was used in research. The chemical composition of cement and chalcedonite powder were given in Table 1.

Fine aggregate fraction 0-2 mm and tap water were used in the experiments. The mortar mix proportion were detailed in Table 2.

Table 1. Chemical composition of cement and chalcedonite powder [%]

Material	SiO_2	Al_2O_3	Fe_2O_3	CaO	MgO	SO_3	K_2O	Na_2O	Cl	P_2O_5	TiO_2	Fe_2O_3	ZrO_2	BaO	F
Cement	19.49	4.75	3.25	62.3	2.08	3.0	0,55	0.79	0.06	–	–	–	–	–	–
Chalcedonite powder	91.8	3.04	1.28	0.45	0.15	0.05	0.42	0.09	–	0.04	0.11	1.28	0.01	0.04	0.06

Table 2. Composition of tested mortars [g]

Series of mortar	Cement	Chalcedonite powder	Fine aggregate	Water
CH0	450.0	0	1350.0	225.0
CH5	427.5	22.5	1350.0	225.0
CH20	360.0	90.0	1350.0	225.0
CH35	292.5	157.5	1350.0	225.0
CH50	225.0	225.0	1350.0	225.0

Additive in the form of chalcedonite powder, which was applied in these research, came from the mine of chalcedonite broken aggregates in Inowłódz. It was a final waste lying on the piles. In order to receive more homogeneous material, with a smaller granulation, it has also undergone 4 hours of grinding in a ball mill. Cement (C symbol), chalcedonite powder before (CHP symbol) and after grinding (CHPG symbol) were examined for particle size distribution with a laser diffractometer HELOS KR producted by Sympatec GmbH (Fig. 1).

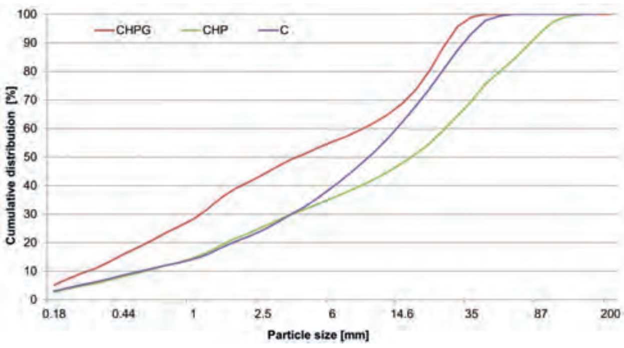

Fig. 1. Particle size distribution of cement and chalcedonite powder

Chalcedonite powder before grinding (CHP) has the particle size ranging from 0 to 175 µm, but chalcedonite powder after grinding (CHPG) has the particle size ranging from 0 to 51 µm, which gives a grain size smaller than cement (C). In the case of the CHPG sample, 50% of the grain size are grains up to 4.2 µm, while the CHP sample contains about 50% of grains with dimensions up to 17.4 µm.

The measurements of standard consistency were done according to PN-EN 1015-3 (as a flow) [22] and PN-B-04500 (as a cone penetration) [23] standards.

The air content was determined in accordance with PN-EN 1015-7 standard [24].

The research of mechanical properties were carried out on 40 x 40 x 160 mm mortars bars according to the PN-EN 196-1 standard [25] (after demoulding, were stored in tap water at 20 ±2°C). Each value was the average of three measurements of bending strength and the average of six measurements of compressive strength. The samples were tested after 28 and 90 days.

The hydration kinetics was carried out by calorimetry operating under non-isothermal and non-adiabatic conditions, using the calorymeter BT 2.15 produced by SETARAM. Tests were made on 7.5 g samples (pastes – Table 3) – 5 g of binder (cement or cement and chalcedonite powder) and 2.5 g of distilled water at constant water to binder ratio = 0.5, in the temparature of 20°C. The samples were placed each time in plastic bags, which were put in the measuring cell of the calorimeter. Results were read every 30 seconds for a period of 48 hours.

Table 3. Composition of tested pastes

Series of pastes	Cement [g]	Chalcedonite powder [g]	Water [ml]
CH0	5.00	0.00	2.5
CH5	4.75	0.25	2.5
CH20	4.00	1.00	2.5
CH35	3.25	1.75	2.5
CH50	2.50	2.50	2.5

Additionally, on the basis of calorimetric measurements (diagrams of total heat evolved), the hydration degree of the pastes was calculated, using the formula [26]:

$$SH = \left(\frac{x_1}{x_2}\right)\cdot 100 \qquad (1)$$

where:
SH – hydration degree;
x_1 – value measured after the period of hydration;
x_2 – value measured after full hydration or after a certain period of time taken as a refernce.

In the article, the measurements of the heat of hydration of CH0 paste after 48 hours were adopted as the value of x_2.

XRD images were obtained in a X-ray Diffractometer Empyrean produced by PANalytical. The research of X-Ray diffraction analysis were carried out on pastes after 2 days of maturing (the composition of the pastes was the same as in the calorimetric tests).

3. TEST RESULTS AND DISCUSSION

The results of mortar consistency tests were shown in Table 4. Replacing the cement in 5% (CH5) with chalcedonite powder increased the flow from 155 mm (CH0) to 160 mm (CH50), what can be explained by the lubricating effect of this material, which can be related to the physical interaction of this dust grains [27]. In other cases, an increase in the amount of chalcedonite powder resulted in a decrease in the flow (from 155 to maximum 142 mm – by about 9%). In the case of the consistency test using the cone penetration method, the addition of chalcedonite powder reduced the tested parameter (from 5.1 cm maximum to 4.2 cm). The highest reduction was observed in CH50 mortar containing 50% addition (by about 17.6%).

Table 4. Consistency and air content of the tested mortars

Sample of mortar	Flow [mm]	Cone Penetration [cm]	Air content [%]
CH0	155	5.1	9.0
CH5	160	4.6	11.0
CH20	147	4.5	11.5
CH35	145	4.4	16.0
CH50	142	4.2	19.5

Air content (Table 4) for the reference mortar (CH0) was 9%. The greater the amount of the additive, the greater the air entrainment of the mortars. The content of chalcedonite powder in the amount of 5% to 20% by weight in relation to cement caused a slight increase in the air content (from 9% to 11.5%). The air content was more than twice as high in CH50 mortar than in reference mortar (CH0). This may be retalted to the properties of chalcedonite. According to the publication [3], the porosity of chalcedonite ranges from 14-35%.

In Tables 5 and 6 were presented the results of determining the bending and compressive strength for the mortars modified with chalcedonite powder. These measurements were compared with the values of the reference mortar CH0 (without additive).

Comparing the results of the bending strength of the reference mortar and chalcedonite powder modified mortars, it can be seen that its increase causes a reduction in the mortar strength after 28 and 90 days. The smallest changes in mechanical properties were noted in the case of CH5 and CH20 mortars (9-17% relative to the CH0 sample). Chalcedonite powder addition of 5% and 20% caused slight increase of compressive strength of mortars after 28 days of hardening, in comparison with the reference mortar. Compressive strength of CH5 mortar after 90 days of research was similiar to the result for CH0 mortar. However, the higher addition brings the strength reduction. The findings from the tests performed after 28 and 90 days were also least favourable for the CH50 sample. CH35 and CH50 mortars with the smallest bending and compressive strength were characterized by a much higer air content compared to the others, which had an impact on their mechanical properties. The strength of the mortars (CH5 and CH20) may be due to the filling effect (sealing the structure) and the pozzolanic properties of this additive.

On the basis of calorimetric research shown in Figures 2 and 3 it may be stated, that chalcedonite powder delays the process of cement hydration. The total heat released by tested pastes after 12, 24, 36, 48 h of hydration and hydration degree of each pastes are given in Table 7.

Table 5. Bending strength of mortars

Sample of mortar	Bending strength after 28 days [MPa]	Standard deviation of bending strength [MPa]	Bending strength after 90 days [MPa]	Standard deviation of bending strength [MPa]
CH0	2.3	0.14	2.4	0.43
CH5	2.1	0.00	2.1	0.05
CH20	2.0	0.05	2.0	0.05
CH35	1.6	0.00	1.6	0.08
CH50	0.2	0.05	0.2	0.05

Table 6. Compressive strength of mortars

Sample of mortar	Compressive strength after 28 days [MPa]	Standard deviation of compressive strength [MPa]	Compressive strength after 90 days [MPa]	Standard deviation of compressive strength [MPa]
CH0	60.8	2.91	70.3	3.62
CH5	65.3	2.53	72.1	3.49
CH20	62.3	2.57	62.6	2.52
CH35	41.5	2.20	43.3	0.76
CH50	26.5	1.75	26.0	1.91

Table 7. Heat of hydration of tested pastes

Sample of pastes	Heat after hours of hydration [J/g]				Degree of hydration			
	12 h	24 h	36 h	48 h	12 h	24 h	36 h	48 h
CH0	134.91	239.75	287.52	317.50	42.49	75.51	90.56	100.00
CH5	132.61	235.85	281.62	307.83	41.77	74.28	88.70	96.95
CH20	112.61	203.04	240.97	263.23	35.47	63.95	75.90	82.91
CH35	110.90	185.62	216.90	234.19	34.93	58.46	68.31	73.76
CH50	90.19	149.87	175.62	191.12	28.41	47.20	55.31	60.20

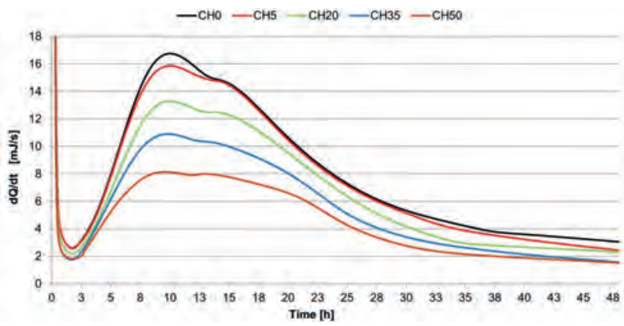

Fig. 2. The heat evolution curves as a function of time for tested pastes

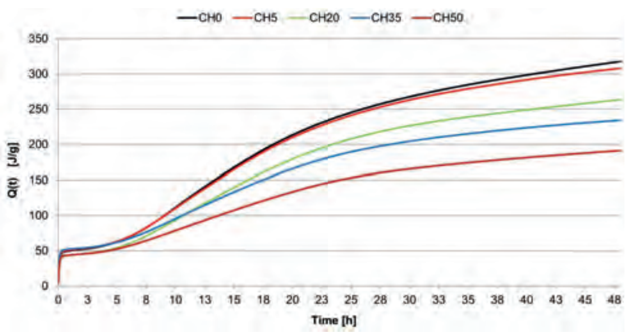

Fig. 3. Total heat evolved as a function of time for tested pastes

The hardening heat of individual pastes is differential – it's maximum for CH0 paste and significantly lower in the case of CH50 paste. The microcalorimetric curves for paste containing 5% chalcedonite powder show that both the total amount of evolved heat and the rate of heat evolution over time do not differ significantly, as compared to a base paste CH0 without chalcedonite powder. It may be noticed, that the addition in the amount of 5% acts as a cement substitute. The increase of chalcedonite powder content effects in „dilution" of active material with the additive and increase in the effective water-cement ratio [28]. It can be seen that the addition affects the reduction of the thermal effect after 12, 24, 36 and 48 hours for pastes in which the cement was replaced with 20, 35 and 50 % chalcedonite powder (for the reference sample). In the case of CH0÷CH35 pastes, two maxima (between 8 and 18 hours) are clearly visible in Figure 2 (the amount of heat released varies). In the case of the CH50 paste, both maxima are at a similar level. It can be noted that the biggest heat emission from the hydration process was obtained with the CH0 and CH5 samples, and in the case of these pastes, the biggest compressive strength were achived after 28 and 90 days. The highest degree of hydration after 48 hours was recorded for the CH0 paste, and the lowest for the CH50 sample. The degree of hydration for CH50 paste was about 40% less than the degree of hydration for CH0.

XRD patterns of reference sample (CH0) and pastes containing 5, 20, 35 and 50% chalcedonite powder replacing after 2 days of hydration are presented in Figure 4. There have been shown the peaks characteristic of the cement phases, non-hydrated clinker phases [29] and the peaks of mineral contained in the chalcedonite powder such as quartz [1-5].

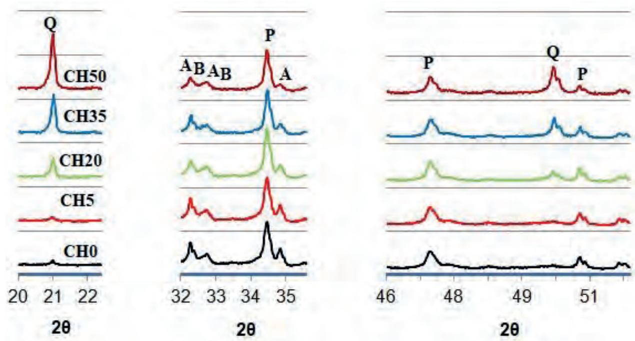

Fig. 4. XRD patterns of tested pastes (denotation: Q – quartz, A – alite, B – belite, P – portlandite)

The most intense peaks for all pastes were recorded for portlandite and quartz. Portlandite intensity was the biggest for CH0, CH5 and CH20 samples, but quartz intensity was the biggest for CH50 sample (due to the highest chalcedonite powder content).

4. CONCLUSIONS

The test results reveal that partial replacement of cement with chalcedonite powder has a noticeable effect on the technological and mechanical properties of mortars:

1. The 5% addition of this dust has a positive effect on the consistency of the mortar. Chalcedonite powder in an amount greater than 5% in relation to the weight of cement contributed to the reduction of the flow of the mortar, which may result in a necessity of superplasticizer application (especially when replacing cement with 35 and 50% of chalcedonite powder).
2. With a share of chalcedonite powder as a cement substitute with 5% and 20% by weight, the compressive strength slightly increases after 28 days in relation to mortar without addition. More of the additive reduces the compressive strength.
3. Chalcedonite powder affects the delay of hydration process. This effect is rising with the increase of addition amount.

The results of these research point the fact, that the chalcedonite powder may be a good component of mortars in the amount to 20% (based on the weight of cement). Partial replacement of cement by chalcedonite powder can be profitable from an economic and ecological point of view.

REFERENCES

[1] Michel M.M.: *Charakterystyka chalcedonitu ze złoża Teofilów pod kątem możliwości wykorzystania w technologii uzdatniania wody i oczyszczania ścieków*. Gospodarka Surowcami Mineralnymi, T. 27, z.1, 2011, pp. 49-67.

[2] http://przeglad-techniczny.pl/artykuly?id=2721 [accessed 31 October 2022].

[3] Tchórzewska D., Pabis J., Kosk I., Nieć M.: *Nowe zastosowania chalcedonitu jako sorbentu w procesie oczyszczania wód*, Przegląd Geologiczny, Vol. 49, Nr 4, 2001, pp. 303-306.

[4] Owsiak Z., Mazur A., Zapała-Sławeta J.: *The evaluation of the effect of chalcedony dust on the reaction of alkalis with reactive aggregate in cement mortars*, Structure and Environment, T. 10, z. 1, 2018, 19-27, doi: 10.30540/sae-2018-002.

[5] Kotwa A., Spychał E.: *Influence of mineral additives properties of concrete.* Structure and Environment, T. 8, z. 2, 2016, pp. 15-20.

[6] Dachowski R., Komisarczyk K.: *Investigation of physico-chemical poperties of sand-lime products modified of diabase aggregate and chalcedonite meal*, IOP Conference Series: Materials Science and Enginnering, T. 245, Zeszyt 22095, 2017, pp. 1-8.

[7] Vyšvařil M., Krebs M., Bayer P.: *Use of chalcedonite powder as a supplementary material in lime mortars*. Conference: REHABEND 2022, Construction Pathology, Rehabilitation Technology and Heritage Management, Granada, Spain, 2022, pp. 1314-1320.

[8] Baran T.: *The use of waste and industrial by-products and possibilities of reducing CO_2 emission in the cement industry-industrial trials*, Cement Wapno Beton, 25(3), 2021, pp. 169-184, doi: 10.32047/CWB.2021.26.3.1.

[9] Czapik P., Cebulski M.: *The properties of cement mortar with natural zeolite and silica fume additions*, Structure and Environment, T. 10, z. 2, 2018, pp. 105-113, doi: 10.30540/sae-2018-010.

[10] Jaworska-Wędzińska M., Jasińska I.: *Durability of mortars with fly ash subject to freezing and thawing cycles and sulfate attack*, Materials, 15(1), pp. 220, 2022, doi: 10.3390/ma15010220.

[11] Manzoor S., Ganesh S., Danish P.: *Effect on properties of concrete by utilization of metakaolin and marble powder*, Materials Today: Proceedings, Vol. 62, 12, 2022, pp. 6689-6694, doi: 10.1016/j.matpr.2022.04.718.

[12] Szaj P.: *Wpływ wybranych dodatków mineralnych na właściwości reologiczne zaczynów cementowych*, Prace Naukowe Instytutu Górnictwa Politechniki Wrocławskiej, T. 134, Studia i Materiały, Nr 41, 2012, pp. 285-294.

[13] Dobiszewska M.: *Waste materials used in making mortar and concrete*, Journal of Materials Education, Vol. 39 (5-6), 2017, pp. 133-156.

[14] Dobiszewska M.: *Kompozyty cementowe z dodatkiem pyłu bazaltowego*, Wydawnictwo Uczelniane Uniwersytetu Technologiczno-Przyrodniczego, Bydgoszcz, 2019.

[15] Chajec A., Sadowski Ł., Mój M.: *The adhesive and functional properties of cementitious overlays modified with granite powder*, International Journal of Adhesion and Adhesives, 10, 2021, doi: 10.1016/j.ijadhadh.2021.103008.

[16] Chajec A.: *Granite powder vs. fly ash for the sustainable production of air-cured cementitious mortars*, Materials, 14(5), 1208, 2021, doi: 10.3390/ma14051208.

[17] Abdelaziz M.A., El-Aleem S.A., Menshawy W.M.: *Effect of fine materials in local quarry dusts of limestone and basalt on the properties of Portland cement pastes and mortars*, International Journal of Engineering Research, 3,6, 2014, pp. 1038-1056.

[18] Aliabdo A.A., Abd Elmoaty A.E.M., Auda E.M.: *Re-use of waste marble dust in the production of cement and concrete*, Construction and Building Materials, 50, 2014, pp. 28-41, doi: 10.1016/j.conbuildmat.2013.09.005.

[19] Karakurt C., Dumangöz M.: *Rheological and durability properties of self-compacting concrete producted using marble dust and blast furnace slag*, Materials, 15(5):1795, 2022, doi:10.3390/ma15051795.

[20] Szaj P.: *Zastosowanie w technologii betonu mączek mineralnych powstających przy produkcji kruszyw łamanych*, Konferencja Dni Betonu, Wisła, 13-15 października 2014.

[21] Kotwa A., Spychał E.: *Parameters of mortars supplemented with chalcedonite powder*. IOP Conference Series: Earth and Envoronmental Science, 214 (1):012127, 2019, doi:10.1088/1755-1315/214/1/012127.

[22] PN-EN 1015-3:2000 Metody badań zapraw do murów. Określenie konsystencji świeżej zaprawy (za pomocą stolika rozpływu).

[23] PN-B-04500:1985 Zaprawy budowlane. Badanie cech fizycznych i wytrzymałościowych.

[24] PN-EN 1015-7:2000 Metody badań zapraw do murów. Określenie zawartości powietrza w świeżej zaprawie.

[25] PN-EN 196-1:2016-07 Metody badania cementu. Część 1: Oznaczanie wytrzymałości.

[26] Westfal L.: *Oznaczanie stopnia hydratacji cementu*, Rozprawa doktorska, Kraków 1974.

[27] Yahia A., Tanimura M., Shimoyama Y.: *Rheological properties of highly flowable mortar containing limestone filler-effect of powder content and W/C ratio*, Cement and Concrete Research, 35, 3, 2005, pp. 532-539, doi:10.1016/j.cemconres.2004.05.008.

[28] Laibao L., Yunsheng Z., Wenhua Z., Zhiyong L., Lihua Z.: *Investigating the influence of basalt as mineral admixture on hydration and microstructure formation mechanism of cement*. Construction and Building Materials, 48, 2013, pp. 434-440, doi:10.1016/j.conbuildmat.2013.07.021.

[29] Bobrowski A., Gawlicki M., Łagosz A., Nocuń-Wczelik W.: *Cement. Metody badań. Wybrane kierunki stosowania*. Wydawnictwo AGH, Kraków 2010.


environment
environment

Karolina Sadko, Jerzy Zbigniew Piotrowski
Structure and Environment 2022, vol. 14, (4), pp. 126-141, Article number: el 015
https://doi.org/10.30540/sae-2022-015

Structure and Environment
ISSN 2081-1500
e-ISSN 2657-6902
https://content.sciendo.com/sae
https://sae.tu.kielce.pl

sciendo

Kielce University of Technology

DOI: 10.30540/sae-2022-015

NUMERICAL INVESTIGATIONS OF THE THERMAL PROPERTIES OF WINDOW SYSTEMS: A REVIEW

PRZEGLĄD NUMERYCZNYCH METOD OKREŚLANIA WŁAŚCIWOŚCI CIEPLNYCH OKIEN

Karolina Sadko*, Jerzy Zbigniew Piotrowski
Kielce University of Technology, Poland

Abstract

Windows are an essential part of building envelopes since they enhance the appearance of the building, allow daylight and solar heat to come in, and allow people to observe outside. However, conventional windows tend to have poor U-values, which cause significant heat losses during the winter season and undesired heat gain in summer. Modern glazing technologies are therefore required to improve thermal resistance and comfort of the occupants, whilst mitigating the energy consumption of buildings. In the present work, a comprehensive review of the numerical investigations of the thermal properties of window systems and glazed buildings partitions is presented. However, the proposed models to predict the thermal performance most often concern only specific cases of window systems related to geometry and used material solutions, focused on specific physical processes, thus they contain a lot of simplifications, such as omitting the influence of radiation, temperature changes or velocity profiles.

Keywords: windows, windows thermal resistance, thermal transmittance, heat transfer coefficient, mathematical modelling

Streszczenie

Istotnymi elementami budynków są okna, które wpływają na ich wygląd, umożliwiają dostęp światła dziennego i ciepła pochodzącego z promieniowania słonecznego, a także pozwalają na obserwowanie otoczenia. Jednakże w porównaniu do pozostałych przegród budowlanych konwencjonalne okna charakteryzują się zwykle gorszymi wartościami współczynnika przenikania ciepła U, generując znaczne straty ciepła w sezonie zimowym i niepożądane zyski ciepła w lecie. W związku z tym konieczne jest poszukiwanie nowoczesnych rozwiązań w technologii okiennej, które poprawią opór cieplny i komfort mieszkańców, jednocześnie zmniejszając zużycie energii przez budynki. W niniejszej pracy przedstawiono przegląd numerycznych metod określania właściwości cieplnych okien i przeszklonych przegród budowlanych. Analiza literatury pokazuje, że proponowane modele dotyczą jednak najczęściej tylko konkretnych przypadków systemów okiennych, związanych z określoną geometrią i zastosowanymi rozwiązaniami materiałowymi, w których uwzględnia się jedynie wybrane procesy fizyczne. Skutkiem tego jest przyjmowanie podczas modelowania wymiany ciepła szeregu uproszczeń, takich jak pomijanie wpływu promieniowania czy nieuwzględnianie zmian temperatury i prędkości.

Słowa kluczowe: okna, opór cieplny okien, przenikalność cieplna, współczynnik przenikania ciepła, modelowanie matematyczne

*Kielce University of Technology, Poland, e-mail: ksadko@tu.kielce.pl

1. INTRODUCTION

Windows represent essential elements of buildings' envelope, which determine natural daylight and direct solar energy gains, provide view of the outdoors and supply fresh air [1, 2]. In addition, they significantly contribute to the heat transfer between the outside and inside environments, thus have a significant impact on overall building energy consumption [3, 4]. Nevertheless, glazing systems usually have the lowest energy efficiency of building envelope components [5, 6]. They are the most problematic in terms of heat loss, generating to 60% of the total energy loss through the building envelopes [7, 8]. Changes in architectural trends have shown that the number and dimensions of windows in buildings are increasing. Today large glazing windows and curtain walls are frequently designed and integrated in modern housing, which makes it necessary to ensure their high thermal resistance [9-11]. On the other hand, in existing buildings old window structures have low thermal resistance, thus an effective way to improve buildings envelope energy performance and reduce heat loss, is the replacement of old window structures by modern windows. Innovative windows should control solar radiation and have high thermal resistance which allow to decrease heat loss in the winter and heat gain in the summer, dynamically responding to varying weather conditions and occupant preferences [12]. There is thus a call for new advances aiming at improving the overall performance of building fenestration by considerably decrease both building energy demand and peak heat loads. Heat transfer in tall cavities where aspect ratio is high such as glazing, takes place through conduction through the glass panes, convection in the gaseous medium filling the gap between the panes and radiation. Therefore, a reduction in the overall heat transfer coefficient of windows can be achieved by minimizing the convective and radiative components [13].

Recently, a variety of technologies have been developed to improve the thermal resistance of windows and building glazing systems. Inhibiting convection in the gaseous medium filling the gap can be achieved by using approaches such as multiple glass panes [14, 15], optimization of the gap width [16-19], inert gases as gap fill [20, 21] and vacuum glazing [22, 23]. Glass used in windows provide adequate illumination levels in the interior of buildings receiving the visible part of solar radiation. The other part of solar radiation in the infrared region entering through windows causes increase of interior temperature, thus glazing is a significant component in investigating problems such as energy demands, assessment of heating and cooling loads and thermal comfort in a building [24, 25]. Proper selection of glazing material can reduce the solar heat gain component in summer as also heat loss in winter [26]. Controlling solar radiation and daylight can be achieved through application of tinted coatings, reflective coatings [27], solar control films [28, 29], interstitial shading devices (e.g, external blinds' [30, 31], single and double curtains [32, 33], roller shades [34], window shutters [35], angular selective shading systems [36-39] and smart window techniques (e.g. electrochromic [40], thermochromic [41], photochromic [42] glazing). Windows are also expected to facilitate sufficient air change rates [43]. To achieve these attributes, various transparent building components have been developed, including ventilated windows [44-48] and ventilated double skin facade [49-52].

This paper presents a review of the modeling of heat transfer in windows systems with the aim of identifying the different approaches and applications implemented, as well as the research gaps. Firstly, the methods of the numerical investigations of the thermal properties of window systems present in the literature are summarized. Then, the most common thermal models are described, considering the influence of the gap thickness, internal surface temperature difference and the radiative heat transfer. Finally, the shortcomings and research gaps are discussed.

2. THE NUMERICAL INVESTIGATIONS OF THE THERMAL PROPERTIES OF WINDOW SYSTEMS

There are two ways of numerical investigation of the thermal properties of window systems: (1) one-dimensional calculation based on standard calculation methods and (2) two- or three-dimensional mathematical modeling using finite element or finite volume models [12]. Standards describing the thermal properties of window systems include International Standards ISO 10292 [53], ISO 15099 [54] and European Standard EN 673 [55]. A crucial parameter characterizing thermal properties of windows is the overall heat transfer coefficient *U*, which defines the heat flow through 1 m^2 of building partition surface with a temperature difference on both sides $\Delta T = 1$ K. Under these standards, the *U*-factor of window systems can be expressed as (Fig. 1):

$$U = \frac{1}{R_T} = \frac{1}{\frac{1}{h_i} + \sum_{s=1}^{n} \frac{\delta_g}{k_g} + \sum_{s=1}^{n-1} \frac{1}{h_{gap}} + \frac{1}{h_o}} \tag{1}$$

where R_T is total thermal resistance of window, h_i, h_{gap}, and h_o are the heat transfer coefficients at the inner surface of the window, the gap between the glass panes, and the outer surface of the window, respectively, $h_{gap} = h_{rad,gap} + h_{conv,gap}$ is the combined radiation and convection heat transfer coefficient of the gap between the glass panes, is the thickness of the glass pane, k_g is the thermal conductivity of the glass pane, n is a number of glass panes.

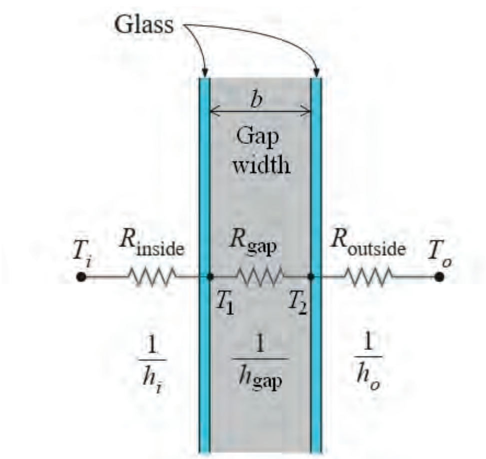

Fig. 1. The thermal resistance network for heat transfer through a double-pane window

Heat transfer in enclosed spaces, such as gap between glass panes, is complicated by the fact that the gas in the enclosure, in general, does not remain stationary. While the gas flows over the glass surface as a result of gravitational movements, there is a significant influence of the gas viscosity on its velocity. The region of the flow over the glass panes, in which the viscous effects and the velocity changes are significant is called the boundary layer [56]. Close to the panes surfaces, value of the velocity is zero, and it increases with increasing distance from the glass surface. In the inviscid flow region, the frictional effects are negligible and the velocity remains essentially constant. The thickness of the boundary layer depends on the temperature and the physical properties of the gas, thus the heat transfer by convection is influenced by physical parameters of the fluids such as specific heat, density, thermal diffusivity and viscosity. It follows from the above that the convective heat transfer coefficients (i.e. h_i, h_{gap}, h_o from eq. 1) are a function of the temperature of the heat exchanging surface as well as the flow velocity, temperature and physical properties of the gaseous medium.

The accuracy of heat transfer calculations is a function of three dimensionless parameters: the aspect ratio of the gap, the Prandtl number, Pr, and the control parameter of the flow, the Rayleigh number, Ra. The relative thickness of the velocity and the thermal boundary layers is best described by the dimensionless parameter Prandtl number, defined as

$$Pr = \frac{\nu}{a} = \frac{c_p \mu}{k} \tag{2}$$

where ν is kinematic viscosity, a is thermal diffusivity, c_p is specific heat, is dynamic viscosity, k is the thermal conductivity of the fluid.

The Rayleigh number, which is the product of the Grashof and Prandtl numbers, can be expressed as:

$$Ra = Pr \cdot Gr \tag{3}$$

The Grashof number, Gr, is a dimensionless number which approximates the ratio of the buoyancy to viscous force acting on a fluid, can be expressed through following equation:

$$Gr = \frac{g \beta \Delta T L^3}{\nu^2} \tag{4}$$

where g is gravitational acceleration, β is coefficient of volume expansion, ΔT is internal glass surface temperatures difference across the gap, L is the characteristic length, which in the case of double pane window is the distance between the two glass panes ($L = b$, where b is width of the gap between two glass panes).

In particular, for $Ra < 1750$ viscosity prevents the onset of buoyancy-driven convective motions. Within the range $1750 < Ra < 3000$ the onset of convection is increasing, depending on the geometric parameters. For $Ra > 3000$ heat transfer is a growing function of the Rayleigh number, which means a reduction of thermal resistance caused by the thermal conductance [57]. The ratio between the pure conduction resistances to a convection resistance represents the Nusselt number, given by:

$$Nu = \frac{hL}{k} = Const\left(Gr \cdot Pr\right)^e \tag{5}$$

where $Const$ is a constant and e is an exponent that makes it possible to account for the orientation of the glazing. For vertical glazing, these are 0.035 and 0.38, respectively [52]. Apart from standard equation calculation methods, the most common approach used in order to determine the thermal properties of window systems are finite element or finite volume simulations, especially when the air flow pattern in the gap between glass panes is investigated. Modeling methods are numerous but the majority of models incorporate CFD analysis [58-63]. In the CFD model, the fluid medium is modeled based on two- or three-dimensional assumptions by meshing the fluid region into a finite number of control volumes. The finite volume method used to study natural convection in the gap of double pane windows, follows assumptions below: 1) heat transfer through a double-pane windows is considered in a stationary two-dimensional formulation; 2) free-convective flow of a gas medium in the window′s compartments is considered laminar and is described by a system of Navier–Stokes equations for a compressible medium; 3) the glass panes surfaces facing into the gap are set as two isothermal walls each with a different temperature to represent the temperature difference between indoor and outdoor environments; 4) the top and bottom surfaces bounding the gap are assumed to be adiabatic; 5) the influence of separating frames is disregarded; 6) all thermophysical properties of the fluid are assumed to be constant, except for the gas medium density and viscosity, which are considered temperature-dependent by the linear law. The governing equations for these finite volume models for steady two-dimensional flow of a fluid with constant density are:

Mass balance:

$$\frac{\partial u}{\partial x}+\frac{\partial v}{\partial y}=0 \tag{6}$$

Momentum balance:

$$\frac{\partial u^2}{\partial x}+\frac{\partial uv}{\partial y}=$$

$$-\frac{1}{\rho}\frac{\partial p}{\partial x}+v\left(\frac{\partial^2 u}{\partial x^2}+\frac{\partial^2 u}{\partial y^2}\right)\frac{\partial uv}{\partial x}+\frac{\partial v^2}{\partial y}= \tag{7}$$

$$-\frac{1}{\rho}\frac{\partial p}{\partial y}+v\left(\frac{\partial^2 v}{\partial x^2}+\frac{\partial^2 v}{\partial y^2}\right)+g\beta\left(T_1-T_2\right)$$

Energy balance:

$$C_p\rho\left(\frac{\partial uT}{\partial x}+\frac{\partial vT}{\partial y}\right)=k\left(\frac{\partial^2 T}{\partial x^2}+\frac{\partial^2 T}{\partial y^2}\right)+S_h \tag{8}$$

where u is velocity component in x-direction, v is velocity component in y-direction, is density, S_h is the radiative heat transfer.

However, in most of these studies, long-wave radiation heat transfer, which accounts for two thirds of the total heat transfer across the air cavity [63], is neglected in the numerical modeling. This means the radiative heat transfer, S_h, in Equation (8) was not included.

2.1. The influence of the gap thickness and internal glass surface temperatures difference across the gap

The thermal resistance of a tall air cavity associated with conductive heat transfer increases with the width of gap filling by gaseous medium, thus increasing the width between two panes of glass decreases the thermal transmittance and improves the insulation effect in windows systems. Manz investigated overall convective heat transfer in an air layer within a rectangular cavity using a commercial CFD code [64]. It was reported that Nusselt numbers do not deviate more than 20% from the correlations based on experimental data. A similar numerical study is conducted in paper [65] considering both laminar and turbulent natural convection in cavity for aspect ratios of 20, 40 and 80 and for Rayleigh numbers in the range of 102 to 108. They presented convective Nusselt number correlations for both laminar and turbulent flows. However, it is known that there is a limit in the effect of increasing the gap on the improvement of insulation. This limit is the ‘optimum’ separation of the panes and depends on the phenomenon of free convection within the gap, which depends both on the geometry (characteristic size and aspect ratio) and on the temperature boundary conditions. In particular, convection enhances the heat flux through the window, reducing thermal insulation. In the case of narrow gaps ($Nu < 1$) it is assumed that convection does not occur and thermal resistance of the gap increases linearly with its width. The influence of convection is taken into account while a certain gap width limit (for $Nu = 1$) is exceeded. In the case of non-linear range (for $Nu > 1$) thermal resistance of the double-pane window does not improve [66]. For cases with a small gap width, the heat transfer by convection is insignificant due to the low values of the velocity of free convective gas flow. With an increase in the distance between the glasses, the thermal resistance of the thermal conductivity of the gas layer increases. However, in this case, due to a decrease in the hydrodynamic resistance of the plane-parallel channel, represented by two vertical glasses, the flow of the gaseous medium is intensified and, as a result, the convective heat transfer in the gaseous layer increase. As a result of the interaction of two opposite tendencies, the total convective heat flux on the inner surfaces of the glasses first decreases with increasing distance between the glasses, and then begins to increase. The influence of the width of gap between the panes and temperature difference on the thermal resistance of double-pane window were presented in paper [16]. Figure 2 shows the predicted heat transfer coefficients for the same temperature difference between the internal surfaces of 10 K. When the width of gap is larger than 25 mm, the convective heat transfer coefficient increases slightly with air space, because the increase in the convective heat transfer is larger than the decrease in the conductive heat transfer. For the internal surface temperature difference of 10 K the predicted overall heat transfer coefficient was 3.33, 2.93 and 2.71 W/m^2 K, for an air space width of 5, 10 and 25 mm, respectively. If the air gap width exceeds 25 mm, the window's thermal transmittance remains almost constant, because a slight increase in convective heat transfer is offset by a similar magnitude of the decrease in radiative heat transfer. The thermal transmittance vary with the temperature difference. Figure 2 shows the variation of *U*-value with the width of gap for internal surface temperature differences of 5 K, 10 K, 15 K and 20 K, respectively. As seen in the figure, the *U*-value decreases with the width of air space up to 25 mm regardless of the magnitude of the temperature difference.

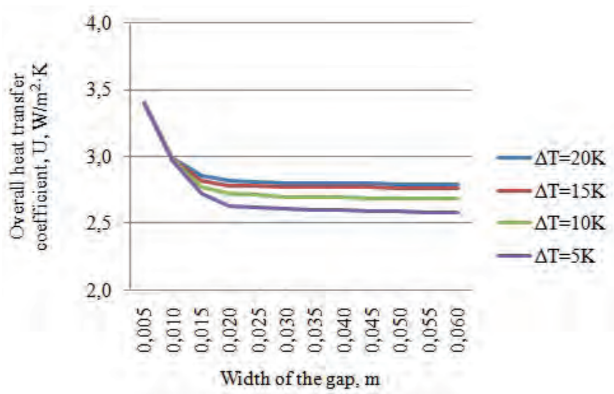

Fig. 2. Variation of overall heat transfer coefficient with the width of gap

The value of the optimum gap related to the velocity and temperature fields in double-pane window were investigated in paper [63]. Authors assigned fourth-kind conditions on the pane surfaces facing the interior of the window, taking into account the presence of radiant heat fluxes between pane surfaces. The distributions of the vertical velocity and temperature over the gap are presented in Figure 3. Figure 3 shows that near the heated pane occurs ascending flow, and near the cold pane, descending flow. In this case the temperature distribution within the gap is different from the linear one, and natural convection in the gap now exerts an appreciable influence on the process of heat transfer. The distributions of the dimensionless vertical velocity, the dimensionless temperature and heat-flux densities on the exterior and interior surfaces of double-pane window are presented in Figure 4 and Figure 5. As can be seen, the maximum heat-flux densities are observed on the upper portion of the outside pane (curve 2) and there is no region in which the heat-flux densities are constant, in practice. This also points to the significant impact of natural convection on the process of heat transfer in double-pane window. The value of the total heat flux is Q = 127.5 W. Although convective heat transfer in double-pane window is appreciable, its share in the total heat flux amounts to only 34% of the overall heat flux. The radiative heat flux is Q_r = 84.7 W (i.e., 66% of the total heat flux). The thermal resistance of double-pane window of the indicated geometry is equal to R = 0.19 m^2·K/W.

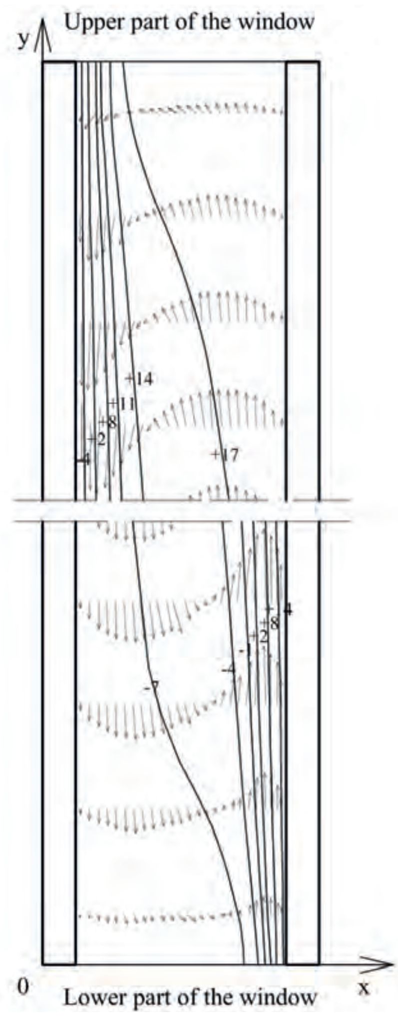

Fig. 3. Temperature fields (°C) and directions of velocity of the gas medium in vertical cross sections of the double-pane window

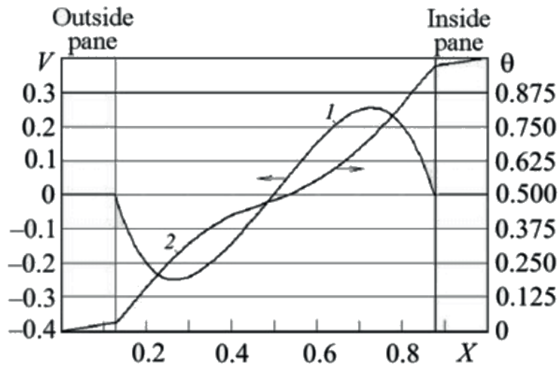

Fig. 4. Distributions of the dimensionless vertical velocity (1) in gap and of the dimensionless temperature (2) across the thickness of the double-pane window [63]

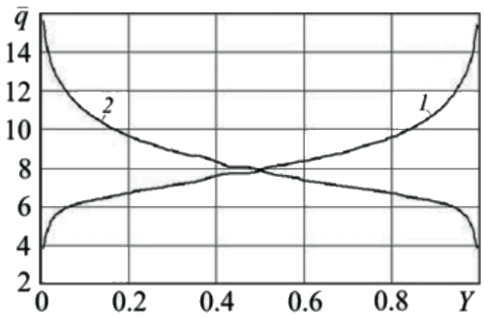

Fig. 5. Distributions of the dimensionless heat-flux densities on the exterior (1) and interior (2) surfaces of the double-pane window [63]

Arıcı et al. carried out numerically flow and conjugate heat transfer in double-glazed windows considering five different gap widths (L = 6 mm, 9 mm, 12 mm, 15 mm and 18 mm) and five different emissivity values (ε = 0, 0.25, 0.50, 0.75 and 1.0) [18]. Surface to Surface (S2S) mathematical model which ignores any absorption, emission or scattering of gas is employed to account radiative heat transfer between panes. Solar heat gain are not considered in the computations. Figure 6 shows variation of the *overall heat transfer coefficient* of air-filled double-pane window with various emissivity values and gap widths. As seen in the figure, while the overall heat transfer coefficient decreases considerably up to gap width of 12 mm, beyond this value the influence of gap width on the overall heat transfer coefficient diminishes. The overall heat transfer coefficient curves of gap width of 12 mm, 15 mm and 18 mm are almost overlapped, thus the most adequate value of the gap width is 12 mm.

The velocity and temperature profiles presented in Figure 7 signify why the U-value is almost constant beyond gap width of L = 12 mm. At its value of L = 6 mm, the gas flow velocity is low, so heat transfer by convection is negligible. In this case, the Nusselt number (except for the bottom and top of the window) is about 1, so heat transfer occurs equally by heat convection and conduction.

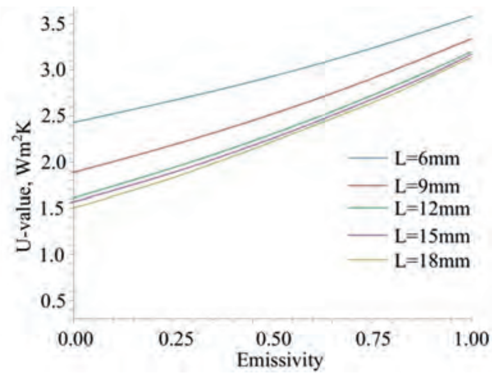

Fig. 6. Variation of the overall heat transfer coefficient of air-filled double-pane window with various emissivity values and gap widths

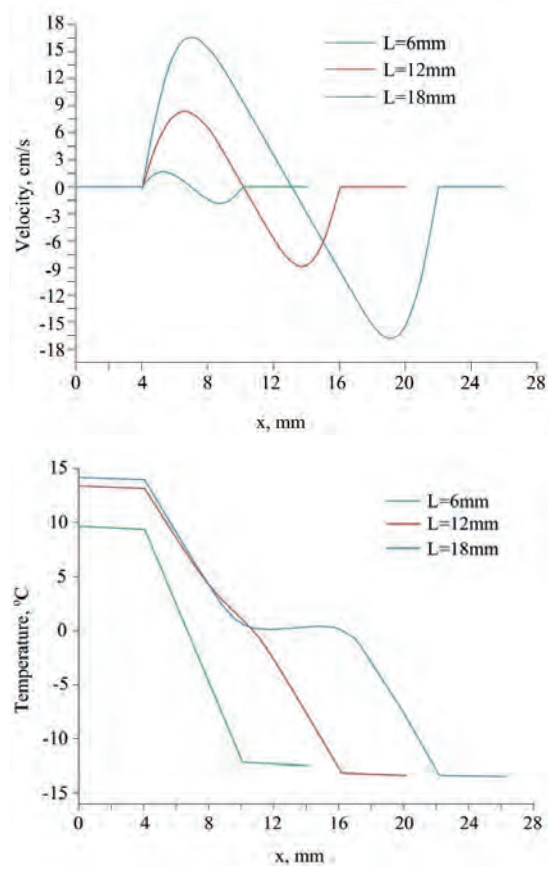

Fig. 7. Effect of gap width on the velocity and temperature profiles of air-filled double-pane window

As the gap width increases, the magnitude of velocity increases, thus the importance of convection and consequently the Nusselt number also increases. At this stage, it is observed that the Rayleigh number exceeds 6300, causing a transition flow between laminar and turbulent and degradation of the linearity of the temperature profiles. The heated air is transported from hot side to cold side horizontally and creates a short cut in heat transfer, which causes a deteriorating the linearity of temperature profiles. Thus, the decrease in the overall heat transfer coefficient is insignificant for L > 12 mm.

The thermal properties of double-glazed window depending on the changes in outdoor temperatures are presented in paper [67]. Figure 8 shows dependence of distance between the panes and external air temperature on overall heat transfer coefficient.

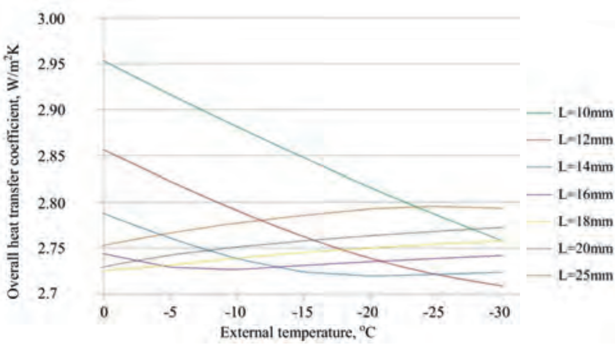

Fig. 8. Dependence of overall heat transfer coefficient of a double-pane window on distance between the panes and external air temperature

As can be seen, the decrement of the external air temperature causes a decrement of the overall heat transfer coefficient for small gap width of 10 and 12 mm. However, for larger distances between the panes, the U-factor slightly changed (mainly increased) to 2%. The decrement of thermal transmittance with the decrease in external air temperature can be considered a positive phenomenon at extremely low temperatures and slight changes in the U-factor value can be treated as insignificant. These results confirm why the change in the heat transfer coefficient of double-pane window due to the outside temperature has been ignored in the past. The thermal behavior of ventilated double-pane window with varying gap width was developed in paper [68]. The model takes into account the physical phenomena present in the heat and flow processes and also the real boundary conditions while in normal operation. The numerical simulations were compared with available results and the agreement was found satisfactory. Effects of the gap width on the temperature distribution, the velocity field, the coefficient of the total heat gain, the coefficient of the solar heat gain and the shading coefficient were investigated. Ignoring at least for the moment, the solar radiation, the heat gain or loss due to the temperature difference between the internal and the external temperatures depends of width of the gap between glass panes. Figure 9 shows the heat gain due to the temperature difference in terms of the gap between the window sheets. As can be seen the increase of the size of the gap leads to increasing the thermal resistance.

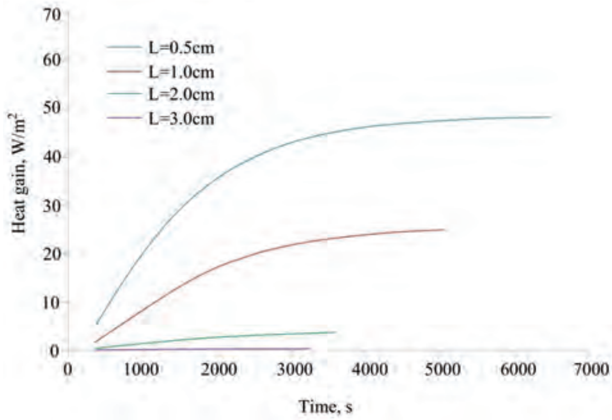

Fig. 9. Effect of the gap width on the heat gain due to temperature difference for a ventilated double-pane window

Table 1. Summary of heat transfer coefficients of windows depending on the geometry, the width of the gap and the internal surface temperature difference

Ref.	Gap width [mm]	*H* [m]	*L* [m]	Δ*T* [K]	*ε*	*U* [W/m²K]
[16]	5	1.50	1.50	10	0.84	3.33
	10	1.50	1.50	10	0.84	2.93
	25	1.0	1.50	5	0.84	2.63
	25	1.0	1.50	10	0.84	2.71
	25	1.0	1.50	15	0.84	2.78
	25	1.0	1.50	20	0.84	2.85
[18]	6	1.0	0.50	35	0.84	3.39
	9	1.0	0.50	35	0.84	3.05
	12	1.0	0.50	35	0.84	2.90
	15	1.0	0.50	35	0.84	2.86
	18	1.0	0.50	35	0.84	2.81
[63]	24	1.08	0.75	30	0.84	2.78
[67]	10	1.48	1.23	20	0.84	2.95
	10	1.48	1.23	30	0.84	2.88
	10	1.48	1.23	45	0.84	2.79
	14	1.48	1.23	20	0.84	2.79
	14	1.48	1.23	30	0.84	2.74
	14	1.48	1.23	45	0.84	2.72
	25	1.48	1.23	20	0.84	2.75
	25	1.48	1.23	30	0.84	2.78
	25	1.48	1.23	45	0.84	2.80

Table 1 present the summary of overall heat transfer coefficients of windows depending on the geometry, the width of the gap and the internal surface temperature difference.

2.2. The influence of the radiative heat transfer

Solar irradiance, incident on the window glass, which consists of the direct component from the Sun and the diffuse component from the sky, clouds, and surrounding objects, is partly transmitted and reflected, while the remaining portion is absorbed within the glass material. The absorbed portion is transmitted inward, as well as outward, by the processes of conduction, convection and longwave radiation, thus causes increase of interior temperature. The total energy transmittance is quantified by the solar heat gain coefficient, SHGC, which is the sum of the direct transmitted solar radiation plus the inward thermal convection and radiation heat transfer due to the increased inner glazing temperature above the room environment, then normalized by the incoming solar irradiance. The sum of this combined solar heat transfer, which depends on SHGC and the convective heat transfer, which depends on *U*-factor, is the total room heat gain through window system [69]. The significant impact on such energy distributions have also the polarization, frequency spectrum as well as the directions of the incident rays. An experimental approach to measure the light transmittance and solar energy transmittance of double-pane window separated by argon filled space and solar controlling film at any incidence angle was developed by Rosenfeld et al. [70] Van Nijnatten [71] measured the directional reflectance and transmittance of coated and uncoated glass samples by setting new accessories in a spectrophotometer. The thermal performance of glazing with films of different types under solar radiation was analyzed in the paper [72]. Ismail and Henríquez [73] numerically investigated solar heat gain coefficient and shading coefficient of double glass panels filled with PCM. Later, author extended his study and developed the mathematical models of heat transfer through windows formed by a single glass sheet and double glass sheets with natural or forced air flow between them under incident solar radiation [68, 74, 75]. The airflow is induced by the buoyancy forces due to the thermal effects in a gap formed by two parallel walls with non-symmetric heating as shown in Figure 10. The heat transfer consist of incident solar radiation, convection and also radiation exchange between the walls and the internal and external ambient. The two-dimensional transient model is formulated based upon the fundamental equations of mass conservation, momentum and energy, the associated constant and time varying boundary conditions.

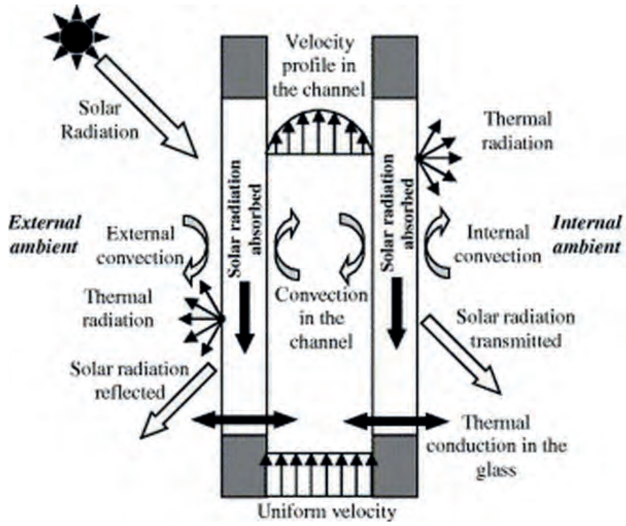

Fig. 10. Heat transfer in a ventilated window [68]

As a result, the heat gain due to the solar radiation, composing of the heat gain due to incident solar radiation which crosses directly to the internal ambient and the solar radiation absorbed by the glass sheets and reemitted to the internal ambient, was determined. Figure 11 shows the solar heat gain for three different values of gap width.

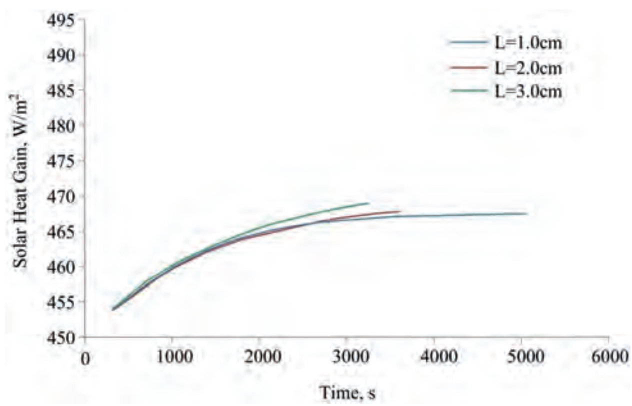

Fig. 11. Effect of the gap width on the solar heat gain of a ventilated double-glazed window

As can be seen, there is a little difference between the solar heat gain of the three arrangements, because of the optical transmittance of the arrangements is nearly the same. The results indicate that the gap width has little effect on the mean coefficient of solar heat gain and the mean shading coefficient. Jaber and Ajib [76] investigated the optimum window type and size for heating demands in three different climate zones – Amman, Aqaba and Berlin. The results showed that as the overall heat transfer coefficient decreases, the annual heating energy for all sites decreases. The heat demand depends on the location of the façade in relation to the directions of the world, thus on the intensity of the incidence of solar radiation. The highest occurres at the Northern façade at all sites, as it received a low solar incident radiation. On the other hand, the Southern façade induced the lowest heating energy because of high solar incident radiations. Alvarez et al. [77] developed heat transfer model to evaluate the convective heat transfer coefficient and heat gain coefficient due to the optical properties of coated glass in the visible and solar spectra region. The overall heat transfer coefficient of window and the solar heat gain of building interior were predicted from the simulation to evaluate the glazing performance in increasing the inside temperature due to the incidence of global radiation through window [26]. A solar simulation model was developed to predict the glazing temperature due to global radiation consisting of direct, diffuse and reflected components and hence the solar heat gain of building interior. The another thermal model was concerned with laminar heat transfer for natural and forced convection process according to the variation of inside and outside atmosphere with seasons and was solved by finite difference technique. For the outer glazing surface, time-dependent incident solar radiation acts as source of heat flux. Heat flow from simulation are presented in Figure 12.

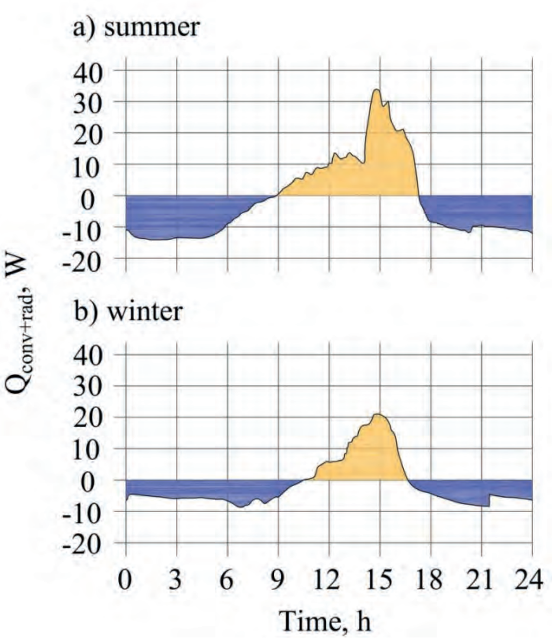

Fig. 12. Heat flow from simulation

Figure 12 shows that heat flow increases with time, due to the increase of global radiation on window and ambient temperature. In the model of heat transfer through windows, the phenomenon of solar radiation beam reflection from the internal environment of the building, is proposed in paper [78]. A correlation created by the authors takes into account the entering solar radiation effective absorption coefficient, which depends upon the optical and geometrical properties of the indoor environment and the transmission coefficient of the diffuse radiation of the transparent surfaces. Solar energy absorbed by the indoor environment is calculated as the sum of three contributions: the first optical, produced by solar radiation transmitted by glazed surfaces, the second direct convective-radiative, which evaluates the fraction of solar radiation absorbed and provided to the indoor environment by the glazed surface which is radiated directly by the sun, the third indirect convective-radiative, produced by solar radiation reflected by internal surfaces and absorbed by glazed surfaces. The proposed new calculation procedure of solar heat gains allows for more accurate monthly evaluations. Some improved simulation methods were investigated by Avedissian and Naylor [79] and Sun et al. [80], who used a "surface-to-surface" (S2S) model to take into account radiation during heat transfer through ventilated window systems. All the surfaces were assumed to be grey bodies, diffuse and opaque to thermal radiation. The air in the cavity was assumed to be a non-participating medium. The view factors, which depend on surfaces' size, separation distance and orientation, were computed before simulating the radiation. A mathematical model of the long-wave radiation heat transfer between the inside room surfaces and the outside environmental surface through a glazing considering the transmittance of glass is presented in paper [81]. The effects of the transparence radiation characteristics of glass, convection heat transfer coefficient of inside and outside of the glazing, and the difference between the surface temperature (including inside room surface temperature and outside environmental surface temperature) and the air temperature (including indoor and outdoor air temperature) on the overall heat flux and the ratio of the heat flux due to the transparence radiation to the overall heat flux are developed. However, short-wave radiation (solar radiation) was neglected by the authors in the process of model developing.

In some advanced windows systems, the absorbed portion of solar radiation can be extracted through other means such as electricity conversion and natural airflow, thus can be taken as the additional heat source. Numerical solutions to the energy equations for laminar natural convection in the air gap of double-pane window with integrated see-through PV glass with low-e coating were investigated in paper [82]. The study provides obtaining of U-value and accurate heat transfer model which is significant for predicting the PV conversion efficiency considering solar cell temperature and investigating the thermal behaviors of see-through PV double-pane window. Results show that a large quantity of heat transfer by radiation within the air gap can be reduced by employing PV double-pane window with low-e coating. A comprehensive review of the modeling of transparent- and semi-transparent Building Intagreted PV systems in windows is presented in paper [83]. Despite the interest in the topic, there are relatively few studies on modeling the performance due to these technologies. Some models were investigated for obtaining the windows overall heat transfer coefficient and SHGC, taking into account the PV effect. In this sense, a methodology for estimating the thermal behavior of a photovoltaic–thermal (PVT) double semi-transparent façade was proposed in paper [84]. The transmission losses and ventilation gains were presented with four parameters (thermal transmittance, ventilation thermal transmittance, solar gain and ventilation solar gain, which were calculated by the one-dimensional single-node energy balance, including the electric production on the PV surface. Another one-dimensional power balance model for a PV window was developed by Misara et al. [85] to obtain the U, SHGC, and solar reduction ratio values. Authors indicated that the normative methods used in the calculations are not applicable to PV windows, thus the models need to be adjusted to include the internal heat sources of PV modules and the new thermal parameters, such as the internal and external heat transfer coefficient and heat transfer coefficient of insulated glass. More detailed two-dimensional models were investigated into T- and ST- BIPV windows in order to evaluate the impact of natural and forced convection in the window gaps on the vertical axis, as is shown in Figure 13.

Two-dimensional model for a ventilated double-pane window was developed in paper [87] to compare the PV output, heat transmission, daylight, and energy use varying with the orientation and transparency.

A similar modeling approach was developed and validated by Han et al. [88] in order to determinate accurate heat transfer coefficients for a see-through glazing system with the integration of Semi-transparent building-integrated photovoltaic (ST-BIPV) with naturally ventilated air gaps.

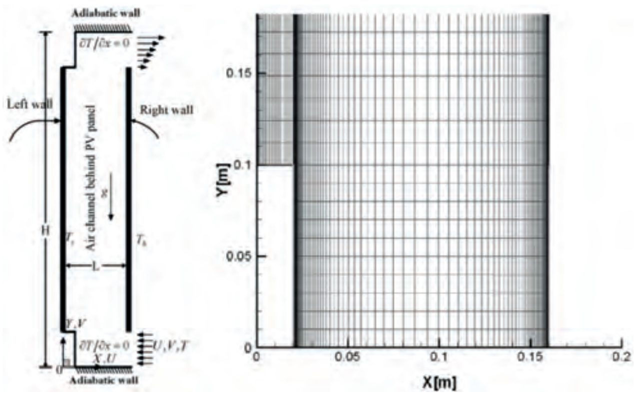

Fig. 13. Two-dimensional model for a ventilated double-sided PV façade [86]

A double-pane semi-transparent and transparent building-integrated photovoltaic (T-BIPV) cladding window were evaluated in paper [89], finding that façade orientation, the window-to-wall ratios, and lighting power density did not affect the selection of the ST- and T-BIPV optical properties. In opposite, Ng et al. [90] compared single-pane window, double-pane window, double-pane window with low-e glaze and double-pane window with low-e tinted glass with ST- BIPV systems (six combinations of thin-film and amorphous silicon modules in a single- or double-glass configuration). Results showed that all BIPV systems outperformed conventional windows by reducing the overall energy use, including heating, cooling, lighting, and PV output. Gevers et al. [91] investigated a prototype of frame-integrated BIPV systems in which the glazing system is used to redirect part of the radiation to the frame, thus acting as a solar control window. Nourozi et al. evaluated the Energy Active Windows (EAW) to minimize the building's thermal losses in winter, providing a modern architecture sustainability and interior comfort [92]. EAW utilizes low-grade energy, such as waste heat from the gap between the window panes, provided by built-in heat exchanger combined with a fan. Nusselt numbers for forced convection [93], occurring between symmetrically heated parallel plates with the same surface temperature, have been adapted for use in EAW because of different surfaces temperatures due to the supply of warm air and the large temperature difference between the inside and the outside. Thus, the constant value in the Nusselt number correlations have been changed to more accurately account for the effect of asymmetrically heated windows. The Nusselt number for panes with asymmetric surface temperatures is about 1.9 times lower than for panes with the same surface temperatures [92]. In the EAW, the influence of the gap width on the value of the heat transfer coefficient turns out to be insignificant, while the change of the temperature of the supplied air is significant. In order to maintain a low heat transfer coefficient, the temperature of the air supplied to the window must be higher than the room's internal temperature. The results indicated that windows can reduce the heating load by about 2.2 W/m^2 for window to floor area ratio of 10%. Controlling short and long wave solar radiation passing through the window can be achieved by use the smart glasses. They can regulate the temperature and illumination level indoors depending on the change of the environmental parameters or due to the electric current passing through an active layer of the laminated glass. Some types of modern smart glasses and chromogenic materials are listed in Table 2.

Table 2. Types of glass or chromism and mechanism of action

Type of glass/chromism	Mechanism of action	Ref.
Low-emissivity	Visible spectrum transmission and IR reflection	[94]
Electrochromism	Change in transparency and color on passing electric current	[95]
Thermochromism	Change in reflectance and transmittance at a specific critical temperature	[96]
Thermotropism	Temperature dependent change of light scattering	[97]
Photochromism	Transmission varies with intensity of incident shortwave UV or visible light	[98]
Gasochromism	Change in transmittance by interaction with diluted hydrogen gas	[99]
Mechanochromism	Color change due to change in pH of solution	[100]
Magnetochromic	Controlled by the magnetic field intensity	[101]

3. CONCLUSIONS

The thermal properties of windows systems listed above may vary depending on the ambient temperature, on solar radiation, on infiltration of outside air passing through leaks in the windows, and on their dimensions and geometry. Due to those differences the theoretical (i.e., calculated) and actual values of energy consumption in buildings differ. Therefore, the detailed relationship between the flow, heat transfer condition and the performances of windows are not fully investigated. Therefore, there is still a need to perform in-depth study on the flow and heat transfer characteristics of windows and other glazed buildings partitions.

Abbreviations:

AR – aspect ratio (H/L),
CFD – Computational Fluid Dynamics,
EAW – Energy Active Windows,
Low-E – low emissivity coating,
PCM – phase change material,
PV – photovoltaic,
PVT – photovoltaic–thermal,
SHGC – solar heat gain coefficient,
ST-BIPV – Semi-transparent building-integrated photovoltaic,
T-BIPV – Transparent building-integrated photovoltaic.

Nomenclature:

a – thermal diffusivity, m^2/s,
b – width of the gap with gas layer; distance between panes, m; mm,
β – coefficient of volume expansion, 1/K,
C_p – specific heat, J/kg·K,
ε – emissivity,
g – gravitational acceleration, m/s^2,
Gr – Grashof number,
h – convection heat transfer coefficient, $W/m^2 \cdot K$,
H – high of window, m,
k – thermal conductivity, W/m·K,
L_c – the characteristic length, m; mm,
L – length of window, m,
Nu – Nusselt number,
p – pressure, Pa,
Pr – Prandtl number,
q – heat flux density, W/m^2,
Q – heat flux, W,
Ra – Rayleigh number,
Re – Reynolds number,
RT – thermal resistance, $m^2 \cdot K/W$,
ρ – density, kg/m^3,
T – temperature, K,
t – time, s,
u – velocity component in x-direction, m/s,
U – overall heat transfer coefficient, $W/m^2 \cdot K$,
v – velocity component in y-direction, m/s,
μ – dynamic viscosity, kg/m·s,
ν – kinematic viscosity, m^2/s,
x, y – horizontal and vertical coordinates, m.

REFERENCES

[1] Fasi M.A., Budaiwi I.M.: *Energy performance of windows in office buildings considering daylight integration and visual comfort in hot climates*, Energy and Buildings, 108 (2015), pp. 307-316, https://doi.org/10.1016/j.enbuild.2015.09.024.

[2] Rezaei S.D., Shannigrahi S., Ramakrishna S.: *A review of conventional, advanced, and smart glazing technologies and materials for improving indoor environment*, Sol. Energy Mater. Sol. Cells, 159 (2017), pp. 26-51, https://doi.org/10.1016/j.solmat.2016.08.026.

[3] Sun Y., Liang R., Wu Y., Wilson R., Rutherford P.: *Development of a comprehensive method to analyze glazing systems with Parallel Slat Transparent Insulation material (PS-IM).* Applied Energy, 205 (2017), pp. 951-63, https://doi.org/10.1016/j.apenergy.2017.08.041.

[4] Cuce E., Riffat S.B.: *A state-of-the-art review on innovative glazing technologies*, Renewable and Sustainable Energy Reviews, 41 (2015), pp. 695-714, https://doi.org/10.1016/j.rser.2014.08.084.

[5] Wang B., Koh W.S., Liu H., Yik J., Bui V.P.: *Simulation and validation of solar heat gain in real urban environments,* Build. Environ., 123 (2017), pp. 261-276, https://doi.org/10.1016/j.buildenv.2017.07.006.

[6] Wang Y., Shukla A., Liu S.: *A state of art review on methodologies for heat transfer and energy flow characteristics of the active building envelopes,* Renew. Sustain. Energy Rev., 78 (2017), pp. 1102-1116, https://doi.org/10.1016/j.rser.2017.05.015.

[7] Tian Z., Zhang X., Jin X., Zhou X., Shi X.: *Towards adoption of building energy simulation and optimization for passive building design: a survey and a review*, Energy Build., 158(1), (2018), pp. 1306-1316, https://doi.org/10.1016/j.enbuild.2017.11.022.

[8] Lizana J., Chacartegui R., Padura A.B., Ortiz C.: *Advanced low-carbon energy measures based on thermal energy storage in buildings*: a review, Renewable and Sustainable Energy Reviews, 82(3), (2018), pp. 3705-3749, https://doi.org/10.1016/j.rser.2017.10.093.

[9] Casini M.: *Active dynamic windows for buildings*: a review, Renewable Energy, 119 (2018), pp. 923-934, https://doi.org/10.1016/j.renene.2017.12.049.

[10] Hee W.J., Alghoul M.A., Bakhtyar B., OmKalthum E., Sopian K.: *The role of window glazing on daylighting and energy saving in buildings*, a review, Renewable and Sustainable Energy Reviews, 42 (2015), pp. 323-343, https://doi.org/10.1016/j.rser.2014.09.020.

[11] Aguilar-Santana J.L., Velasco-Carrasco M., Riffat S.: *Thermal Transmittance (U-value) Evaluation of Innovative Window Technologies, Future Cities and Environment*, 6(1), (2020), pp. 12, http://doi.org/10.5334/fce.99.

[12] Sun Y., Wu Y., Wilson R.: *A review of thermal and optical characterisation of complex window systems and their building performance prediction*, Appl. Energy, 222(15), (2018), pp. 729-747, https://doi.org/10.1016/j.apenergy.2018.03.144.

[13] Basok B., Davydenko B., Novikov V., Pavlenko A.M., Novitska M., Sadko K., Goncharuk S.: *Evaluation of Heat Transfer Rates through Transparent Dividing Structures, Energies*, 15(13), (2022), pp. 4910, https://doi.org/10.3390/en15134910.

[14] Gorantla K., Shaik S., Setty A.B.T.P.: *Effects of single, double, triple and quadruple window glazing of various glass materials on heat gain in green energy buildings, Energy and Environment Engineering*, (2017), pp. 45-50, https://doi.org/10.1007/978-981-10-2675-1_5.

[15] Arıcı M., Karabay H., Kan M.: *Flow and heat transfer in double, triple and quadruple pane windows,* Energy Build., 86 (2015), pp. 394-402, https://doi.org/10.1016/j.enbuild.2014.10.043.

[16] Gan G.: *Thermal transmittance of multiple glazing: computational fluid dynamics prediction*, Applied Thermal Engineering, 21(15), (2001), pp. 1583-1592, https://doi.org/10.1016/S1359-4311(01)00016-3.

[17] Aydın O.: *Conjugate heat transfer analysis of double pane windows*, Building and Environment, 41(2), (2006), pp. 109-116, https://doi.org/10.1016/j.buildenv.2005.01.011.

[18] Arıcı M., Kan M.: *An investigation of flow and conjugate heat transfer in multiple pane windows with respect to gap width*, emissivity and gas filling, Renewable Energy, 75 (2015), pp. 249-256, https://doi.org/10.1016/j.renene.2014.10.004.

[19] Arıcı M., Karabay H.: *Determination of optimum thickness of double-glazed windows for the climatic regions of Turkey. Energy and Buildings*, 42 (2010), pp. 1773-1778, https://doi.org/10.1016/j.enbuild.2010.05.013.

[20] Ismail K.A.R., Salinas C.T., Henríquez J.R.: *A comparative study of naturally ventilated and gas filled windows for hot climates. Energy Convers. Manage.*, 50 (2009), pp. 1691-1703, https://doi.org/10.1016/j.enconman.2009.03.026.

[21] Park S., Song S-Y.: *Evaluation of Alternatives for Improving the Thermal Resistance of Window Glazing Edges*, Energies, 12 (2019), 244, https://doi.org/10.3390/en12020244.

[22] Eames P.: *Vacuum glazing: current performance and future prospects*, Vacuum, 82 (2008), pp. 717-722, https://doi.org/10.1016/j.vacuum.2007.10.017.

[23] Fang Y., Eames P.C., Norton B., Hyde T.J., Zhao J., Wang J., Huang Y.: *Low emittance coatings and the thermal performance of vacuum glazing*, Solar Energy, 81 (2007), pp. 8-12, https://doi.org/10.1016/j.solener.2006.06.011.
[24] Wąs K., Radoń J., Sadłowska-Sałęga A.: *Thermal Comfort - Case Study in a Lightweight Passive House*, Energies, 15 (2022), 4687, https://doi.org/10.3390/en15134687.
[25] Souviron J., van Moeseke G., Khan A.Z.: *Analysing the environmental impact of windows*: A review, Building and Environment, 161 (2019), 106268, https://doi.org/10.1016/j.buildenv.2019.106268.
[26] Pal S., Roy B., Neogi S.: *Heat transfer modelling on windows and glazing under the exposure of solar radiation*, Energy and Buildings, 41(6), (2009), pp. 654-661, https://doi.org/10.1016/j.enbuild.2009.01.003.
[27] Xamán J., Jiménez-Xamán C., Álvarez G., Zavala-Guillén I., Hernández-Pérez I., Aguilar J.O.: *Thermal performance of a double pane window with a solar control coating for warm climate of Mexico,* Applied Thermal Engineering, 106 (2016), pp. 257-265, https://doi.org/10.1016/j.applthermaleng.2016.06.011.
[28] Pereira J., Gomes M.G., Rodrigues A.M., Almeida M.: *Thermal, luminous and energy performance of solar control films in single-glazed windows: Use of energy performance criteria to support decision making*, Energy Build., 148(198), (2019), pp. 431-443, https://doi.org/10.1016/j.enbuild.2019.06.003.
[29] Teixeira H., Gomes M.G., Rodrigues A.M., Pereira J.: *Thermal and visual comfort, energy use and environmental performance of glazing systems with solar control films*, Build. Environ., 168 (2020), 106474, https://doi.org/10.1016/j.buildenv.2019.106474.
[30] Bavaresco M.V., Ghisi E.: *Influence of user interaction with internal blinds on the energy efficiency of office buildings,* Energy Build., 166(1), (2018), pp. 538-549, https://doi.org/10.1016/j.enbuild.2018.02.011.
[31] Jain S., Garg V.: *A review of open loop control strategies for shades, blinds and integrated lighting by use of real-time daylight prediction methods*, Build. Environ., 135(1), (2018), pp. 352-364, https://doi.org/10.1016/j.buildenv.2018.03.018.
[32] Lee A.D., Shepherd P.: Evernden M.C., Metcalfe D., *Optimizing the architectural layouts and technical specifications of curtain walls to minimize use of aluminium*, Structures, 13 (2018), pp. 8-25, https://doi.org/10.1016/j.istruc.2017.10.004.
[33] Bedon C., Zhang X., Santos F., Honfi D., Lange D.: *Performance of structural glass facades under extreme loads – design methods, existing research, current issues and trends*, Constr. Build. Mater., 163(28), (2018), pp. 921-937, https://doi.org/10.1016/j.conbuildmat.2017.12.153.
[34] Ghosh A., Neogi S.: *Effect of fenestration geometrical factors on building energy consumption and performance evaluation of a new external solar shading device in warm and humid climatic condition*, Sol. Energy, 169(15), (2018), pp. 94-104, https://doi.org/10.1016/j.solener.2018.04.025.
[35] Lai K., Wang W., Giles H.: *Solar shading performance of window with constant and dynamic shading function in different climate zones*, Sol. Energy, 147(1), (2017), pp. 113-125, https://doi.org/10.1016/j.solener.2016.10.015.
[36] Silva T., Vicente R., Amaral C., Figueiredo A.: *Thermal performance of a window shutter containing PCM: numerical validation and experimental analysis*, Appl. Energy, 179(1), (2016), pp. 64-84, https://doi.org/10.1016/j.apenergy.2016.06.126.
[37] Naylor D., Lai B.Y.: *Experimental study of natural convection in a window with a between-panes Venetian blind,* Experimental Heat Transfer, 20 (2007), pp. 1-17, https://doi.org/10.1080/08916150600977358.
[38] Dalal R., Naylor D., Roeleveld D.: *A CFD study of convection in a double glazed window with an enclosed pleated blind,* Energy Build, 41 (2009), pp. 1256-1262, https://doi.org/10.1016/j.enbuild.2009.07.024.
[39] Collins M., Tasnim S., Wright J.: *Numerical analysis of convective heat transfer in fenestration with between-the-glass louvered shades,* Build Environ, 44 (2009), pp. 2185-2192, https://doi.org/10.1016/j.buildenv.2009.03.017.
[40] Granqvist C., Bayrak P.I., Niklasson G.A.: *Electrochromics on a roll: web-coating and lamination for smart windows,* Surf. Coat. Technol., 336 (2018), pp. 133-138, https://doi.org/10.1016/j.surfcoat.2017.08.006.
[41] Ji C., Wu Z., Wu X., Wang J., Jiang Y.: *Al-doped VO2 films as smart window coatings: reduced phase transition temperature and improved thermochromic performance*, Solar Energy Mater. Sol. Cells, 176 (2018), pp. 174-180, https://doi.org/10.1016/j.solmat.2017.11.026.
[42] Wu Y., Krishnan P., Zhang M.H., Yu L.E.: *Using photocatalytic coating to maintain solar reflectance and lower cooling energy consumption of buildings*, Energy Build., 164(1), (2018), pp. 176-186, https://doi.org/10.1016/j.enbuild.2018.01.011.
[43] Feist W., Schnieders J., Dorer V., Haas A.: *Re-inventing air heating: Convenient and comfortable within the frame of the Passive House concept,* Energy Build., 37 (2005), pp. 1186-1203, https://doi.org/10.1016/j.enbuild.2005.06.020.
[44] Danza L., Barozzi B., Belussi L., Meroni I., Salamone F.: *Assessment of the Performance of a Ventilated Window Coupled with a Heat Recovery Unit through the Co-Heating Test.* Buildings, 6 (2016), 3, https://doi.org/10.3390/buildings6010003.

[45] Zhang C., Wang J., Xu X., Zou F., Yu J.: *Modeling and thermal performance evaluation of a switchable triple glazing exhaust air window,* Applied Thermal Engineering, 92 (2016), pp. 8-17, https://doi.org/10.1016/j.applthermaleng.2015.09.080.
[46] Khalvati F., Omidvar A.: *Summer study on thermal performance of an exhausting airflow window in evaporatively-cooled buildings*, Appl. Therm. Eng., 153 (2019), pp. 147-158, https://doi.org/10.1016/j.applthermaleng.2019.02.135.
[47] Carlos J.S.: *Optimizing the ventilated double window for solar collection*, Solar Energy, 150 (2017), pp. 454-462, https://doi.org/10.1016/j.solener.2017.04.063.
[48] Bhamjee M., Nurick A., Madyira D.M.: *An experimentally validated mathematical and CFD model of a supply air window*: Forced and natural flow, Energy and Buildings, 57 (2013), pp. 289-301, https://doi.org/10.1016/j.enbuild.2012.10.043.
[49] Fallahi A., Haghighat F., Elsadi H.: *Energy performance assessment of double-skin façade with thermal mass,* Energy Build, 42 (2010), pp. 1499-1509, https://doi.org/10.1016/j.enbuild.2010.03.020.
[50] Ding C., Ngo T., Mendis P., Lumantarna R., Zobec M.: *Dynamic response of double skin façades under blast loads,* Engineering Structures, 123 (2016), pp. 155-165, https://doi.org/10.1016/j.engstruct.2016.05.051.
[51] Zanghirella F., Perino M., Serra V.: *A numerical model to evaluate the thermal behaviour of active transparent façades*. Energy Build, 43 (2011), pp. 1123-1138, https://doi.org/10.1016/j.enbuild.2010.08.031.
[52] Ghadamian H., Ghadimi M., Shakouri M., Moghadasi M.: *Analytical solution for energy modeling of double skin façades building*, Energy Build., 50 (2012), p. 50, 158-165, https://doi.org/10.1016/j.enbuild.2012.03.034.
[53] ISO 10292: Glass in building – Calculation of steady-state U values (thermal transmittance) of multiple glazing; 1994.
[54] ISO 15099: Thermal performance of windows, doors and shading devices – Detailed calculations; 2003.
[55] EN 673: Glass in building – Determination of thermal transmittance (U value) – Calculation method; 2011.
[56] Cengel Y.A.: *Heat Transfer*: A Practical Approach, 2nd ed., McGraw-Hill, 2003.
[57] Giorgi L., Bertola V., Cafaro E.: *Thermal convection in double glazed windows with structured gap,* Energy and Buildings, 43(8), (2011), pp. 2034-2038, https://doi.org/10.1016/j.enbuild.2011.03.043.
[58] Gosselin J.R., Chen Q.: *A computational method for calculating heat transfer and airflow through a dual-airflow window,* Energy Build, 40 (4), (2008), pp. 452-458, https://doi.org/10.1016/j.enbuild.2007.03.010.
[59] Najaf Khosravi S., Mahdavi A.: *A CFD-Based Parametric Thermal Performance Analysis of Supply Air Ventilated Windows*, Energies, 14 (2021), p. 2420, https://doi.org/10.3390/en14092420.
[60] Xamán J., Olazo-Gómez Y., Chávez Y., Hinojosa J.F., Hernández-Pérez I., Hernández-López I., Zavala-Guillén I.: *Computational fluid dynamics for thermal evaluation of a room with a double glazing window with a solar control film*, Renewable Energy, 94 (2016), pp. 237-250, https://doi.org/10.1016/j.renene.2016.03.055.
[61] Ganguli A.A., Pandit A.B., Joshi J.B.: *CFD simulation of heat transfer in a two-dimensional vertical enclosure,* Chem Eng Res Des, 87 (2009), pp. 711-727, https://doi.org/10.1016/j.cherd.2008.11.005.
[62] Ganguli A.A., Pandit A.B., Joshi J.B.: *Numerical predictions of flow patterns due to natural convection in a vertical slot*, Chem Eng Sci, 62 (2007), pp. 4479-4495, https://doi.org/10.1016/j.ces.2007.05.017.
[63] Basok B., Davydenko B., Isaev S.A., Goncharuk S.M., Kuzhel L.N.: *Numerical modeling of heat transfer through a triple-pane window*, Journal of Engineering Physics and Thermophysics, 89(5), (2016), pp. 1277-1283, https://doi.org/10.1007/s10891-016-1492-7.
[64] Manz H.: *Numerical simulation of heat transfer by natural convection in cavities of facade elements*, Energy and Buildings, 35 (2003), pp. 305-311, https://doi.org/10.1016/S0378-7788(02)00088-9.
[65] Xaman J., Alvarez G., Lira L., Estrada C.: *Numerical study of heat transfer by laminar and turbulent natural convection in tall cavities of façade elements*, Energy and Buildings, 37 (2005), pp. 787-794, https://doi.org/10.1016/j.enbuild.2004.11.001.
[66] Respondek Z.: *Heat Transfer Through Insulating Glass Units Subjected to Climatic Loads*, Materials, 13 (2020), 286. https://doi.org/10.3390/ma13020286.
[67] Banionis K., Kumžienė J., Burlingis A., Ramanauskas J., Paukštys V.: *The Changes in Thermal Transmittance of Window Insulating Glass Units Depending on Outdoor Temperatures in Cold Climate Countries,* Energies, 14 (2021), 1694, https://doi.org/10.3390/en14061694.
[68] Ismail K.A.R., Henríquez J.R.: *Two-dimensional model for the double glass naturally ventilated window*, International Journal of Heat and Mass Transfer, 48 (2005), pp. 461-475, https://doi.org/10.1016/j.ijheatmasstransfer.2004.09.022.
[69] Chow T., Li V., Lin Z.: *Innovative solar windows for cooling-demand climate,* Solar Energy Materials and Solar Cells, 94(2), (2010), pp. 212-220, https://doi.org/10.1016/j.solmat.2009.09.004.
[70] Rosenfeld J.L.J., Platzer W.J., van Dijk H., Maccari A.: *Modelling the optical and thermal properties of complex glazing: overview of recent developments*, Solar Energy, 69(6), (2001), pp. 1-13, https://doi.org/10.1016/S0038-092X(01)00028-7.

[71] Van Nijnatten P.A.: *A spectrophotometer accessory for directional reflectance and transmittance of coated glazing*, Solar Energy, 73 (2002), pp. 137-149, https://doi.org/10.1016/S0038-092X(02)00047-6.
[72] Chaiyapinunt S., Phueakphongsuriya B., Mongkornsaksit K., Khomporn N.: *Performance rating of glass windows and glass windows with films in aspect of thermal comfort and heat transmission*, Energy and Buildings, 37 (2005), pp. 725-738, https://doi.org/10.1016/j.enbuild.2004.10.008.
[73] Ismail K.A.R., Henríquez J.R.: *Thermally effective windows with moving phase change material curtains*, Applied Thermal Engineering, 21 (2001), pp. 1909-1923, https://doi.org/10.1016/S1359-4311(01)00058-8.
[74] Ismail K.A.R., Henríquez J.R.: *Modeling and simulation of a simple glass window*, Solar Energy Materials and Solar Cells, 80 (2003), pp. 355-374, https://doi.org/10.1016/j.solmat.2003.08.010.
[75] Ismail K.A.R., Henríquez J.R.: *Simplified model for a ventilated glass window under forced air flow conditions*, Applied Thermal Engineering, 26 (2006), pp. 295-302, https://doi.org/10.1016/j.applthermaleng.2005.04.023.
[76] Jaber S., Ajib S.: *Thermal and economic windows design for different climate zones*, Energy Build, 43 (2011), pp. 3208-3215, https://doi.org/10.1016/j.enbuild.2011.08.019.
[77] Alvarez G., Flores J.J., Aguilar J.O., Gomez-Daza O., Estrada C.A., Nair M.T.S., Nair P.K.: *Spectrally selective laminated glazing consisting of solar control and heat mirror coated glass: preparation, characterization and modeling of heat transfer*, Solar Energy, 78 (2005), pp. 113-124, https://doi.org/10.1016/j.solener.2004.06.021.
[78] Oliveti G., Arcuri N., Bruno R., De Simone M.: *An accurate calculation model of solar heat gain through glazed surfaces*, Energy and Buildings, 43 (2-3), 2011, pp. 269-274, https://doi.org/10.1016/j.enbuild.2010.11.009.
[79] Avedissian T., Naylor D.: *Free convective heat transfer in an enclosure with an internal louvered blind*, Int International Journal of Heat and Mass Transfer, 51(1-2), (2008), pp. 283-293, https://doi.org/10.1016/j.ijheatmasstransfer.2007.03.042.
[80] Sun Y., Wu Y., Wilson R., Sun S.: *Thermal evaluation of a double glazing façade system with integrated Parallel Slat Transparent Insulation Material (PS-TIM)*, Build Environ, 105 (2016), pp. 69-81, https://doi.org/10.1016/j.buildenv.2016.05.004.
[81] Wang T.P., Wang L., Li B.: *A model of the long-wave radiation heat transfer through a glazing*, Energy and Buildings, 59 (2013), pp. 50-61, https://doi.org/10.1016/j.enbuild.2012.12.027.
[82] Han J., Lu L., Yang H.: *Numerical evaluation of the mixed convective heat transfer in a double-pane window integrated with see-through a-Si PV cells with low-e coatings*, Applied Energy, 87(11), (2010), pp. 3431-3437, https://doi.org/10.1016/j.apenergy.2010.05.025.
[83] Romaní J., Ramos A., Salom J.: *Review of Transparent and Semi-Transparent Building-Integrated Photovoltaics for Fenestration Application Modeling in Building Simulations*, Energies, 15(9), (2022), 3286, https://doi.org/10.3390/en15093286.
[84] Infield D., Mei L., Eicker U.: *Thermal performance estimation for ventilated PV facades*, Solar Energy, 76 (2004), pp. 93-98, https://doi.org/10.1016/j.solener.2003.08.010.
[85] Misara S., Henze N., Sidelev A.: *Thermal Behaviours of BIPV-Modules (U-Value and g-Value)*, In Proceedings of the 26th European Photovoltaic Solar Energy Conference and Exhibition, 2011, pp. 4107-4115, https://doi.org/10.4229/26thEUPVSEC2011-5BV.1.17.
[86] Han J., Lu L., Peng J., Yang H.: *Performance of ventilated double-sided PV façade compared with conventional clear glass façade*, Energy Build, 56 (2013), pp. 204-209, https://doi.org/10.1016/j.enbuild.2012.08.017.
[87] Chow T.T., Fong K.F., He W., Lin Z., Chan A.L.S.: *Performance evaluation of a PV ventilated window applying to office building of Hong Kong*, Energy Build, 39 (2007), pp. 643-650, https://doi.org/10.1016/j.enbuild.2006.09.014
[88] Han J., Lu L., Yang H.: *Thermal behavior of a novel type see-through glazing system with integrated PV cells*, Build. Env, 44 (2009), pp. 2129-2136, https://doi.org/10.1016/j.buildenv.2009.03.003.
[89] Kapsis K., Athienitis A.K.: *A study of the potential benefits of semi-transparent photovoltaics in commercial buildings*, Sol. Energy, 115 (2015), pp. 120-132, https://doi.org/10.1016/j.solener.2015.02.016.
[90] Ng P.K., Mithraratne N., Kua H.W.: *Energy analysis of semi-transparent BIPV in Singapore buildings*, Energy Build, 66 (2013), pp. 274-281, https://doi.org/10.1016/j.enbuild.2013.07.029.
[91] Gevers R.H., Pretorius J.H.C., van Rhyn P.: *Novel approach for concentrating and harvesting solar radiation in hybrid transparent photovoltaic façade's in Southern Africa*, Renew. Energy Power Qual. Journal, 1 (2015), pp. 245-250, https://doi.org/10.24084/repqj13.295.
[92] Nourozi B., Ploskić A., Chen Y., Ning-Wei Chiu J., Wang Q.: *Heat transfer model for energy-active windows – An evaluation of efficient reuse of waste heat in buildings*, Renew. Energy, 162 (2020), pp. 2318-2329, https://doi.org/10.1016/j.renene.2020.10.043.
[93] Churchill S.W., Chu H.H.S.: *Correlating equations for laminar and turbulent free convection from a vertical plate*, International Journal of Heat and Mass Transfer, 18(11), (1975), pp. 1323-1329, https://doi.org/10.1016/0017-9310(75)90243-4.

[94] Jelle B.P., Kalnæs S.E., Gao T.: *Low-emissivity materials for building applications: A state-of-the-art review and future research perspectives*, Energy and Buildings, 96 (2015), pp. 329-356, https://doi.org/10.1016/j.enbuild.2015.03.024.

[95] Brzezicki M.: *A Systematic Review of the Most Recent Concepts in Smart Windows Technologies with a Focus on Electrochromics*, Sustainability, 13 (2021), 9604, https://doi.org/10.3390/su13179604.

[96] Aburas M., Soebarto V., Williamson T., Liang R., Ebendorff-Heidepriem H., Wu Y.: *Thermochromic smart window technologies for building application: A review*, Applied Energy, 255 (2019), 113522, https://doi.org/10.1016/j.apenergy.2019.113522.

[97] Sun Y., Liu X., Ming Y., Liu X., Mahon D., Wilson R., Liu H., Eames P., Wu Y.: *Energy and daylight performance of a smart window: Window integrated with thermotropic parallel slat-transparent insulation material,* Applied Energy, 293 (2021), p. 116826, https://doi.org/10.1016/j.apenergy.2021.116826.

[98] Heidari M.N., Eydgahi A., Matin P.: *The Effect of Smart Colored Windows on Visual Performance of Buildings*, Buildings, 12 (2022), 861, https://doi.org/10.3390/buildings12060861.

[99] Feng W., Zou L., Gao G., Wu G., Shen J., Li W.: *Gasochromic smart window: optical and thermal properties, energy simulation and feasibility analysis*, Solar Energy Materials and Solar Cells, 144 (2016), pp. 316-323, https://doi.org/10.1016/j.solmat.2015.09.029.

[100] Zhou Y., Fan F., Liu Y., Zhao S., Xu Q., Wang S., Luo D., Long Y.: *Unconventional smart windows: Materials, structures and designs*, Nano Energy, 90 (2021), 106613, https://doi.org/10.1016/j.nanoen.2021.106613.

[101] Heiz B.P.V., Pan Z., Su L., Le S.T., Wondraczek L.: *A large-area smart window with tunable shading and solar-thermal harvesting ability based on remote switching of a magneto-active liquid*, Adv. Sustain. Syst., 2 (2018), 1870001, https://doi.org/10.1002/adsu.201700140.

Ewa Zender-Świercz, Michał Polański
Structure and Environment 2022, vol. 14, (4), pp. 142-152, Article number: el 016
https://doi.org/10.30540/sae-2022-016

Structure and Environment
ISSN 2081-1500
e-ISSN 2657-6902
https://content.sciendo.com/sae
https://sae.tu.kielce.pl

sciendo

Kielce University of Technology

DOI: 10.30540/sae-2022-016

INFLUENCE OF ROAD TRAFFIC ON INDOOR AIR QUALITY

WPŁYW RUCHU DROGOWEGO NA JAKOŚĆ POWIETRZA WEWNĘTRZNEGO

Ewa Zender-Świercz*, Michał Polański
Kielce University of Technology, Poland

Abstract

The quality of air that people breathe has become a very important parameter of quality of life. Pollution contributes to numerous diseases, problems with the absorption of knowledge, and also reduces work efficiency. The article attempts to find the relationship between road traffic and indoor air quality. The parameter used to assess air pollution was particulate matter (smog). The research was carried out in three localisations with different traffic volumes, in three places for each localisation, in the summer, autumn, and winter periods. It was found that in areas with heavy road traffic, this traffic causes an inflow of pollutants into the rooms. In low – traffic localisations, sources other than road traffic have a greater impact on the indoor air quality, especially in the cool periods (autumn, and winter).

Keywords: particulate matter PM2.5, PM10; Indoor Air Quality; road traffic

Streszczenie

Jakość powietrza, jakim oddycha człowiek, stała się bardzo istotnym parametrem jakości życia. Zanieczyszczenia przyczyniają się do licznych zachorowań, problemów z przyswajaniem wiedzy, a także obniżają wydajność pracy. W artykule podjęto próbę odnalezienia zależności pomiędzy natężeniem ruchu drogowego i jakością powietrza wewnętrznego. Parametrem, który wykorzystano do oceny zanieczyszczenia powietrza, był pył zawieszony (smog). Badania przeprowadzono w trzech lokalizacjach o różnym natężeniu ruchu, w trzech miejscach dla każdej lokalizacji, w okresach lato, jesień i zima. Stwierdzono, że w lokalizacji o dużym natężeniu ruchu pojazdów ruch ten powoduje napływ zanieczyszczeń do pomieszczeń. W lokalizacjach o małym natężeniu ruchu większy wpływ na jakość powietrza wewnętrznego mają inne niż ruch drogowy źródła, szczególnie w okresach chłodnych (jesień, zima).

Słowa kluczowe: pyły zawieszone PM2.5, PM10; jakość powietrza wewnętrznego; ruch drogowy

1. INTRODUCTION

The quality of the air that people breathe, especially in the centre of crowded cities, has become an extremely important parameter of the quality of human life [1]. Air pollution is a major contributor to noncommunicable diseases around the world [2]. Evidence collected by scientists shows the damaging effects of pollutants on the respiratory and cardiovascular systems [3], and epidemiological and toxicological studies also indicate negative effects on the central nervous system [4-11]. In particular, traffic-related pollutants, including carbon monoxide,

*Kielce University of Technology, Poland, e-mail: ezender@tu.kielce.pl

nitric oxide, and particulate matter less than 2.5 μm in diameter, have been associated with a number of adverse neurodevelopmental effects in children (eg. autism spectrum disorders) and neurodegenerative disorders in adults (eg. Alzheimers disease) [12-14].

Breathing polluted air is associated with more frequent hospitalizations [15], and exhaust gases, semi-volatile, and gaseous pollutants containing organic compounds present in the air are mutagenic and cause genetic damage [16]. In addition, air pollutants can cross the placental barrier and directly affect the embryo and the foetus [17, 18]. Several studies have shown that city dwellers spend almost 90% of their time indoors [19]. If the air we breathe for such a long period of time is of poor quality, it has a significant impact on our health and well-being. It should be noted that due to the lack of immediate health effects, the problem of indoor air pollution is underestimated. This is an extremely dangerous activity. We live in a time when, in the name of modernity, huge amounts of harmful substances are released into the atmosphere. Hardly anyone is aware of the scale of this problem. The industries, transportation, and electricity production sectors emit millions of tons of pollutants. The effects of these emissions often spread over time. There is a widespread belief in society that closed windows or doors effectively isolate us from air pollutants outside. However, it should be remembered that they are never perfectly tight and that the contaminants that enter can even be 10 μm or less. Furthermore, it has been shown that the level of indoor pollution can be up to 10 times higher than the level of outdoor pollution [20]. These indoor pollutants that can contribute to the so-called sick building syndrome, SBS, cause several respiratory and cardiovascular diseases, and reduce work efficiency. US data estimate that SBS-related health problems generate $ 57 billion in losses annually [21]. The WHO (World Health Organization) [22] also reports that 3.8 million deaths worldwide in 2016 were caused by air pollution. In contrast, particulate matters PM2.5 is responsible for approximately 4.5 million of these deaths [23]. In the UK alone, around 40.000 premature deaths are caused by air pollution each year, about half of which are related to pollution from transport [24]. In Poland, PM 2.5 particulate matter is also responsible for 82% of the burden of diseases resulting from exposure to indoor air pollution [25].

The WHO regularly publishes guidelines to improve them as much as possible, and government institutions are taking steps in the right direction, trying to reduce the amount of harmful substances emitted into the atmosphere. Despite this, millions of people around the world are chronically exposed to air pollutants in concentrations well above legal safety standards [26]. The concentrations of particulate matter currently recommended by the WHO are 5 μg/m^3 for PM2.5 and 15 μg/m^3 for PM10 per year, 15 μg/m^3 for PM2.5 and 45 μg/m^3 for PM10 per day.

Indoor air pollution most often comes from the external environment. They penetrate the inside through leaks in window openings, doors, and through ventilation [27]. Particularly important from the point of view of the amount of incoming pollutants is the type of ventilation system. Mechanical air exchange systems are equipped with filters that are not present in natural ventilation. In the case of natural ventilation, only systems that inform about the need to close windows [28] due to the high pollution of the outdoor air can help reduce the flow of pollutants into the rooms. The main ones are carbon oxides (CO, CO_2), nitrogen oxides (NO_x), polycyclic aromatic hydrocarbons (PAHs), ozone (O_3), and PM (particulate matter). The dominant component of air pollution in cities and suburban areas is dust pollution, among which we distinguish particulate matter with an aerodynamic diameter: 2.5 to 10 μm (PM 10), fine particles below 2.5 μm (PM 2.5) and ultrafine particles less than 0.1 μm [29]. Furthermore, it is important that dust (especially PM 2.5) can stay in the air for a long time, can be transported over hundreds of kilometres, and can penetrate inside buildings [30].

The source of particulate matter is mainly industry [31], but, as Merzkisz [32] reports, particulate matter also arises in transport as a result of wear of the vehicle's consumables, such as the braking system, and tires, and are products of incomplete combustion of fuels, in the combustion chamber. In addition, the research by Xiong et al. [33] proved the impact of vehicle traffic on the increase in PM 2.5 concentration in the air. They observed a reduction in pollution during mobility limitation during the SARS Cov2 pandemic. Particulate matter emitted during the combustion process increases in mass as the temperature of the exhaust gas decreases. The main reason for this phenomenon is the fact that soot, which is the main component of exhaust gas solids, has strong absorption properties. Models describing the process of soot formation in the cylinders of internal combustion engines describe the dehydrogenation of hydrocarbons followed by their decomposition into ethyne. Subsequent processes include polymerization, cyclization, and coagulation of polymers, which consequently lead to the formation of a porous carbon black structure. The course of PM formation is shown in Figure 1. The harmfulness of these particles is mainly related to the heavy organic substances and heavy metals absorbed in the soot particles. It is worth remembering that the smaller the molecule, the more dangerous it is to human health. The smallest ones can penetrate deep into the human blood system and its internal organs.

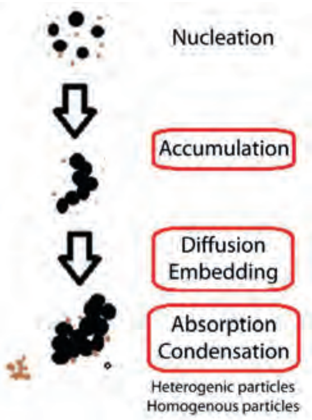

Fig. 1. Formation of particulate matter in vehicle exhaust gas

The correct assessment of indoor air quality should begin with recognition and characterization of the source of pollutant emission [34]. This research work attempts to check whether indoor air quality is related to road traffic volume in the area and which place in the apartment is most exposed to possible pollution. Air quality was assessed on the basis of the amount of particulate matter in the air. The study was carried out at three localisations that differ in terms of road traffic intensity in their vicinity.

2. MATERIALS AND METHODS

In order for the study to show differences in air quality depending on the volume of vehicle traffic, the localisations of the research were selected in such a way that the differences in traffic intensity were obvious and noticeable. For this purpose, 3 sites were selected in Kielce, Poland (Table 1).

The concentration of particulate matter was measured with meters (Table 2), located outside the building (P I), in a room facing the road – 10 m from the road (P II) and in the room located on the other side of the building – 100 m from the road (P III). The concentration of PM1, PM2.5, PM10 particulate matter, the temperature of the air, and the relative humidity of the air were measured. The measurement was carried out around the clock with a time step of 15 minutes.

The buildings analysed are single-family houses equipped with natural ventilation. The building in the L1 location was equipped with a district heating system, the buildings in the L2 and L3 locations were equipped with wood-fired fireplaces with a closed combustion chamber. The users of all facilities opened their windows in the summer, whereas in autumn and winter they opened them for several minutes in the morning and evening to ventilate the rooms. In L1, users stayed mainly in the morning and afternoon hours; in L2 and L3, they stayed constantly. The dust was not removed during the tests.

The content of particulate matter was measured on the basis of laser light scattering technology, air temperature with a silicon bandgap sensor, and relative air humidity with a capacitive sensor. Research was carried out in three series of measurements in three different seasons of the year: summer, autumn, and winter.

Table 1. Localisation of research objects

Localisation	Geographical coordinates	Road traffic	Building
L 1	50°52'2.38"N, 20°39'38.141"E	heavy	low, compact, urban
L 2	50°51'45.305"N, 20°39'37.204"E	moderate	low, compact, outskirts of the city
L 3	50°51'55.8"N, 20°49'25.907"E	low	low, low density, countryside

Table 2. Characteristics of the particulate matter concentration meters

Parameter	Measurement range	Accuracy	Resolution of Indications
Concentration of particulate matter	0 – 500 mg/m^3	± 10 mg/m^3 for 0 – 99 mg/m^3 ± 10% for 100 – 500 mg/m^3	1 mg/m^3
Temperature	-40 – 100°C	± 0.5°C for -20 – 80°C	0.01°C
Relative humidity	0 – 100%	± 3% for -20 – 80%	1%

3. RESULTS AND DISCUSSION

3.1. Experimental Studies

The data obtained allowed the development of diagrams showing the course of changes in dust concentration over time, depending on the localisation and for different localisations of the meters within the analysed building. In Figures 2-10 the measurement accuracy (10 $\mu g \cdot m^{-3}$) is marked. The concentrations of particulate matter recorded during the tests often reached values below the accuracy of the measurement.

L 1 (Fig. 2) is a building on the road with the highest traffic. It is an exit road from Kielce to Lublin, characterized by particularly increased traffic at night until 9:00 and in the afternoon. The course of changes in the concentration of particulate matter in the outside air is significantly higher at night and in the afternoon. The concentration of particulate matter in the room near the road is higher than the concentration of particulate matter in the room located away from the road. This clearly shows the impact of road traffic on the condition of the internal air.

L 2 (Fig. 3) is characterized by moderate traffic intensity with visible intensity in the morning (6:30-9:00) and afternoon (14:30-18:00) hours. This is reflected in the concentration of particulate matter in those hours. At ‘P I’ there is a clear increase in the concentration of particulate matter in the morning, evening, and night, and the lowest concentration is visible during the day. Greater concentrations can be seen inside the room facing the street than in the room located away from the road. This also means that the influx of pollutants from the road into the interior has a greater impact on indoor air quality.

In L 3 (Fig. 4), due to low road traffic, no effect of vehicle traffic on the concentration of particulate matter in the air during the summer was observed. There was no tendency to change the concentration

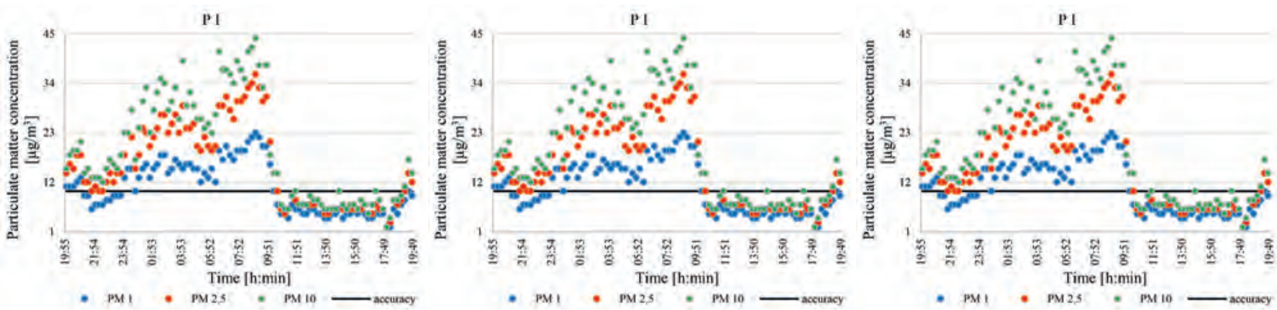

Fig. 2. Changes in particulate matter concentration for L 1. Season – summer

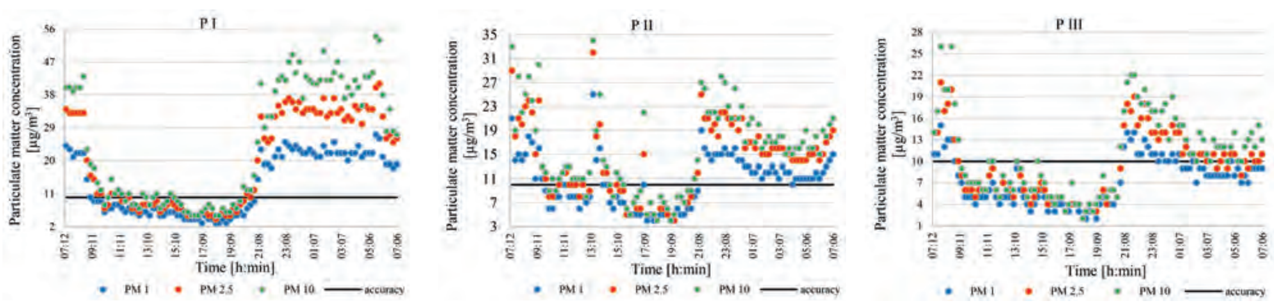

Fig. 3. Changes in particulate matter concentration for L 2. Season – summer

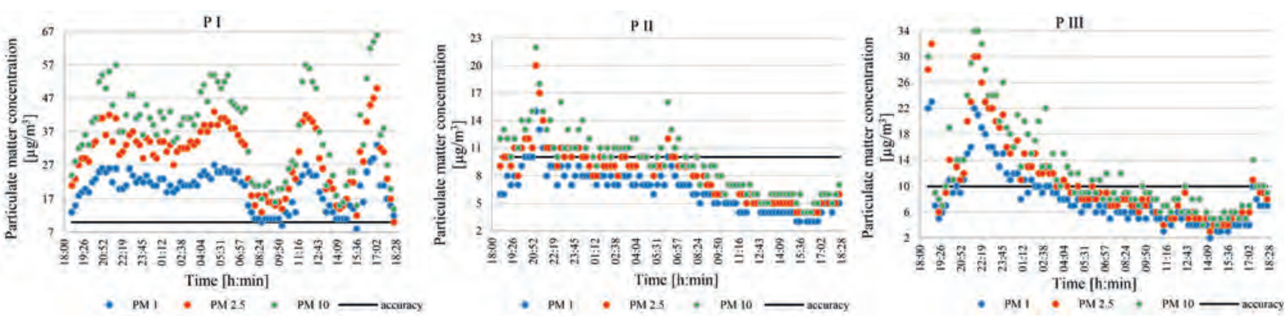

Fig. 4. Changes in particulate matter concentration for L 3. Season – summer

of particulate matter outside the building depending on the time of day. In the rooms within the building, increased concentrations were observed in the evening hours. This is related to the increase in heat production for the purpose of preparing domestic hot water for bathing. This is also evidenced by a higher concentration of particulate matter in ‘P III’ than in ‘P II’, i.e. in a room located away from the road and close to other residential buildings. During the night and during the day, the concentration was lower. At the same time, the highest concentration of particulate matter was found outside the building, which means that the main source of pollution is the surroundings of the building.

In the autumn period, at L 1 (Fig. 5), the concentrations of particulate matter outside the building were the highest, and, similarly to the summer period, in the room located away from the road, they were the lowest.

In the autumn period, for L 2 (Fig. 6) outside, the daily differences in the concentrations of particulate matter are smaller than in summer. The beginning of the heating season is of significant importance for the equalization of the concentration of particulate matter throughout the day. It means a significant influence of the particulate matter from the furnaces. In this case, the concentration of particulate matter in the room located away from the road was also the lowest.

In autumn, at L 3 (Fig. 7), the highest concentrations of particulate matter were observed outside the building, and, similarly to summer, the concentration of particulate matter increased in the afternoon and evening hours. Particulate matter concentrations in the indoor air reached higher values in a room located away from the road, confirming the low impact of road traffic in a low-traffic localisation.

In winter, at L 1 (Fig. 8), the highest concentrations of particulate matter were recorded outside in the

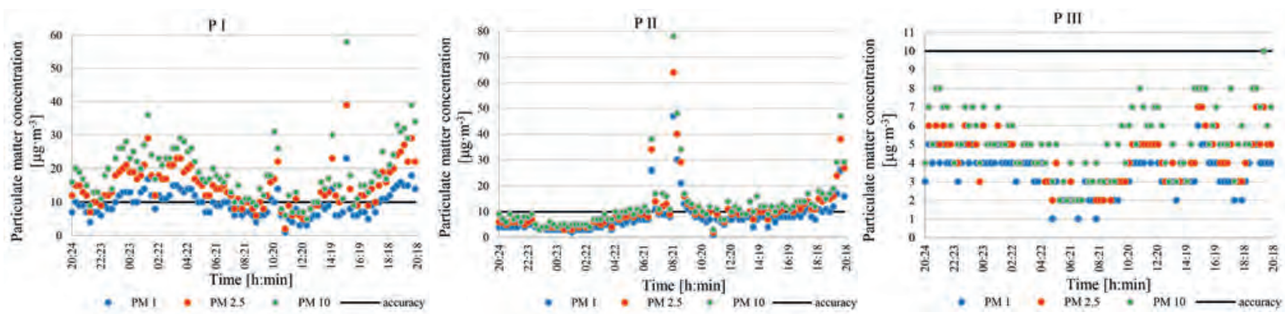

Fig. 5. Changes in particulate matter concentration for L 1. Season – autumn

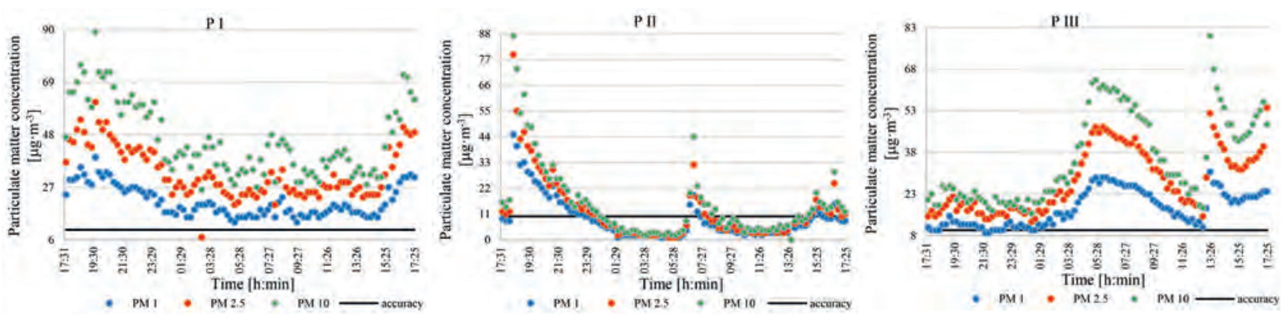

Fig. 6. Changes in particulate matter concentration for L 2. Season – autumn

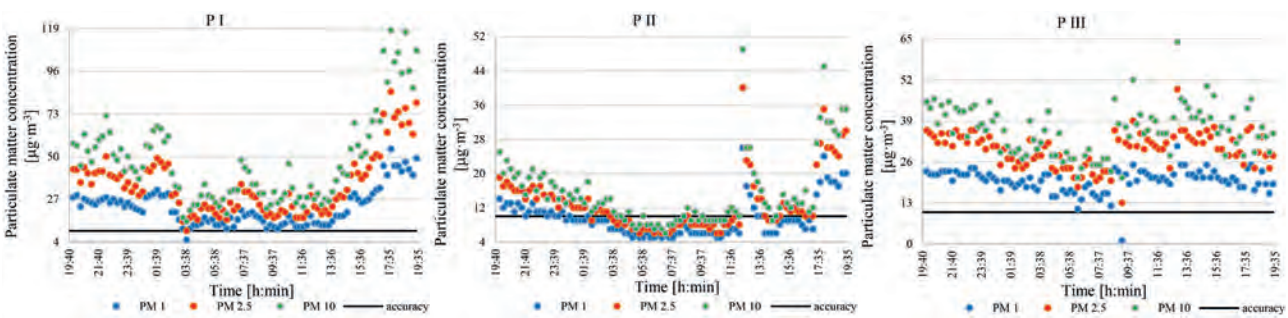

Fig. 7. Changes in particulate matter concentration for L 3. Season – autumn

evening and night hours. In the room located away from the road, the concentrations of particulate matter in the indoor air were higher than in the room near the road, which means that the particulate matter coming from outside also has a source other than transport. Taking into account the ongoing heating period, this was particulate matter from the furnaces. This room also does not exhibit diurnal variability similar to the outdoor concentration of particulate matter. In turn, the course of changes in the concentration of particulate matter in the room near the road is similar to the variability in the outside air.

In the winter period, at L 2 (Fig. 9), the highest outdoor concentrations of particulate matter were recorded with a visible difference in concentrations for night and day hours. As in the autumn period, the difference in the concentration of particulate matter at different times of the day is smaller than in summer. The diurnal differences are more pronounced in the room facing the road (P II). The lowest concentrations occurred in the room on the other side of the building (P III).

In winter, at L 3 (Fig. 10), the daily difference in the concentrations of particulate matter is visible. Lower concentration values appear during daylight hours. In this case, the highest concentration of particulate matter values were also found outside the building (P I) and the lowest in the room on the other side of the building (P III). The diurnal variability is also visible at P III, where higher concentrations of particulate matter occur between 10 pm and 6 am.

3.2. Statistical Analysis

Figures 11 to 13 present the box plots, which show the distribution of *the concentration of particulate matter (pm 2.5 and PM 10)* characteristic in groups

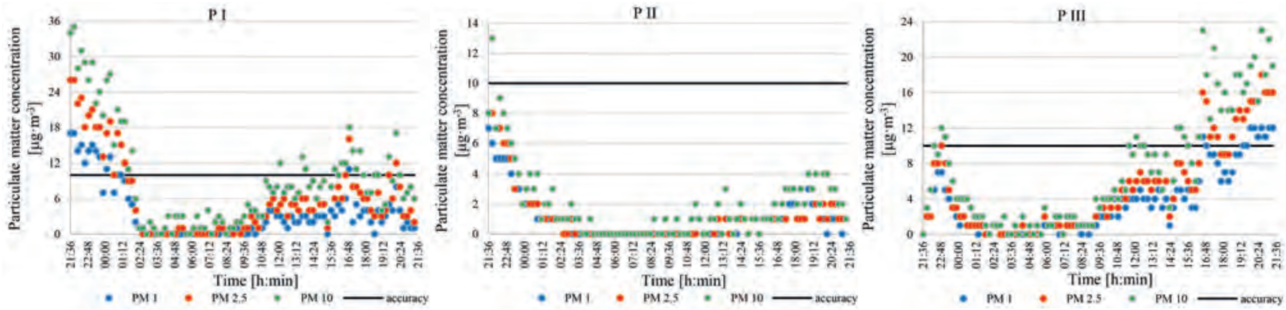

Fig. 8. Changes in particulate matter concentration for L 1. Season – winter

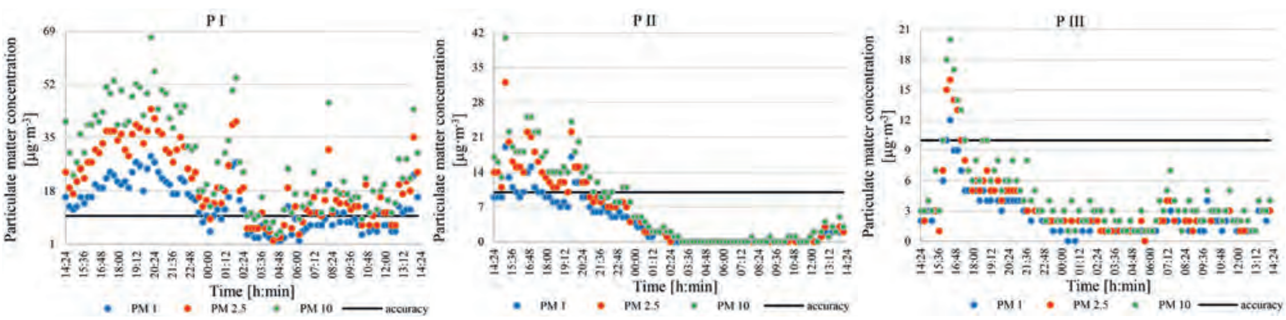

Fig. 9. Changes in particulate matter concentration for L 2. Season – winter

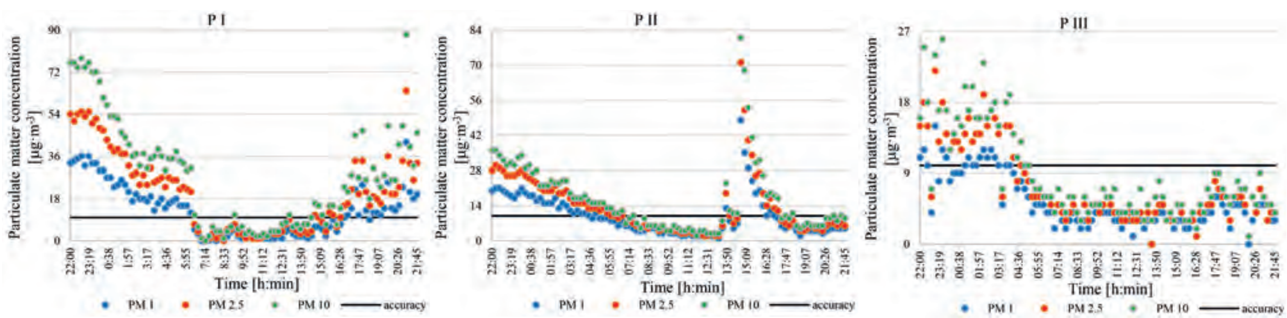

Fig. 10. Changes in particulate matter concentration for L 3. Season – winter

determined by *localisation* characteristic. The single box plot presents: the smallest value, the lower quartile, the median, the upper quartile, and the largest value of the examined characteristic, as well as the mean value using the marker. The difference between the upper and the lower quartiles, called the interquartile range, indicates how long the range covering half the centrally located values of the examined characteristic is.

Figure 11 shows that the lowest average value of the concentration of PM 2.5 particulate matter outside the building can be expected in summer, autumn, and winter for L 1. Furthermore, in the cooler period (autumn and winter), the average values of the PM 2.5 particulate matter concentration are similar. This means that fuel combustion is more important than road traffic for air quality.

In the case of the concentration of PM 10 particulate matter, as for the concentration of PM 2.5 particulate matter, the lowest average value outside the building in summer, autumn, and winter can be expected for L 1. Furthermore, in the cooler period (autumn and winter), the average values of the PM 10 particulate matter concentrations are similar to each other. This means that fuel combustion is more important than road traffic for air quality.

According to Figure 13, in the localisation with the highest road traffic, the concentration of PM 2.5 particulate matter is the lowest at all three measurement points, which confirms that the amount of PM 2.5 particulate matter in the air is mostly affected by fuel combustion, and not by road traffic itself. At the same time, in localisations where fuels are not burned and traffic is heavy, the presence of

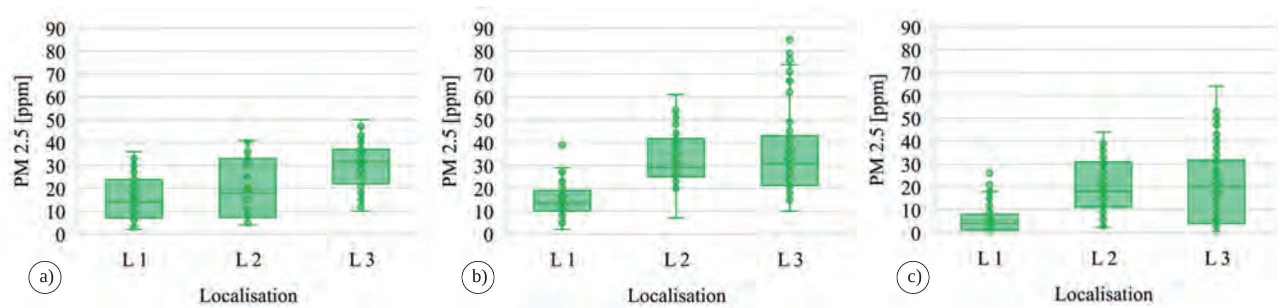

Fig. 11. Box plots of the concentration of PM 2.5 particulate matter outside the building: (a) Summer, (b) Autumn, and (c) Winter

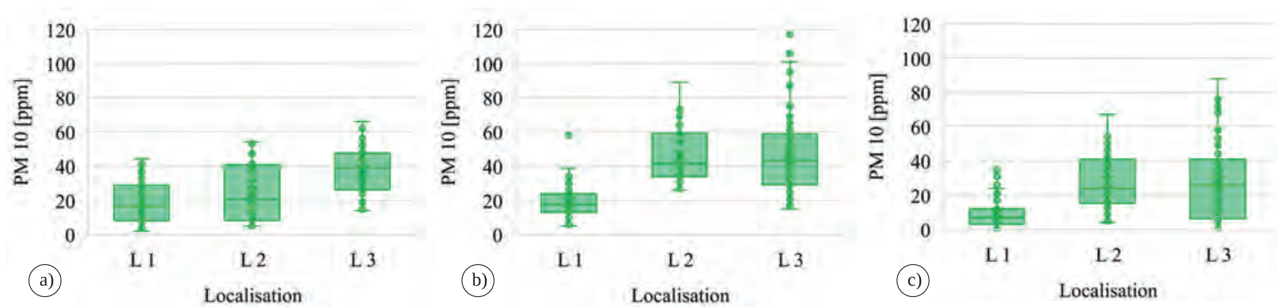

Fig. 12. Box plots of the concentration of PM 10 particulate matter outside the building: (a) Summer, (b) Autumn, and (c) Winter

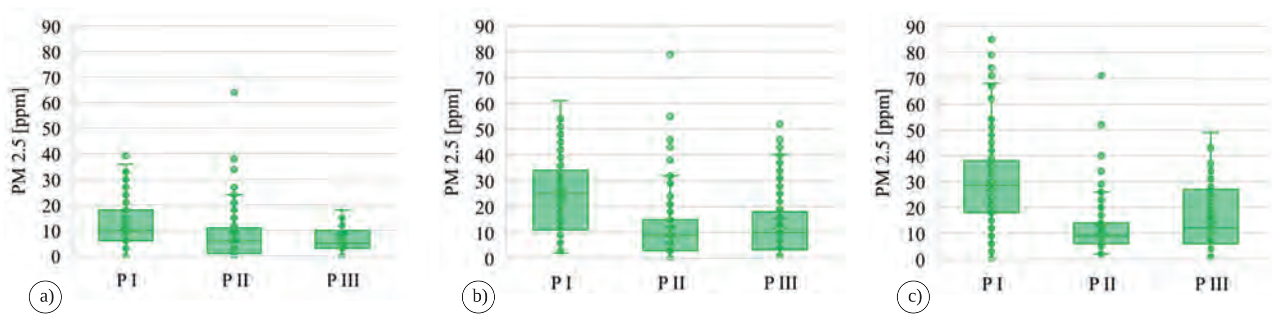

Fig. 13. Box plots of the concentration of PM 2.5 particulate matter outside the building: (a) L 1, (b) L 2, and (c) L 3

environment

indoor particulate matter was recorded, and therefore road traffic is a source of indoor air particulate matter in areas with heavy traffic. L 2 and L 3 show higher concentrations of particulate matter in indoor air. At L 3, the concentration of particulate matter in the room located away from the road is highest, which means that the road with the lowest traffic has little effect on indoor air quality.

3.3. Discussion

The results of the conducted tests do not indicate a clear increase in the concentration of particulate matter in the morning and afternoon hours, i.e. those with increased road traffic. There is a tendency to increase concentrations of particulate matter in the afternoon and night and a relatively stable level during the day. An important factor here is movement, which during the hours of our activity causes, e.g. a more frequent exchange of air in the rooms. Also, especially in summer, open windows facilitate faster air exchange. This means that pollutants enter the room as quickly as they are removed from it, for example, due to the air flow caused by passing cars. In the afternoon and at night, when this movement is very limited, harmful substances stay in the air longer, maintaining this concentration for a relatively long time. The second factor is heating, where heat is produced by burning solid fuels, such as coal or wood, or liquid fuels, such as gas and fuel oil. Fuel combustion releases the products of incomplete combustion into the atmosphere, that is, solid particles that create smog. The figures show the dependence of the increase in particulate matter concentration in the afternoon and their maintenance at a high level for a longer period of time.

In the literature, you can find various research works on the subject of the dependence of air quality on the intensity of vehicle traffic in the environment. An example may be the article by Badyda, Majewski [35], who attempted to check the relationship between vehicle traffic and air pollution near traffic roads, taking into account weather conditions. Their 168-hour study showed a relationship between air quality and traffic in the area. For this purpose, they monitored the number of cars passing at different times of the day, broken down into passenger cars, trucks, and buses, measured the level of carbon monoxide, nitrogen oxides, benzene, ethylbenzene, toluene, xylene, sulphur dioxide, and PM10 particulate matter, and recorded the prevailing meteorological conditions such as air temperature and humidity. The results of their research are unequivocal. During the peak traffic period, along with the increase in traffic, the amount of pollutants in the air increases. This is especially visible between 8:00 am and 9:00 am and 4:00 pm and 6:00 pm on working days. However, it should be mentioned that the intensity of traffic in the afternoon does not usually coincide with the increase in pollution. This intensification occurs about 5 hours later. This is precisely related to the meteorological conditions at the measurement site. The authors indicate that in addition to the intensity of traffic itself, the measurement results are significantly influenced by variables such as wind speed, air temperature, solar radiation intensity, precipitation height, and relative humidity of the air. Depending on the season, the above – mentioned variables affect air quality to a different extent.

Another example in the literature dealing with the same topic is the article by Gliniak et al. [36], in which the authors attempted to investigate the relationship between vehicle traffic and air pollution in the form of PM 10 and PM 2.5 particulate matter. The study was carried out from March to July 2013 on different days of the week, from 12:00 p.m. to 3:00 p.m. and from 10:00 p.m. to 1:00 p.m. The results of their tests do not show any relationship between the intensity of road traffic and the amount of particulate matter in the air. The increase in the number of vehicles passing near the measurement point did not increase the concentration of particulate matter. Such results indicate that in Krakow, the share of road traffic in the emission of air particulate matter pollutants is negligible and comes from completely different sources.

The Pearson correlation analysis conducted for the concentration of outdoor particulate matter (Table 3) showed that in the summer the correlations of the L 1 and L 2 localisations are stronger than the correlations of the L 1 and L 3 localisations, in the autumn the correlations for both variants of localisations are moderate, and for the winter period, there is a stronger correlation between the L 1 and L 3 localisations than between L 1 and L 2. In summer, the only source of particulate matter outdoors is vehicle traffic; hence, the weaker correlation between the localisation with the smallest and largest vehicle traffic. The correlation analysis also confirms the large impact of fuel combustion on the concentration of particulate matter in the outdoor air in places with little traffic and solid fuel heat sources.

environment

Table 3. Pearson's correlation between localisations for each period

Summer	L 1 / L 2	L 1 / L 3
	0.7	0.2
Autumn	L 1 / L 2	L 1 / L 3
	0.5	0.5
Winter	L 1 / L 2	L 1 / L 3
	0.4	0.6

To clearly determine the impact of vehicle traffic on indoor air quality, a Pearson's correlation analysis was performed between the measurement points for each localisation (Table 4). The winter period was selected as the most authoritative period, as the windows in each of the buildings were closed most of the time. There is a stronger correlation between P I/P II in localisations with more traffic. In L 3, a stronger correlation occurred for P I/P III, confirming the greater influence of fuel combustion on the concentration of particulate matter.

Table 4. Pearson's correlation between measurement points for each localisations

	Winter	
	P I/P II	P I/P III
L 1	0.8	0.3
L 2	0.7	0.6
L 3	0.4	0.7

Taking into account the current WHO recommendations for the concentration of suspended particulate matter during the day, it is worth noting that in all localisations the concentration of PM 2.5 particulate matter exceeded the recommended value. In L 1, in winter, the concentrations of PM 2.5 were exceeded at night, i.e. during the period of increased vehicle traffic. In L 2 and L 3, temporary exceedances of PM 10 concentrations were also observed.

The research carried out for the purposes of the article and the analysis of the literature show that it is necessary to conduct further research, extended to the monitoring of a larger number of parameters, in order to unequivocally determine the impact of road traffic on air quality. In this case, it would be important to take into account the type of engine in the vehicles to determine whether the fuel combustion of the engines or the wear of roads and tires has a significant impact.

3.4. Limitations of the study

The findings of this study must be seen in light of some limitations. Meters detect the presence of particulate matter in the air, but do not allow us to determine the source of air pollution, which may be vehicle traffic, fuel combustion, and other activities in households. To overcome this limitation, more research is needed with a greater variety of building localisations, and this study is a good introduction for further analyses.

4. CONCLUSIONS

The conducted analysis showed that:

1. In localisations with heavy vehicle traffic, the concentration of particulate matter in the air is lower in rooms located away from the road, regardless of the season. For the period of autumn and winter there is a percentage difference of 53-84% in the summer period 2%.
2. Indoor air quality depends on the intensity of road traffic.
3. In a localisation with low traffic, fuel combustion for heat production has a greater impact on the concentration of particulate matter, than road traffic.
4. Further analysis is necessary to assess the significance of the share of road traffic as a source of particle matter pollution, taking into account other sources (mainly fuel combustion) and the parameters of the outside air and the floor of the building. It is also important to take into account the direction of the wind, which can cause differences in the inflow of pollutants into the interior from different sides of the building.

REFERENCES

[1] Kleeberger S.R.: *Genetic aspects of suscepti-bility to air pollution,* Eur. Respirat. J. 2003, Volume 21, pp. 52-56, https://doi.org/10.1183/09031936.03.00403003.

[2] Cohen A.J., Brauer M., Burnett R., Anderson H.R., Frostad J., Estep K., Balakrishnan K., Brunekreef B., Dandona L., Dandona R., Feigin V., Freedman G., Hubbell B., Jobling A., Kan H., Knibbs L., Liu Y., Martin R., Morawska L., Pope C.A., Shin H., Straif K., Shaddick G., Thomas M., van Dingenen R., van Donkelaar A., Vos T., Murray C.J.L., Forouzanfar M.H.: *Estimates and 25- year trends of the global burden of disease attributable to ambient air pollution: an analysis of data from the Global Burden of Diseases Study 2015*, The Lancet, 2017, Volume 389, Issue 10082, pp. 1907-1918, https://doi.org/10.1016/S0140-6736(17)30505-6.

[3] Thurston G.D., Kipen H., Annesi-Maesano I., Balmes J., Brook R.D., Cromar K., De Matteis S., Forastiere F., Forsberg B., Frampton M.W., Grigg J., Heederik D., Kelly F.J., Kuenzli N., Laumbach R., Peters A., Rajagopalan S.T., Rich D., Ritz B., Samet J.M., Sandstrom T., Sigsgaard T., Sunyer J., Brunekreef B.: *A joint ERS/ATS policy statement: What constitutes an adverse health effect of air pollution? An analytical framework*, Eur. Respir. J., 2017, Volume 49, 1600419, https://doi.org/10.1183/13993003.00419-2016.

[4] Block M.L., Elder A., Auten R.L., Bilbo S.D., Chen H., Chen J.C., Cory-Slechta D.A., Costa D., Diaz-Sanchez D., Dorman D.C., Gold D.R., Gray K., Jeng H.A., Kaufman J.D., Kleinman M.T., Kirshner A., Lawler C., Miller D.S., Nadadur S.S., Ritz B., Semmens E.O., Tonelli L.H., Veronesi B., Wright R.O., Wright R.J.: *The outdoor air pollution and brain health workshop*, Neurotoxicology, 2012, Volume 33, pp. 972-984, https://doi.org/10.1016/j.neuro.2012.08.014.

[5] Grandjean P., Landrigan P.J.: *Neurobehavioural effects of developmental toxicity*, The Lancet Neurol., 2014, Volume 13, pp. 330-338, https://doi.org/10.1016/S1474-4422(13)70278-3.

[6] Guxens M., Sunyer J.: *A review of epidemiological studies on neuropsychological effects of air pollution*, Swiss Med. Wkly. 2012, 142, https://doi.org/10.4414/smw.2011.13322.

[7] Patten K.T., González E.A., Valenzuela A., Berg E., Wallis C., Garbow J.R., Silverman J.L., Bein K.J., Wexler A.S., Lein P.J.: *Effects of early life exposure to traffic-related air pollution on brain development in juvenile Sprague Dawley rats*, Transl. Psychiatry, 2020, 10, pp. 1-12, https://doi.org/10.1038/s41398-020-0845-3.

[8] Danzer S.C.: *Postnatal and adult neurogenesis in the development of human disease*, Neuroscientist, 2008, Volume 14, Issue 5, pp. 446-458, https://doi.org/10.1177/1073858408317008.

[9] Hwang L.: *Environmental stressors and violence: Lead and polychlorinated biphenyls*, Reviews on Environmental Health, 2007, Volume 22, pp. 313-328, https://doi.org/10.1515/REVEH.2007.22.4.313.

[10] Stein J., Schettler T., Wallinga D., Valenti M.: *In harm's way: Toxic threats to child development*, Journal of Developmental and Behavioral Pediatrics, 2002, Volume 23, pp. 13-22, https://doi.org/10.1097/00004703-200202001-00004.

[11] Wigle D.T., Arbuckle T.E., Walke R.M., Liu S., Krewski D.: *Environmental hazards: Evidence for effects on child health*, Journal of Toxicology and Environmental Health, Part B: Critical Reviews, 2007, Volume 10, Issue 1-2, pp. 3-39, https://doi.org/10.1080/10937400601034563.

[12] Power M.C., Adar S.D., Yanosky J.D., Weuve J.: *Exposure to air pollution as a potential contributor to cognitive function, cognitive decline, brain imaging, and dementia: A systematic review of epidemiologic research*, Neurotoxicology, 2016, Volume 56, pp. 235-253, https://doi.org/10.1016/j.neuro.2016.06.004.

[13] Suades-González E., Gascon M., Guxens M., Sunyer J.: *Air pollution and neuropsychological development: A review of the latest evidence*, Endocrinology, 2015, Volume 156, pp. 3473-3482, https://doi.org/10.1210/en.2015-1403.

[14] Cipriani G., Danti S., Carlesi C., Borin G.: *Danger in the Air: Air Pollution and Cognitive Dysfunction*, American Journal of Alzheimer's Disease & Other Dementias, Volume 33(6), pp. 333-341, https://doi.org/10.1177/1533317518777859.

[15] Brook R.D., Franklin B., Cascio W., et al.: *Air pollution and cardi ovascular disease: a statement for healthcare professionals from the Expert Panel on Population and Prevention Science of the American Heart Association*, Circulation, 2004, Volume 109, Issue 21, pp. 2655-2671, https://doi.org/10.1161/01.CIR.0000128587.30041.C8.

[16] Pope C.A. III, Burnett R.T., Thun M.J., et al.: *Lung cancer, cardio pulmonary mortality, and long-term exposure to fine particulate air pollution,* JAMA, 2002, Volume 287(9), pp. 1132-1141, https://doi.org/10.1001/jama.287.9.1132.

[17] Curtis D.J., Sood A., Phillips T.J., et al.: *Secretions from placenta, after hypoxia/ reoxygenation, can damage developing neurones of brain under experimental conditions*, Exp Neurol., 2014, Volume 261, pp. 386-395, https://doi.org/10.1016/j.expneurol.2014.05.003.

[18] Saunders N.R., Liddelow S.A., Dziegielewska K.M.: *Barrier mechanisms in the developing brain,* Front Pharmacol., 2012, Volume 3(46), https://doi.org/10.3389/fphar.2012.00046.

[19] Allen J.G., Macomber J.D.: *Healthy Buildings. How Indoor Spaces Drive Performance and Productivit,* Publisher: Hardvard University Press 2020.

[20] Wolverton B.C.: *How to grow fresh air: 50 Houseplants that purify your home or office,* Publisher: Penguin Books, 2020.

[21] Tuomainen M., Smolander J., Kurtnitski J., Palonen J., Seppanen O.: *Modelling the cost of effects of the indoor environment,* The 9th International Conference on Indoor Air Quality and Climate "Indoor Air 2002", June 30-July 5, 2002, Monterey, California. Vol 1, pp. 814-819.

[22] World Health Organization. World Health Statistics 2018 (WHO – WHS): Monitoring health for the SDGS.

[23] Turston G.D., Newman J.D.: *Walking to a pathway for cardiovascular efects of air pollution*, The Lancet, 2018, Volume 391(10118), pp. 291-292, https://doi.org/10.1016/s0140-6736(17)33078-7.

[24] Künzli N. et al.: *Public-health impact of outdoor and trafc-related air pollution: a European assessment,* The Lancet, 2000, Volume 356(9232), pp. 795-801, https://doi.org/10.1016/S0140-6736(00)02653-2.

[25] Sowa J.: *Hygienic basics of ventilation – the evolution of opinions in Poland*, Rynek Instalacyjny, 2022, 1-2, pp. 52-58.
[26] Block M.L., Calderòn-Garcidueñas L.: *Air pollution: mechanisms of neuroinflammation and CNS disease,* Trends Neurosci., 2009, Volume 32, Issue 9, pp. 506-516, https://doi.org/10.1016/j.tins.2009.05.009.
[27] Afshari A., Ekberg L.E., Matson U.: *Characterization of indoor sources of fine and ultrafine particles a study conducted in a full-scale chamber,* Indoor Air, 2005, Volume 15, Issue 2, pp. 141-150, https://doi.org/10.1111/j.1600-0668.2005.00332.x.
[28] Kulis C., Müller J.: *Indoor air quality improvement in natural ventilation using a fuzzy logic controller,* Technical transactions, 2020, No 2020/045, https://doi.org/10.37705/TechTrans/e2020045.
[29] Craig L., Brook J.R., Chiotti Q., et al.: *Air pollution and public health: a guidance document for risk managers,* J Toxicol Environ Health A., 2008, Volume 71, Issue 9-10, pp. 588-698, https://doi.org/10.1080/15287390801997732.
[30] Vette A.F., Rea A.W., Lawless P.A., et al.: *Characterization of indooroutdoor aerosol concertation relationship during the Fresno PM Exposure Studies*, Aerosol Sci Technol., 2001, Volume 34(1), pp. 118-126.
[31] https://powietrze.malopolska.pl/baza/wplyw-poszczegolnych-zrodel-na-jakoscpowietrza-w-polsce - Krajowy bilans emisji SO2, NOX, CO, NH3, NMLZO, pyłów metali ciężkich i TZO za lata 2013-2014 w układzie klasyfikacji SNAP i NFR, Raport podstawowy; Krajowy Ośrodek Bilansowania i Zarządzania Emisjami, Instytut Ochrony Środowiska – Państwowy Instytut Badawczy, Warszawa 2016.
[32] Merkisz J.: *Ekologiczne problemy silników spalinowych.* Wydawnictwo Politechniki Poznańskiej. *Tom I i II*. Poznań1999.
[33] Xiong C., Zhang Y., Yan J., Yang X., Wang Q., Tu R., He Y.: *Chemical composition characteristics nad source analysis of PM 2.5 in Jiaxing, China: Insights into the effect of COVID-19 outbreak,* Environmental Technology, 2021, https://doi.org/10.1080/09593330.2021.1979104.
[34] Zabiegała B.: *Związki organiczne, ich źródła emisji i wpływ na jakość powietrza wewnętrznego. Problemy jakości powietrza wewnętrznego w Polsce*, 2007, pp. 233-254.
[35] Badyda A., Majewski G.: *Analiza zmienności stężenia zanieczyszczeń komunikacyjnych w aglomeracji miejskiej na tle natężenia ruchu pojazdów i warunków meteorologicznych*, Przegląd Naukowy Inżynieria i Kształtowanie Środowiska, 2006, Volume 1, Issue 33, pp. 146-157.
[36] Gliniak M., Zuśka Z., Miczyński J.: *Ocena poziomu pyłowego zanieczyszczenia powietrza w aglomeracji krakowskiej na przykładzie al. A. Mickiewicza,* Logistyka, 2015, Volume 4(1), pp. 8876-8881.

Farhaj Hasan, Nazmul Alam, Al Amin, Mahadi Hasan
Structure and Environment 2022, vol. 14, (4), pp. 153-160, Article number: el 017
https://doi.org/10.30540/sae-2022-017

Structure and Environment
ISSN 2081-1500
e-ISSN 2657-6902
https://content.sciendo.com/sae
https://sae.tu.kielce.pl

sciendo

Kielce University of Technology

DOI: 10.30540/sae-2022-017

BEHAVIOR OF MAT FOUNDATION FOR A TEN-STORY BUILDING: FIXED BASE VS THREE-DIMENSIONAL SOIL MODEL

ZACHOWANIE SIĘ PODŁOŻA Z MATĄ DLA BUDYNKU DZIESIĘCIOPIĘTROWEGO: STAŁA BAZA A TRÓJWYMIAROWY MODEL GRUNTU

Farhaj Hasan*, Nazmul Alam
University of Asia Pacific (UAP), Bangladesh
Al Amin
European University of Bangladesh (EUB), Bangladesh
Mahadi Hasan
Engineering & Research Associates (ERA), Bangladesh

Abstract

Soil is an anisotropic, heterogeneous, and inelastic complex material. It is difficult to represent the exact behavior of soil by numerical modelling in practice. Conventionally, soil is simplified to an idealized model where it is considered isotropic, homogeneous, and behaves elastically under loads. The idealization, in this case, is done using the proper elastic modulus, Poisson's ratio, and unit weight of soil depending upon the soil type. Although the exact soil behavior is simplified, using Finite Element Analysis (FEA) a more effective result can be obtained. A superstructure was modelled using ETABS using a fixed-base system and the base reaction forces were obtained. A mat and a soil element on which the mat was laid were modelled as a flexible-base system in Midas GTS NX. The base reactions obtained from ETABS were applied to the mat in the soil model to determine the settlements and, consequently, the spring stiffness. The superstructure was then modelled again, incorporating springs under the respective columns. Convergence in settlement, and base reactions were reached by iteration, and the final results from the flexible-base system were then compared with the fixed-base system. The center column settled the most, about 60 mm, and there was a decrease in settlement by 15% between the first model and the final iterated model. The base reaction for center columns decreased by 24% in the flexible base system compared to the fixed base system. However, an increase in base reaction was observed for both side and edge columns. There was an extremely erratic change in grade beams under a flexible base system, which shows that the superstructure elements are also affected by the change in the base system. It is recommended to use this approach, for the analysis of structures considering flexible base systems instead of fixed bases because it enhances the accuracy of analysis with feasible time consumption and less complex effort.

Keywords: Elastic modulus, Poisson's ratio, Finite Element Analysis (FEA), Midas GTS NX, settlement, spring stiffness etc.

Streszczenie

Gleba jest materiałem złożonym anizotropowym, niejednorodnym i nieelastycznym. W praktyce trudno jest dokładnie odwzorować zachowanie gleby za pomocą modelowania numerycznego. Konwencjonalnie glebę upraszcza się do wyide-

*University of Asia Pacific (UAP), Bangladesh, e-mail: farhaj.ce@gmail.com

alizowanego modelu, w którym uważa się ją za izotropową, jednorodną i zachowującą się elastycznie pod obciążeniem. Idealizacja w tym przypadku odbywa się za pomocą odpowiedniego modułu sprężystości, współczynnika Poissona i masy jednostkowej gruntu w zależności od rodzaju gruntu. Chociaż dokładne zachowanie gleby jest uproszczone, można uzyskać bardziej efektywne wyniki za pomocą analizy elementów skończonych (FEA). Konstrukcja nośna została wymodelowana za pomocą ETABS przy użyciu systemu stałej podstawy i uzyskano siły reakcji podstawy. Matę i element gruntu, na którym została położona, zamodelowano jako układ o elastycznej podstawie w programie Midas GTS NX. Reakcje bazowe uzyskane z ETABS naniesiono na matę w modelu gruntowym w celu określenia osiadań, a co za tym idzie sztywności sprężystej. Następnie ponownie wymodelowano konstrukcję nośną, włączając sprężyny pod odpowiednimi kolumnami. Zbieżność osiadania i reakcji bazowych została osiągnięta przez iterację, a końcowe wyniki z systemu o elastycznej podstawie zostały następnie porównane z systemem o stałej podstawie. Kolumna środkowa osiadła najbardziej, około 60 mm, a między pierwszym modelem a ostatecznym modelem iterowanym nastąpił spadek osiadania o 15%. Reakcja podstawy dla kolumn centralnych zmniejszyła się o 24% w systemie z podstawą elastyczną w porównaniu z systemem z podstawą stałą. Zaobserwowano jednak wzrost odczynu zasadowego zarówno dla kolumn bocznych, jak i krawędziowych. Nastąpiła bardzo nieregularna zmiana belek niwelacyjnych pod elastycznym systemem bazowym, co pokazuje, że zmiany w systemie bazowym mają również wpływ na elementy konstrukcji nośnej. Zaleca się stosowanie tego podejścia do analizy konstrukcji z uwzględnieniem elastycznych systemów bazowych zamiast stałych baz, ponieważ zwiększa to dokładność analizy przy możliwej czasochłonności i mniejszym wysiłku.

Słowa kluczowe: moduł sprężystości, współczynnik Poissona, analiza elementów skończonych (FEA), Midas GTS NX, osiadanie, sztywność sprężyny itp.

1. INTRODUCTION

Foundation could be either shallow or deep depending on the bearing capacity of soil and the load from the superstructure. Shallow foundation can be chosen when the demand of the superstructure, the load, can be met by, the bearing capacity of the soil, from shallow depth usually when the depth of foundation is equal or less than the required width. Shallow foundation can be of different types like single footing, combined footing or mat foundation-which is a special type of combined footing. Whereas deep foundation system is considered when the bearing capacity of the soil is not enough at shallow depth. The simplified distinction is when the depth of foundation is four times the width of foundation, the system is called deep foundation. Pile foundation is one of the most common examples of deep foundation system. Mat foundation is adopted when the bearing capacity of soil is not sufficient for individual column footing because of overlapping of footing area. Mat foundation spreads the load over a large area and allows more settlement.

Settlement occurs when a load is applied on the soil, and it is very important for the engineers to be able to predict its settlements. A settlement is comprised of two types, elastic settlement and consolidation settlement. Consolidation settlement can be of two types, primary consolidation and secondary consolidation. The elastic settlement is the immediate settlement that occurs when a load is applied. Settlement mainly depends on the soil properties. For example, when a load is applied on sand, the settlement that occur is only elastic due to the deformation of the soil body. Whereas, the clay soil will have both elastic settlement and consolidation settlement, the deformation of soil particles followed by drainage of water. And in the long term the secondary consolidation will occur when the soil particles will rearrange themselves after the water is drained out. The settlement also depends on the inter-particle properties.

Compared the bending moments between conventional approach and FEM. A raft was modelled in SAFE and the superstructure was modelled in STAAD. The bending moment in x and y direction as well settlements were converged. Bending moment was found to be lesser in FEM than conventional approach for loose and medium soil, however, the difference is not much for stiff soil and between the centre column spaces for all types of soil (Limkar et al., 2017). A New Approach for Estimating Thickness of Mat Foundations under Certain Conditions by (Al-Shayea, Zeedan, 2012) estimates the thickness of the mat foundation for engineering practice. The mat thickness was estimated using FEM analysis of soil, mat, and superstructure in STAAD PRO, where the mat was analysed as a 3D finite element plate, and the soil and the superstructure were considered as elastic materials with different elastic properties using Poisson's ratio and elastic modulus. The following insights were found in the paper: The distribution of stress on the foundation is affected by both mat rigidity and soil type; for rigid plates, moment is

environment

more important than shear; for flexible plates, shear is more important.

Cement columns in peat soil were compared between an analytical model and a finite element (FE) model. The FE model was done using PLAXIS 3D foundation software, and for the analytical model, Brom's analytical methods were used. The analytical model consistently predicts less settlement than the FE model (Banadaki et al., 2012). Settlements of hydro-digesters on mat foundation were both measured and analysed using numerical analysis tools by (Shah et al., 2006) two digesters were modelled using FE software, where the superstructures were analysed in STAAD Pro and the subsurface soil model was analysed in Plaxis software. Springs were incorporated into the superstructure model, which used the subgrade modulus from the soil model as the spring stiffness of the springs. The results from both the models were iterated and converged before analyzing the results. It was seen that the FE model predicted more settlement, but it was close to the measured values.

The modulus of subgrade reaction, *k*. In this study, a value of *k* was computed using Vlasov's model from a concentrated load, which was then used in the Winkler's model. The value of *k* from Vlasov's model and the corresponding value for maximum displacement were converged by the process of the iteration method. An equation for *k* was developed, which can be computed if the properties of the soil as well as the geometry are known (Daloglu et al., 2000). In Practical Subgrade Model for Improved Soil-Structure Interaction Analysis: Software Implementation by (Horvath, Colasanti, 2011), they proposed an improved model for plate-like structures coupling of the virtual springs underneath the mat foundation. The paper uses both the Modified Kerr mechanical model (Horvath, Colasanti, 2010) and the Reissner model to introduce a new method called the Modified Kerr- Reissner Model (MK/R), which is done by introducing a tensioning thin membrane between layers of springs and using an equivalent single layer of elastic and isotropic soil instead of the multi-layered soil which was introduced by Reissner's Model.

A three-stage design approach to ensure an optimum design system. The three stages are: finding the number of piles, location of the piles; and a detailed analysis to confirm the optimum number of piles for practical design. It was also noted that increasing the number of piles after a certain point gives no additional benefits to the structure (Poulos, 2001). the applicability and accuracy of various approaches offered for determining the coefficient of subgrade reaction, k. The geotechnical parameters of a site on the Tabriz Marl were used as a baseline, and settlement study findings from different methods were compared to those obtained from advanced soil model analyses utilizing Safe and Plaxis software. The soft soil model was shown to be the best governing model for Tabriz Marl, and the Vesic relation among the techniques of determining k_s leads to low inaccuracy when compared to the soft soil model. It is also suggested that mean elasticity modulus should be used to obtain more accurate findings from these methods (Sadrekarimi, Akbarzad, 2009).

Three soil samples were taken from the research area at various elevations. A variety of tests were carried out to determine some of the soil's prerequisite qualities. The use of piles, regardless of raft thickness, results in a significant reduction in foundation settlements. The use of piled rafts can also be used to reduce raft settlements as well as material resources by reducing raft thickness. Midas GTS NX has proven to be effective software for analyzing piled raft foundations (Saini, Goyal, 2019).

2. METHODOLOGY

A 10-story residential building will be modelled in ETABS, and linear static analysis will be carried out to determine the base reaction of the columns under vertical load. The behavior of mat foundation system will be analyzed using the finite element method. As a result, a mat on soil model will be created in Midas GTS NX. The settlement will be then determined for the superstructure's base reaction force. Using the base reaction force and settlement, the spring stiffness (coefficient of subgrade reaction) will be calculated, and the superstructure will be modelled using springs under each base column. The new base reaction will be obtained and used in the FE model to determine the new settlement, and hence another spring stiffness will be calculated and used in the spring model. The process will be repeated and the settlement, spring stiffness, and base reaction will be determined using this incremental iteration process. These parameters will be compared with the original fixed base system.

The plan's *X* span was 17 m, with 5 columns spaced at 4.27 m intervals and 4 columns spaced at 4.88 m intervals in the *Y* direction for a total span of 48 ft. Each story height was 3 m, with a foundation level 2.44 m below the existing ground level and a total height of 29.87 m. A reinforced concrete structure was considered for the superstructure analysis. The concrete material was to be elastic and isotropic.

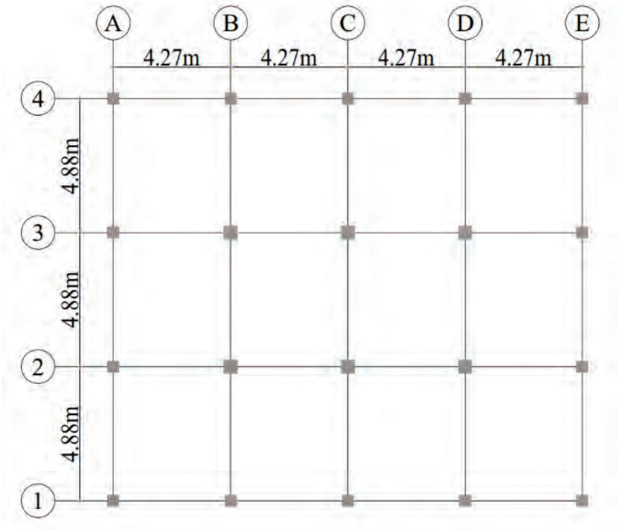

a) Plan view

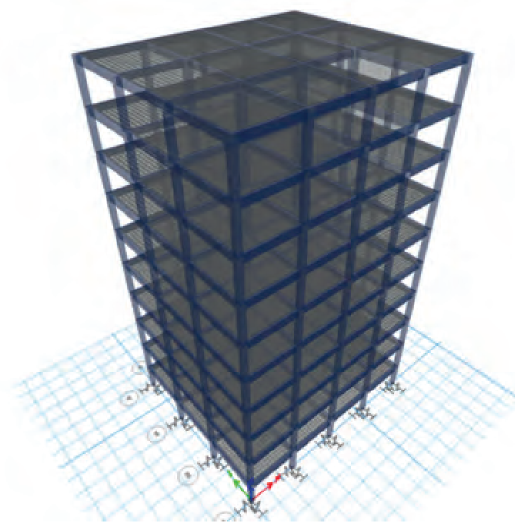

b) 3D view

Fig. 1. Building interpretation

Table 1. Lateral loads parameters (BNBC-2020)

Wind load		Seismic Load	
Windward coefficient, C_{pw}	0.8	Response reduction factor, R	8
Leeward coefficient, C_{pl}	0.5	System over-strength factor, Ω_0	3
Wind Speed, V (m/s)	65	Deflection amplification factor C_d	5.5
Exposure type	B	Importance factor, I	1
Importance factor, I	1.0	0.2 seconds spectral acceleration, S_s	0.5
Gust factor, G	0.85	1 second spectral acceleration, S_1	0.2
Directionality factor, K_d	0.85	Site class	F
Topographic factor, K_{zt}	1.0	Site co-efficient, F_a	1.35
		Site co-efficient, F_v	2.7

Five layers of soil were modelled using an idealized soil strata from Dhaka (Dhanmondi Area), in Midas GTS NX software using the Mohr-Coulomb plasticity model. The soil strata are given below.

Table 2. Properties of soil with layer thickness

Thickness	Soil Types	Soil properties	
1.5 m	Soft Clay	$\gamma = 19$ kN/m^3, $E = 12.5$ MPa, $C = 25$ kN/m^3	$\varphi = 0°$, $\upsilon = 0.4$
4.5 m	Medium Stiff Clay	$\gamma = 19.5$ kN/m^3, $E = 29$ MPa, $C = 35$ kN/m^3	$\varphi = 0°$, $\upsilon = 0.35$
6.0 m	Stiff Clay	$\gamma = 20$ kN/m^3, $E = 49$ MPa, $C = 58$ kN/m^3	$\varphi = 0°$, $\upsilon = 0.3$
9.0 m	Medium Dense Sand	$\gamma = 20$ kN/m^3, $E = 35$ MPa, $C = 0$ kN/m^3	$\varphi = 30°$, $\upsilon = 0.3$
9.0 m	Dense Sand	$\gamma = 20$ kN/m^3, $E = 120$ MPa, $C = 0$ kN/m^3	$\varphi = 40°$, $\upsilon = 0.3$

An 85 m × 73 m (five times the mat dimension in both directions) soil body was modelled using Midas GTS NX software with depth taken as 30 m as per the above soil strata.

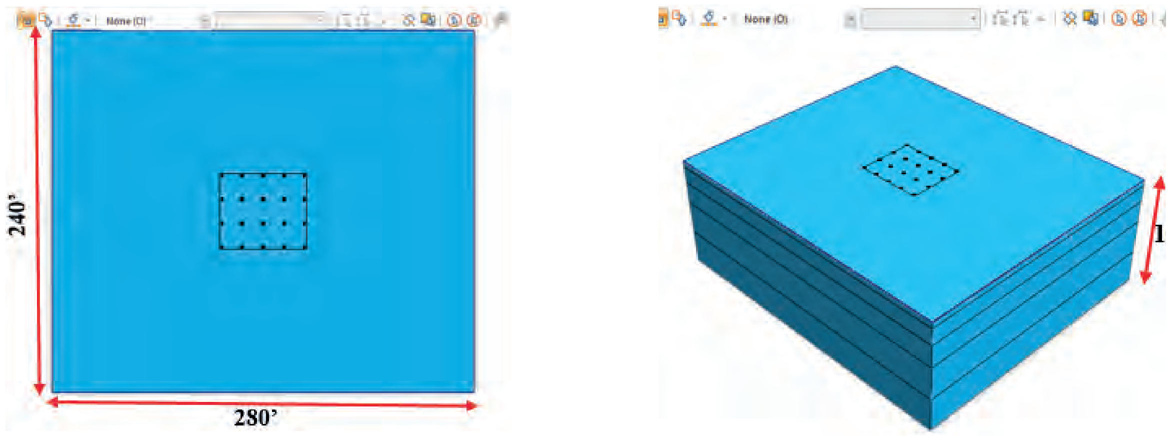

a) Plan of the model b) Three dimensional view

Fig. 2. Soil Model in Midas GTS NX

For meshing the built-in auto mesh feature was used for both mat and soil model. The auto mesh feature in Midas GTS NX generates a combination of hybrid mesh of hexahedral, pentahedral and tetrahedral elements in both two-dimensional and three-dimensional elements.

The analysis for the superstructure was done in ETABS, whereas the soil and mat were analyzed in Midas GTS NX. The procedure of the numerical analysis was as below:

- Base reactions (F_o) under each base column were generated from the ETABS Model using a rigid base system.
- The base reactions were then transferred to the soil model in Midas GTS NX to obtain the resulting vertical displacements under each column (x_o).
- Using the expression, $F = k/x$, we obtained the spring stiffness or coefficient of subgrade reaction (k_o) obtained from these values.
- The spring stiffness was used in the ETABS model under each base column to analyze the superstructure as a flexible base system. This generated new base reactions and vertical displacements.
- The new base reactions were then used in the soil model in MIDAS GTS NX to obtain the new displacement.

A new spring stiffness was calculated again and the procedure continued until the parameters were converged.

3. RESULTS AND DISCUSSSIONS

The convergence in parameters such as settlement, base reactions, and spring stiffness will be represented and discussed. Furthermore, the behavior of the superstructure's elements will be displayed and discussed, which could be a basis for future work.

Differential vertical settlement was encountered when spring was used in the superstructure model than fixed support. However, the settlement difference between the original model (fixed support) and the spring model was around 15% for center columns (after convergence) in comparison to finite element model (FEM).

Table 3. Comparisons of settlement (mm)

Trial	Centre columns		Corner columns		Edge columns	
	ETABS	Midas GTS NX	ETABS	Midas GTS NX	ETABS	Midas GTS NX
Fixed base 0		–65.26	0	–31.30	0	–44.97
Trial-1	–67.39	–60.70	–45.58	–36.05	–55.18	–45.76
Trial-2	–68.22	–59.96	–43.73	–36.83	–54.35	–45.89
Trial-3	–59.75	–59.83	–37.02	–36.94	–45.97	–45.92
Trial-4	–59.78	–59.81	–36.98	–36.96	–45.95	–45.93

The conventional modelling of a superstructure using fixed support cannot account differential settlement between the columns. It can be seen that the difference in settlement between the center columns and the corner columns is around 24 mm. Thereby flexible foundation should be modelled to encounter the differential settlement.

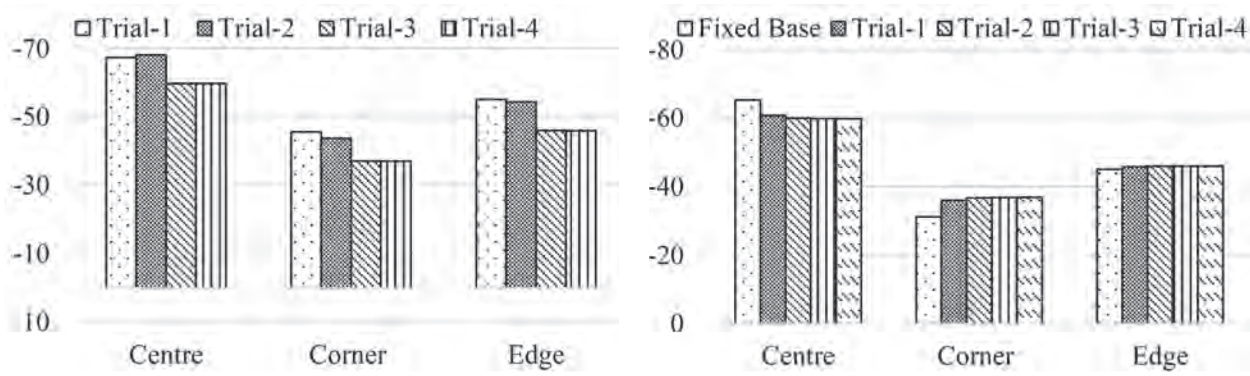

a) Settlement (ETABS) b) Settlement (Midas GTS NX)

Fig. 3. Convergence in settlement (mm) between Midas Model and ETABS Model

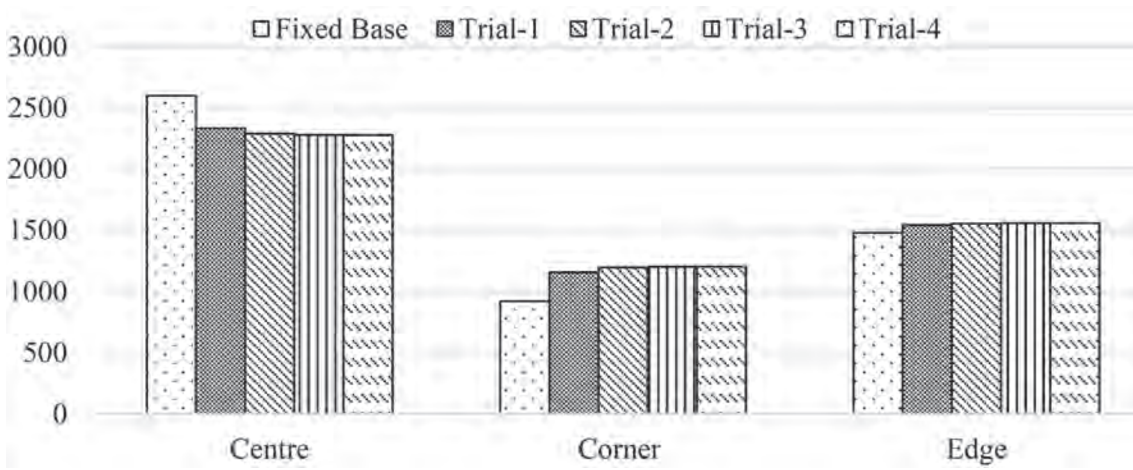

Fig. 4. Graphical representation of convergence in base reactions (kN)

In most conventional practice, the soil flexibility is totally ignored, and it is assumed that the superstructure is supported on a fixed base. This results in overestimating the foundation or worse, underestimating the soil settlement and base reaction. Therefore, it is necessary to analyze the support as a flexible support. This is done by considering virtual springs underneath the superstructure as developed by Winkler. However, Winkler's model assumes constant spring stiffness for the entire area of the foundation system, which again leads to the same problem of both underestimation and overestimation in the foundation system. Therefore, it is critical to use different spring stiffness according to the superstructure and substructure response.

Table 4. Comparisons of spring stiffness (kN/mm)

Trial	Centre columns	Edge columns	Corner columns
Fixed base	39.88	32.85	29.48
Trial-1	38.46	33.71	32.17
Trial-2	38.19	33.85	32.57
Trial-3	38.13	33.88	32.63
Trial-4	38.12	33.89	32.65

The analysis shows that the spring stiffness for the corner columns increased by around 10% whereas, the center columns decreased by as much as 5% and the side columns were not affected much. The base reaction was significantly affected by the change in support. The base reaction for corner columns increased as much as 24% by the introduction of springs in the support instead of fixed support which is concerning. The side columns were least affected by conversion of fixed base to flexible base. The base reaction for corner column also increased by 15%.

4. CONCLUSION

The purpose of this study was to understand the behavior of soil under both fixed base systems and flexible base systems and to find a state-of-the-art solution to analyze mat foundation systems. The new approach to analyzing the mat foundation can be more accurate and efficient at the same time. The settlement in both the soil model and the spring model converged. The maximum settlement in the flexible foundation was reduced to 60 mm from 68 mm, which is not very much. The main concern, however, is the differential settlement, which could be eliminated by knowing the exact settlement from FEM. The change in base reaction was drastic in the flexible base system compared to the fixed base system. In some cases, there would be under design of mat foundation systems if the conventional fixed base system was used. Because the settlement was nearly the same in both models, the spring stiffness changed as the base reaction changed. Again, there would be under design in the mat foundation if a fixed base was to be used in the foundation system. The superstructure's elements' behavior also changed by changing the base system. When the base is changed to flexible, some elements experience increased moment or a reverse in moment direction, or both. This is a big concern, and more study must be done in the future to understand more about the superstructure's elements' behavior under a flexible base system.

REFERENCES

[1] Abdolrezayi A., Khayat N.: *Comparative Three-Dimensional Finite Element Analysis of Piled Raft Foundations*. Computational Engineering and Physical Modeling, 4 (1), 2021, pp. 19-36; Doi.org/10.22115/CEPM.2020.234834.1111.

[2] Al-Shayea N., Zeedan H.: *A new approach for estimating thickness of mat foundations under certain conditions*. Arabian Journal for Science and Engineering, 37(2), 2012, pp. 277-290; Doi.org/10.1007/s13369-012-0178-5.

[3] Al-Taie E., Al-Ansari N., Knutsson S.: *Estimation of Settlement under Shallow Foundation for Different Regions in Iraq Using SAFE Software*. Engineering, 7(07), 2015, p. 379; Doi.org/10.4236/eng.2015.77034.

[4] Banadaki A.D., Ahmad K., Ali N.: *Initial settlement of mat foundation on group of cement columns in Peat–Numerical analysis*. Electronic journal of geotechnical engineering, 17(Bundle O), 2012, pp. 2243-2253.

[5] BNBC (2020): "Bangladesh National Building Code", Housing and building Research Institute, Dhaka.

[6] Chang D.W., Hung M.H., Lien H.W.: *2D Soil Springs for Elastic Settlements of Mat Foundation under Vertically Uniform Loads*. In 2020 International Conference on Mathematics and Computers in Science and Engineering (MACISE), 2020, January, pp. 188-191. IEEE; Doi.org/10.1109/macise49704.2020.00041.

[7] Colasanti R.J., Horvath J.S.: *Practical subgrade model for improved soil-structure interaction analysis: software implementation*. Practice periodical on structural design and construction, 15(4), 2010, pp. 278-286.

[8] Daloglu A.T., Vallabhan C.G.: *Values of k for Slab on Winkler Foundation.* Journal of Geotechnical and Geo-environmental Engineering, 126(5), 2000, pp. 463-471; Doi.org/10.1061/(asce)1090-0241(2000)126:5(463).

[9] Horvath J.S., Colasanti R.J.: *Practical subgrade model for improved soil-structure interaction analysis: Model development*, International Journal of Geomechanics, 11(1), 2011, pp. 59-64; doi.org/10.1061/(asce)gm.1943-5622.0000070.

[10] Loukidis D., Tamiolakis G.P.: *On the Pseudo-Coupled Winkler Spring Approach for Soil-Mat Foundation Interaction Analysis*, In Proceedings of China-Europe Conference on Geotechnical Engineering, 2018, pp. 386-389. Springer, Cham; Doi.org/10.1007/978-3-319-97112-4_86.

[11] Limkar S.D., Kalyanshetti M.G., Halkude S.A.: *Analysis of raft foundation using finite element approach*. Int J Latest Trends Eng Technol, 8(3), 2017, pp. 014-028; Doi.org/10.21172/1.83.003.

[12] Poulos H.G.: *Piled raft foundations: design and applications. Geotechnique*, 51(2), 2001, pp. 95-113; doi.org/10.1680/geot.51.2.95.40292.

[13] Sadrekarimi J., Akbarzad M.: *Comparative study of methods of determination of coefficient of subgrade reaction*. Electronic Journal of Geotechnical Engineering, 14(1), 2009, pp. 45-61.

[14] Shah H.J., Goh S.H., Lacy H.S., Kellogg D.R.: *Numerical Modeling and Analysis of a Large Mat Foundation Supported above a Varved Silt and Clay Formation of New York City*. In GeoCongress 2006: Geotechnical Engineering in the Information Technology Age, 2006, pp. 1-6; Doi.org/10.1061/40803(187)89.

[15] Shah H.J., Goh S.H., Lacy H.S., Kellogg D.R.: *Numerical Modeling and Analysis of a Large Mat Foundation Supported above a Varved Silt and Clay Formation of New York City*. In GeoCongress 2006: Geotechnical Engineering in the Information Technology Age, 2006, pp. 1-6; Doi.org/10.1061/40803(187)89.

[16] Saini S., Goyal, E.T.: *Analysis of piled raft foundation using MIDAS GTS NX.* Int Res J Eng Technol, 6 (5), 2019, pp. 5491-5499.
[17] Tabsh S.W., El-Emam M.: *Influence of Foundation Rigidity on the Structural Response of Mat Foundation*. Advances in Civil Engineering, 2021; Doi.org/10.1155/2021/5586787.

Marta Styś-Maniara*, Edyta Nartowska, Monika Metryka-Telka, Rafał Porowski
Structure and Environment 2022, vol. 14, (4), pp. 161-172, Article number: el 018
https://doi.org/10.30540/sae-2022-018

Structure and Environment
ISSN 2081-1500
e-ISSN 2657-6902
https://content.sciendo.com/sae
https://sae.tu.kielce.pl

sciendo

Kielce University of Technology

DOI: 10.30540/sae-2022-018

INORGANIC SALT HYDRATES AS PHASE CHANGE MATERIALS (PCM) FOR THERMAL ENERGY STORAGE IN SOLAR INSTALLATIONS

NIEORGANICZNE HYDRATY SOLI JAKO MATERIAŁY ZMIENNOFAZOWE (PCM) DO MAGAZYNOWANIA ENERGII CIEPLNEJ W INSTALACJACH SŁONECZNYCH

Marta Styś-Maniara*, Edyta Nartowska, Monika Metryka-Telka
Kielce University of Technology, Poland
Rafał Porowski
AGH University of Science and Technology, Poland

Abstract

The authors present a general idea of using inorganic salt hydrates in solar installations. A key role in this selection is played by thermophysical parameters, so the authors review their test methods and in turn characterize them for the most promising salt hydrates. Next, the authors describe the advantages and disadvantages of inorganic salt hydrates and indicate possibilities for their improvement. The use of salt hydrate converters in PV installations significantly improves the efficiency of photovoltaic modules. We show that at least 18 salt hydrates are promising for solar applications with the best ones being Sodium Hydrogen Phosphate Dodecahydrate, Sodium Carbonate Decahydrate and Calcium Chloride Hexahydrate. The selection of a test method for determining the thermophysical parameters of salt hydrates should be individual depending on the research objective. Comparing the methods presented, we believe that it is the DSC and DTA methods that provide the most accurate and repeatable results.

Keywords: salt hydrates, phase change materials, thermal energy storage, latent heat storage

Streszczenie

Autorzy przedstawiają ogólną koncepcję wykorzystania nieorganicznych hydratów solnych w instalacjach solarnych. Kluczową rolę w tym doborze odgrywają parametry termofizyczne, dlatego autorzy dokonują przeglądu metod ich badania i kolejno charakteryzują je dla najbardziej obiecujących hydratów solnych i ich mieszanin. Następnie autorzy opisują zalety i wady nieorganicznych hydratów solnych oraz wskazują możliwości ich udoskonalenia. Zastosowanie konwerterów hydratów solnych w instalacjach PV znacząco poprawia sprawność modułów fotowoltaicznych. Wykazano, że co najmniej 18 hydratów soli i ich mieszanin jest obiecujących dla zastosowań solarnych ze względu na korzystne parametry termofizyczne, przy czym najlepsze z nich to dodekahydrat wodorofosforan sodu, dekahydrat węglanu sodu i heksadydrat chlorku wapnia. Z przeglądu literatury wynika, że wybór metody badawczej do określenia parametrów termofizycznych hydratów soli powinien być indywidualny w zależności od celu badań. Porównując przedstawione metody, stwierdzono, że to właśnie metody DSC i DTA dają najbardziej dokładne i powtarzalne wyniki.

Słowa kluczowe: hydraty soli, materiały zmiennofazowe, magazynowanie energii cieplnej, magazynowanie ciepła utajonego

*Kielce University of Technology, Poland, e-mail: mmaniara@tu.kielce.pl

1. INTRODUCTION

Consumption of fossil fuels and carbon dioxide is increasing. An energy crisis is on the horizon, legislative standards for environmental disturbance are becoming stricter. In addition, public consciousness is growing and people are moving towards sustainable development. All this is causing the search for alternative energy sources and the continuous development of energy storage mechanisms. Currently, 3 types of TES systems for physical heat storage are known (Fig. 1).

One example of latent heat storage is PCM materials. Latent heat can be stored during the phase transformation of a given material and released under suitable conditions. It is divided according to the type of phase transformation (liquid-solid, solid-liquid and solid-solid). Within the solid-liquid interactions there are compounds:

- organic (waxes, paraffinic-alkane compounds, non-paraffinic compounds, fatty acids, alcohols, ionic liquids);
- inorganic (salts, hydrates-hydrated salts, metals, metal hydrides);
- eutectic mixtures (organic-organic, inorganic-inorganic, inorganic-organic) [1].

The use of PCMs helps to manage energy efficiently. The potential of these materials caused a rapid development of research in their direction in recent years, especially when it comes to salt hydrates [2, 3].

Inorganic salt hydrates, which are a large part of PCMs, have always attracted interest due to their affordable price, good thermal conductivity and high energy storage density. However, disadvantages such as leakage, supercooling and phase separation limit their practical application [4-6]. To reduce these disadvantages, PCMs of stable form have been tested by incorporating PCMs into porous materials or by microencapsulation to prevent leakage and phase separation [7-9]. Research is still being undertaken to improve salt hydrates for specific applications. In order to fully realize the potential of salt hydrates as PCM materials in solar installations, it is necessary to better understand their possibilities and limitations for such solutions.

The authors present a general idea of using inorganic salt hydrates in solar installations. A key

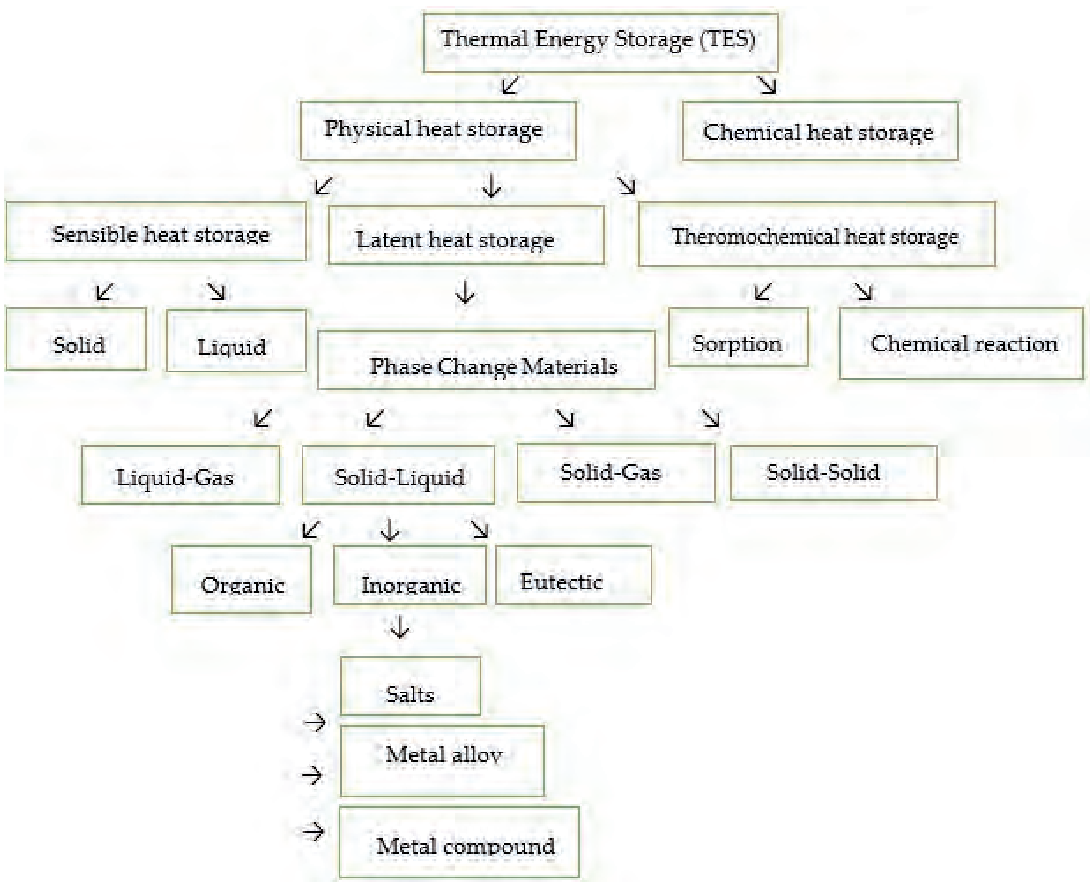

Fig. 1. Classification of thermal energy storage technologies [1]

role in this selection is played by thermophysical parameters, so the authors review their test methods and in turn characterize them for the most promising salt hydrates and their mixtures. Next, the authors describe the advantages and disadvantages of inorganic salt hydrates and indicate possibilities for their improvement. Finally, the authors provide directions for future research necessary to select a suitable inorganic salt hydrate for solar applications.

2. SALT HYDRATES AS PCM MATERIALS IN SOLAR INSTALLATIONS

Solar energy can be collected directly into electricity using a photovoltaic (PV) module. However, when solar radiation arrives at the PV module, it is not only converted into electricity, but also into thermal energy, which increases the temperature of the PV system. There are many factors that affect the output of a PV system [1].

One of them is temperature. The efficiency of a PV module is the inverse of temperature. According to the Standard Test Conditions, if a PV module operates at a temperature higher than the ambient temperature, 25°C, then for every one degree Celsius increase in temperature, the conversion rate of the PV module drops as low as 0.5%. Summer is the season with the highest solar radiation. Daytime temperatures in summer are typically between 40°C and 70°C, which is 2-3 times the ideal operating temperature of solar panels. This puts the overall efficiency of the PV system at risk – a potential drop in conversion factor of (7.5-22.5)%. Overheating of PV modules finally shortens their lifetime (*x, y*). A simple solution to reduce the surface temperature of the current PV system is to cool (by convection) the back of the PV panels by using a phase change material (PCM). PCMs are materials that go through reversible stages that depend on their temperature. They can accept or reject heat. The principle of PCM in a PV module is simple. Excess heat from the panel surface caused by an increase in ambient temperature will be consumed by the attached PCM, until the physical phase of the PCM is completely transformed (e.g., from solid to liquid). As the panel temperature drops, the PCM solidification process should release heat to the working fluid in the PV panel, to the structure, or will act as an insulator in the system. Solutions using PCM in solar installations are well-known in the scientific community.

Karthick et al. [9] integrated Glauber salt ($Na_2SO_4 \cdot 10H_2O$) into a photovoltaic system for the façade of a test building in India. The purpose of the study was to evaluate the improvement in electrical and thermal energy results. Glauber's salt was encapsulated with a sheet of tedlar and then attached right behind each polycrystalline PV cell. To make a single module (Building Integrated Photovoltaics) BIPV, the cells were placed between additional low-iron glass materials. Output power and efficiency were analyzed and the orientation of the module and test room were taken into account to evaluate solar heat gain through the facade. The results showed a 10% increase in electrical output with the PCM. This was due to an 8°C reduction in the system's instantaneous peak temperature. The overall PV cell temperature decreased by 12% [9]. Another BIPV-related study was conducted by Hasan et al. [10]. In this experiment, calcium chloride hexahydrate ($CaCl_2 \cdot 6H_2O$) was tested in 4 different PV-PCM systems. The tests were conducted at low as well as high solar irradiance, in order to fully evaluate the efficiency of the system. Polycrystalline silicon photovoltaic cells with Perspex as a housing were placed on the front of four containers made of different materials. The materials and sizes of the system's containers were carefully selected to study the effects of thermal conductivity (for system A and C made of aluminum) and insulation (for system B and D made of perspex), wall thickness and thermal mass of the PCM on temperature control. While the ambient temperature remained constant (~20°C ±1°C), the results showed that calcium chloride hexahydrate lowered the cell temperature at solar irradiance >750 W/m^2, increasing the temperature deviation time. In the BIPV- PCM system, at 750 W/m^2, the PV cell surface temperature decreased to 18°C, and the constant temperature was maintained for about 30 minutes. In contrast, at 1000 W/m^2, although the reduction in surface temperature was smaller (10°C), the duration increased to 5 hours.

The studies presented above show the suitability of inorganic salt hydrates as PCM materials to improve the efficiency of PV systems. Similarly, Hussein et al. [11] investigated a PV/PCM system with a crystalline silicon panel as the electrical component, a rectangular aluminum chamber filled with PCM as the thermal component (Fig. 2). It was assumed that the aluminum chamber is in ideal thermal contact with the PV panel.

By changing the components in a PV/PCM system, heat can be generated for useful use. The authors observed improvements in all parameters. Combining

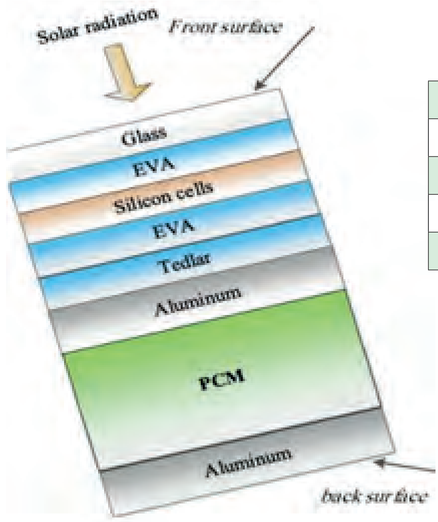

Parameter	Glass	EVA*	Silicon cells	Tedlar	Al. chamber
Thermal conductivity (W/mK)	1.04	0.3	148	0.2	202
Density (kg/m^3)	2500	935	2330	1500	2791
Specific heat capacity (J/kgK)	750	2500	700	1090	871
Thickness (mm)	3.2	0.5	0.2	0.5	5

*ethylene-vinyl acetate

Fig. 2. Cross-section of the PV-PCM system and basic properties of the system layers [11]

the properties of all layers including glass, EVA, silicon cells, tedlar and PCM gives us a cell with better specific heat capacity, better density and higher thermal conductivity.

3. METHODS FOR STUDYING THE THERMOPHYSICAL PROPERTIES OF SALT HYDRATES

The main thermophysical parameters of salt hydrates include *melting point, heat of fusion and density.*

3.1. Melting point and heat of fusion – assumptions of research methods

Chemical substances undergo a variety of physical and chemical transformations due to changes in ambient temperature. In the case of pure substances, these transformations allow for effective identification of their chemical structure, and the study of mixtures allows for their qualitative and quantitative analysis. Among the most commonly studied temperature-dependent physical transformations are:

- melting/solidification – that is, a change in the solid/liquid state of phase. It is a characteristic of pure chemicals having a crystalline structure (both inorganic and organic);
- change in specific gravity – shown by a change in the volume of a liquid substance or a change in the dimension of a solid (contraction or dilation).

Calorimetry is one of the most precise and convenient methods of studying solids by determining their specific heat as a function of temperature, phase transitions of various types, phase diagrams. Calorimeters are used to qualitatively evaluate exo- and endothermic processes, as well as to quantify the progress of a reaction. Frequently used thermal analysis methods include differential tests [12].

Differential Scanning Calorimetry (DSC) relies on the measurement of the difference between the heat flow vs. temperature relation of the sample and the heat flow vs. temperature relation of a standard. Directly measured signal is a change in temperature between a test sample and a reference sample (Fig. 3). This difference is proportional to the flow of the heat flux between the two samples and is automatically converted to the value of the heat flux using special software. The result of calorimetric measurements is a DSC curve shown as the temperature dependence on the heat flux, an endo- and exothermic peaks are recorded on these curves, which result from the temperature differences between a tested sample and a reference sample. The measurements are performed in the controlled inert gas atmosphere of high purity (nitrogen). In shape, the DSC curve shows good agreement with the DTA curve. On the DSC curve we can distinguish sections of the so-called baseline, which are shifted parallel to the temperature axis by a certain small value of dH. They mark the temperature intervals in which no processes related to heat release or absorption take place in the sample. When a reaction or phase transformation occurs, the baseline turns into a peak. This is the part of the curve where it deviates from the baseline and then returns to it. An endothermic peak occurs when the temperature of the test sample is lower than the reference sample, while an exothermic peak occurs when the temperature of the test sample rises

Fig. 3. DSC Q200 (TA Instruments)[own study]

above the temperature of the reference sample. In the first case, heat must be supplied to the test sample (downward-oriented peak), while in the second case, heat is received by the system (upward-oriented peak) [14].

Differential Thermal Analysis (DTA) is a method where the temperature difference between a test substance and a reference substance is recorded as two samples in a controlled heated or cooled environment. The result of the measurement is a DTA curve, which is the temperature difference as a function of temperature or time [13]. One of the instruments for DTA testing is the SDT Q600 (Fig. 4).

The T-history method is based on comparing the history of temperature change over time for a phase change material and a reference material. Analysis of the temperature distribution allows the values of melting point, specific heat and enthalpy of fusion of

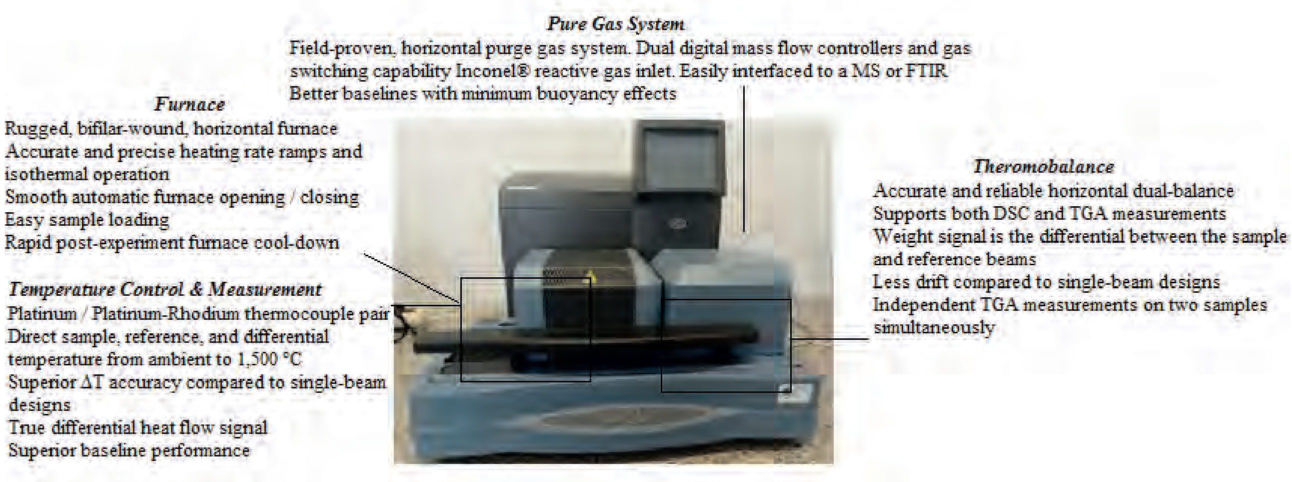

Fig. 4. SDTQ600 [TA Instruments.com]

the PCM material to be obtained [16]. The smallest differences in results are observed at the melting temperature.

When determining thermophysical parameters for mixtures, the so-called ***Dynamic method*** is practiced. It allows the measurement of liquid-solid and liquid-liquid phase equilibria. Measurements involve visual observation of the temperature of disappearance of the last solid-phase crystal (SLE) or disappearance of opacity (LLE) at a controlled heating rate. A diagram of the apparatus used is shown in Figure 5. In practice, the determination of phase diagrams is performed as follows. A small amount of salt hydrate is introduced into the measuring flask, followed by another hydrate. Each time the flask is weighed before and after the addition of the second salt hydrate. A volumetric flask with a mixture of a well-defined composition (1 x) is placed in a water bath. The contents of the flask are slowly heated with an electric heater connected to an autotransformer, which provides precise regulation of the heating rate.

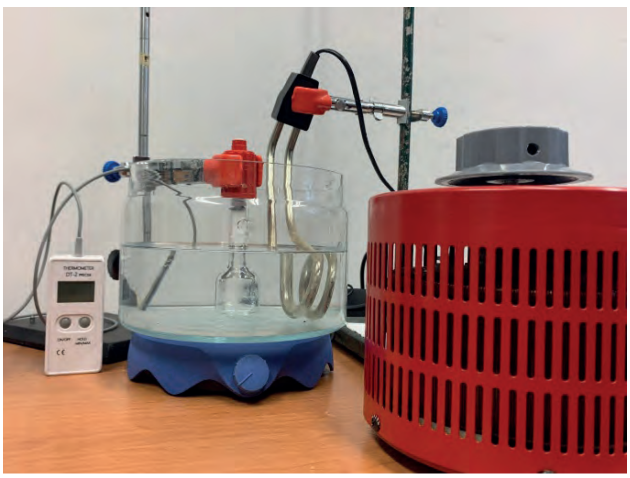

Fig. 5. Apparatus for measuring phase equilibria by dynamic method: electronic thermometer; measuring vessel; electric heater; Teflon-coated magnetic stirrer; stirring element for heating or cooling medium in bath; water, oil or acetone bath; magnetic stirrer [own study]

Under strong light passing through the test sample, the temperature of the disappearance of the last crystal or the disappearance of the opacity is observed. The temperature of the system is measured using a thermometer whose probe has been completely immersed in a water bath. The accuracy of the temperature measurement is estimated at ±0.01 K. During the measurement, both the sample was subjected to continuous stirring using a magnetic and mechanical stirrer, which makes it possible to eliminate concentration and temperature gradients within them [17].

3.2. Melting point and heat of fusion – limitations of methods when testing salt hydrates

DSC is a common instrument in most PV-PCM system performance studies. The quality of the DSC curve depends on many factors. The most important of these are *the mass of the sample, the rate of temperature change used and the positioning of the substance in the vessel*. The optimal mass of the test sample is usually between a few and a dozen milligrams. The greater the mass of the sample, the greater the observed thermal effect. If weak thermal effects are observed, a higher mass should be used. However, when the test substance exhibits closely spaced anomalies, the use of a large mass can cause them to combine into a single anomaly on the DSC curve. The rate of temperature change, can be selected depending on a number of factors. Typically, measurements are made at a rate of 5 or 10 K/min. An increase in the heating rate results in an increase in the size of the anomalies with a simultaneous broadening of the anomalies. Uniform distribution of substances in the vessel ensures good heat transfer and, consequently, correct temperature indications of the phase transitions or chemical reactions taking place (18).

According to some authors, the expensive DSC method may not be suitable for PCM testing because DSC uses only about 10 mg of sample mass [15]. This creates difficulties in determining the problems associated with larger samples during phase isolation, dispersion, high supercooling, etc. during the study. Finally, small sample sizes in testing are usually not indicative of real engineering systems or industrial applications that require huge amounts of PCMs, especially for heterogeneous materials. As a result, the authors [15] believe that other techniques should be considered that allow for larger test sample weights in a study, such as the T-History method. The THM method provides a simple experimental device, the ability to simultaneously measure the melting point, specific heat and thermal conductivity of several PCM samples, and the possibility to observe the phase transformation process of each PCM sample [19]. The major disadvantage may be the inaccuracy of the results. Conducting T-history tests requires special care on the part of the investigator. During the test, it is necessary to watch out for two main factors that have determined significant measurement errors:

inaccuracy of the temperature measurement reading and movement of the thermocouple in the sample during the measurement, which directly affect the decrease in measurement accuracy [19].

For the dynamic method, the experiment is labor-intensive and subject to error, as crystallization from solution was a very difficult and slow process. The method, has been known for more than 100 years, where it was commonly used to determine solubility curves. It allows detailed observation of the full range of molar fractions of the solute. It is a largely subjective method and requires a great deal of feeling on the part of the experimenter.

The literature review shows that the selection of a test method for determining the thermophysical parameters of salt hydrates should be individual depending on the research objective. Comparing the methods presented, we believe that it is the DSC and DTA methods that provide the most accurate and repeatable results.

3.3. Density

The pycnometer method is one of the simplest methods to determine density. The instrument consists of a container of a certain volume and a sealed lid with an opening for the excess liquid under test to flow out. The vessel is weighed before and after filling. Density is calculated as the ratio of the weight of the product to the volume of the pycnometer (Fig. 6).

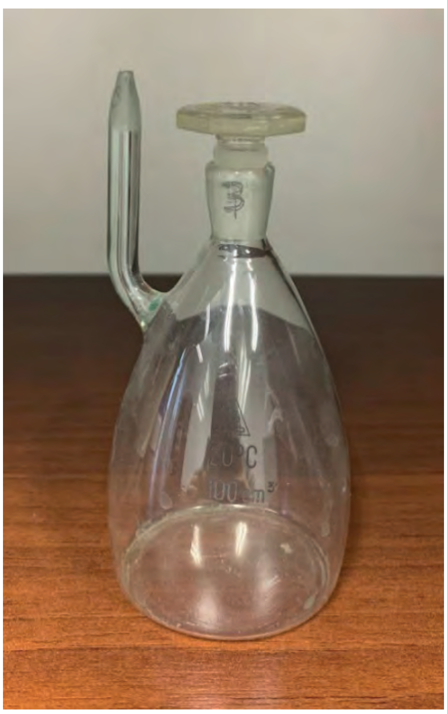

Fig. 6. Pycnometer [own study]

4. THE CHARACTERISTICS OF SALT HYDRATES AND THEIR MIXTURES

4.1. Thermophysical properties

Salt hydrates are described by the general formula $AB - nH_2O$, where n is the number of water molecules, AB indicates the composition of the salt. During the phase transformation, the salt undergoes dehydration [23]. The thermophysical properties of salt hydrates are an important parameter when evaluating these substances. They can regulate the temperature of photovoltaic cells and improve the electrical performance of photovoltaic panels in different temperature environments [24].

In Thermal Energy Storage (TES) systems, usable energy is transferred from the solar collector to the medium (PCM) as sensible or latent heat. Latent heat is most attractive because it has a higher density, so the required volume of material is smaller than for sensible heat storage [25]. Latent heat uses the phase transformation material as the storage medium. When the temperature increases, the phase transformation occurs and the material changes from a solid to a liquid state, absorbing heat and thus compensating for the temperature increase. In the same manner, when the temperature decreases, the PCM goes from a liquid to a solid state, transferring heat to the medium and thus compensating for the decrease in temperature. Such properties are essential for improving the efficiency of photovoltaic panels [25].

The melting point range of salt hydrates is between 15°C and 117°C [26]. They are characterized by high heat capacity and high latent heat of 330 kJ/kg [27], high thermal conductivity and low price. Depending on the phase transformation efficiency, salt hydrates can be divided into three categories: salt hydrates with congruent, incongruent and semi-congruent melting properties. Many salt hydrates that process a high latent heat transition and a moderate phase transformation temperature do not have congruent melting properties. The phase transformation temperature range of a single salt hydrate may not always fit practical applications. Therefore, two or more salt hydrates can be mixed to adjust the melting temperature. Salt hydrate mixtures can be divided into eutectic mixtures with congruent behavior and non-eutectic mixtures with incongruent melting points. Eutectic mixtures usually do not segregate during melting and freezing because they freeze to form crystalline mixtures [28-31]. Multi-component eutectic mixtures with a common melting point and high latent heat can lower the melting point of a single-component salt hydrate, and can then be used in broader fields [32]. In addition, eutectic mixtures can also eliminate the disadvantages of single salt hydrates, including supercooling and phase separation. Liu et al. [33] described eutectics of hydrated salts $Na_2SO_4 \cdot 10H_2O + Na_2HPO_4 \cdot 12H_2O$ and $Na_2CO_3 \cdot 10H_2O + Na_2HPO_4 \cdot 12H_2O$ to find applications in thermal energy storage in solar systems. The eutectics showed no phase separation and the degree of supercooling was reduced [33]. It was found that the inclusion of eutectic PCM improved the efficiency by 12% and lowered the module temperature by 12°C compared to a conventional PV module. Xin et al. [34] determined the optimal ratio of nucleating and thickening agents to reduce the level of supercooling and eliminate phase separation in a binary mixture of eutectic $Na_2SO_4 \cdot 10H_2O$ and $Na_2HPO_4 \cdot 12H_2O$.

Inorganic salt hydrates that can be required for solar applications along with their thermophysical parameters are summarized in Table 1.

Higher values of energy storage density translate into a smaller volume of material required to accumulate a given amount of heat. The best compounds considering heat of fusion to density relationship are Sodium Hydrogen Phosphate Dodecahydrate, Barium Hydroxide Octahydrate and Magnesium Sulfate Heptahydrate. The use of these substances will provide a relatively small converter giving a large enough heat of fusion.

4.2. Advantages and disadvantages

Phase change materials should have properties that are difficult to achieve simultaneously. PCMs absorb, store and release large amounts of energy in the form of latent heat at a constant temperature, which is called the phase change temperature. Such a transformation is an isothermal transformation, that is, the amount of heat stored during the heating of any material is significantly less than the amount of heat accumulated during the phase transformation of that material [9]. Phase-change materials are characterized by properties [4]:

- ***Physical*** (high density, low density variation during phase transformations, low vapor pressure, no supercooling effect, moderate crystallization rate, low viscosity);

Table 1. Thermophysical properties of salt hydrates and their eutectics

Chemical formula	Heat of fusion (J/g)	Density (Solid) (g/cm³)	Melting point (°C)	References
$Na_2HPO_4 \cdot 12H_2O$ Sodium Hydrogen Phosphate Dodecahydrate	280	1.71	35-44	[5]
$Ba(OH)_2 \cdot 8H_2O$ Barium Hydroxide Octahydrate	266	2.18	78	[31]
25% $Na_2SO_4 \cdot 10H_2O$+75%$Na_2HPO_4 \cdot 12H_2O$	262.3	n/a	31.2	[34]
$Na_2SO_4 \cdot 10H_2O$ Sodium Sulfate Decahydrate	248	1.46	32.4	[31]
$Na_2CO_3 \cdot 10H_2O$ Sodium Carbonate Decahydrate	247	1.44	33	[31]
40%$Na_2CO_3 \cdot 10H_2O$+60% $Na_2HPO_4 \cdot 12H_2O$	220.2	n/a	27.3	[33]
$Na_2S_2O_3 \cdot 5H_2O$ Sodium Thiosulfate Pentahydrate	201/206	1.73	48	[23]
$MgSO_4 \cdot 7H_2O$ Magnesium Sulfate Heptahydrate/Epsom salt	202	2.66	48.5	[23]
$MgCl_2 \cdot 4H_2O$ Magnesium Chloride Tetrahydrate	178	1.57	58	[32]
$CaCl_2 \cdot 6H_2O$ Calcium Chloride Hexahydrate	174	1.8	28	[32]
$CuSO_4 7H_2O$ Copper Sulfate Heptahydrate	171	2.28	40.7	[23]
53%$Mg(NO_3)_2 \cdot 6H_2O$+ 47%$Al(NO_3)_2 \cdot 9H_2O$	168	n/a	66	[32]
$Mg(NO_3)_2 \cdot 6H_2O$ Magnesium Nitrate Hexahydrate	163	1.46	89.9	[32]
$Al(NO_3)_2 \cdot 9H_2O$ Aluminium Nitrate Nonahydrate	155	1.058	72	[2]
50%$Mg(NO_3)_2 \cdot 6H_2O$+50% $MgCl_2 \cdot 6H_2O$	132	n/a	58-59	[32]
75%$CaCl_2 \cdot 6H_2O$+25% $MgCl_2 \cdot 6H_2O$	102.3	n/a	21.4	[32]
$CaCl_2 \cdot 4H_2O$ Calcium Chloride Tetrahydrate	99.6	1.566	44.2	[32]
$K_2HPO_4 \cdot 7H_2O$ DiPotassium Hydrogen Phosphate Heptahydrate	99	1.52	48	[33]

- ***Thermal*** (proper phase transformation temperature range adapted to the operating temperature of the PV plant, high latent and specific heat and high thermal conductivity of both phases);
- ***Chemical*** (non-combustible, non-explosive, non-toxic, recyclable, no chemical decomposition);
- ***Economic*** (available in large quantities, cost-effective during application).

When used for solar installations, inorganic salt hydrates show advantages and disadvantages (Table 2).

Table 2. Advantages and disadvantages of inorganic phase change materials [25]

Inorganic salt hydrates as PCM materials	
Advantages	**Disadvantages**
High phase change energy	Chemically unstable
High capacity and thermal conductivity	May cause corrosion
Easily available	Supercooling
Non-combustible	Phase separation
Price	

The advantage is the high heat capacity of the phase change. Thanks to it, PCM materials have the ability to accumulate heat. Also very important in the operating conditions of PCMs is the enthalpy change associated with supercooling or overheating of these materials (hysteresis of the phase transformation), which is a few to several degrees with regard to the melting point. A high value of thermal conductivity provides materials with a more efficient absorption or release of heat between the system and the environment, even for small temperature differences [2]. When a substance does not achieve such a condition, techniques are used to increase the effective thermal conductivity, usually by adding well-conducting materials such as graphite [37]. The economic advantages of PCMs include the low price of these materials [2]. Inorganic materials are described as non-combustible [23]. Inorganic salt hydrates are flexible materials. Even the seemingly good characteristics included as advantages can be improved. Duan et al. [43] prepared composites of $CaCl_2 - 6H_2O$ and EG by adsorbing liquid salt hydrates onto EG. A stably shaped composite was obtained by introducing EG into molten $CaCl_2 \cdot 6H_2O$. In addition, polyoxyethylene-10 alkylphenols were added as an emulsifier to increase the bonding strength between EG and salt hydrate. Thermal conductivity was improved by 82% compared to pure $CaCl_2 \cdot 6H_2O$. Cui et al [53] used vacuum impregnation to prepare a compound of $CaCl_2 \cdot 6H_2O$ and sepiolite. This fibrous clay mineral proved to be a good flame retardant and can be widely used in buildings. The resulting $CaCl_2 \cdot \mathbf{6H_2}O$ composite provided good phase change energy storage performance, but sepiolite reduced enthalpy and thermal stability.

The disadvantages of hydrated salts are the supercooling effect and phase separation problems. These two phenomena are closely related, due to the different densities of water and salt. Thus, during crystallization of hydrated salts, which have a complex structure, a solid-phase sediment is formed in water, which does not have the ability to accumulate heat [36]. Phase separation is a significant problem associated with salt hydrates [37]. A way to minimize and avoid phase separation is to add thickeners to salt hydrates. Thickeners that have been studied include hydroxyethyl cellulose, nanocellulose, cellulose [38-41], polyethylene glycol [42] and some silicone derivatives [43]. Fine-grained auxiliary materials for inorganic materials include such porous materials as expanded graphite [44], diatomaceous earth [45] and titanium nanodioxide [46]. They increase the viscosity of the solution, which allows for uniform distribution of the solids. Effective methods include microencapsulation and microencapsulation combined with impregnation using porous materials. They solve phase separation problems, but can also effectively avoid leakage during PCM synthesis.

Microencapsulated phase transition materials (MEPCMs) typically consist of a polymeric material as the shell and a PCM as the core [47]. Microencapsulated salt hydrates can change reactivity with the external environment. They can be used as a powder and then prevent phase separation and PCM leakage. The microcapsules showed excellent performance, with no leakage or phase separation. PCM microcapsules consisting of $Na_2HPO_4 \cdot 7H_2O$ as the core and methyl methacrylate as the capsule were prepared by Huang et al. [48]. They used a suspension copolymerization method with a volatile solvent. In the polymerization reaction, the primary salt hydrate $Na_2HPO_4 \cdot 12H_2O$ lost five water molecules during heating, while the rest were successfully diverted to the organic solvent. The thermal conductivity seemed to remain unchanged after the formation of the $Na_2HPO_4 \cdot 7H_2O$ microcapsule. Thus, it can be considered a potential material for solar space heating.

Porous materials such as carbon foam, diatomaceous earth, expanded graphite and expanded perlite used as support materials can also effectively eliminate the leakage, phase separation and corrosion problems of PCM. Such composite materials are often synthesized by impregnating PCMs or mixing them with a porous matrix [49]. Supporting materials with large specific surface areas cause liquid materials to be absorbed through their internal pores. Expanded graphite (EG) is a type of carbon material formed by annealing graphite at high temperatures using microwave radiation. Good performance characterizes EG and PCM with high thermal conductivity, low weight, no phase separation leakage and low overcooling due to expanded graphite capillary and surface tension [50-53].

Pichandi et al. considered eutectic PCM by adding magnesium sulfate heptahydrate 30% ($MgSO_4 \cdot 7H_2O$) to sodium carbonate decahydrate 70% ($Na_2CO_3 \cdot 10H_2O$), to eliminate the problems of supercooling and phase separation of sodium carbonate in PV. Through a DSC study, it was found that this substrate content tends to perform best in terms of thermal conductivity and stability, latent heat of fusion, melting point. This eutectic PCM was placed on the back of a 25 W polycrystalline silicon PV module. The experiment was conducted on two specific days selected based on outdoor solar conditions in India. Equipment including a temperature data logger, voltmeter, ammeter, solar radiation sensor and thermoelectric wire were used to evaluate the performance of the PV- PCM system. According to the collected data, the system showed a maximum temperature drop of 7°C, resulting in a 1.21% increase in efficiency. The power output of the system was 17.63 W higher with the eutectic PCM, which improved power production by 12.5%. However, when comparing the cost of this PV- PCM system to the monetary return in the long term, there is very little or no economic benefit, as PCM material preparation and setup cost extra, even in mass production. Therefore, various salt hydrates with similar properties to magnesium sulfate heptahydrates are potential substitutes for this study [9].

Phase-change materials can cause corrosion, then, if the inappropriate tank in which this PCM will be stored is selected. Brass, copper and aluminum are avoided. Glass, polypropylene and stainless steel are good candidates as PCM carriers for long-term storage of PCM salt hydrates [1].

There is no salt hydrate that has the advantages alone. In practice, the choice of material is made on the basis of the amount of heat capacity and phase change temperature, as well as price. Disadvantages of the material are eliminated or reduced by various physical procedures (e.g., using stabilizing additives and nucleators) or by designing the system accordingly [3].

5. CONCLUSIONS

In the article, we highlight the important role played by salt hydrates in PV installations. The use of salt hydrate converters in PV installations significantly improves the efficiency of photovoltaic modules. We show that at least 18 salt hydrates and their mixtures are promising for solar applications due to their beneficial thermophysical parameters with the best ones being Sodium Hydrogen Phosphate Dodecahydrate, Sodium Carbonate Decahydrate and Calcium Chloride Hexahydrate. The literature review shows that the selection of a test method for determining the thermophysical parameters of salt hydrates should be individual depending on the research objective. Comparing the methods presented, we believe that it is the DSC and DTA methods that provide the most accurate and repeatable results.

Salt hydrates have many advantages and disadvantages that are well known in the scientific community. In this paper we show that inorganic salt hydrates are flexible materials and in addition to the disadvantages even the seemingly good characteristics included as advantages can be improved. Research is still needed to assess the potential for changes in the individual properties of salt hydrates during long-term operation of solar systems, which can influence the efficiency of the solar system.

REFERENCES

[1] Singh G.K.: *Solar power generation by PV (photovoltaic) technology*: A review, Energy 2013, 53, pp. 1-13.
[2] Cabeza L.F., Castell A., Barreneche C.D., de Gracia, A., Fernández A.: *Materials used as pcm in thermal energy storage in buildings: a review*, Renew. Sustain. Energy rev. 2011, 15, pp. 1675-1695.
[3] Li T.X., Wu D.L., He F., Wang R.Z.: *Experimental investigation on copper foam/hydrated salt composite phase change material for thermal energy storage*, Int. J. Heat mass transf. 2017, 115, pp. 148-157.
[4] Kenisarin M., Mahkamov K.: *Salt hydrates as latent heat storage materials: thermophysical properties and costs*. Sol. Energy Mater. Sol. Cells 2016, pp. 145, 255-286.
[5] Zhang P., Xiao X., Ma Z.: *A review of the composite phase change materials: fabrication, characterization, mathematical modeling and application to performance enhancement*, Appl. Energy 2016, 165, pp. 472-510.

[6] Raj B., Van de Voorde M., Mahajan Y.: *Phase change nanomaterials for thermal energy storage*. In nanotechnology for energy sustainability, 2017, pp. 459-484.

[7] Wang T., Wang S., Luo R., Zhu C., Akiyama T., Zhang Z.: *Microencapsulation of phase change materials with binary cores and calcium carbonate shell for thermal energy storage*. Appl. Energy 2016, 171, pp.113-119.

[8] Giro-Paloma J., Martínez M., Cabeza L.F., Fernández A.I.: *Types, methods, techniques, and applications for microencapsulated phase change materials (MPCM): A review*. Renew. Sustain. Energy Rev. 2016, 53, pp. 1059-1075.

[9] Choo Y.M., Wei W.: *Salt hydrates as phase change materials for photovoltaics thermal management*. Energy Science & Engineering, 2021, 10, pp. 1630-1645.

[10] Hasan A., McCormack S.J., Huang M.J., Norton B.: *Evaluation of phase change materials for thermal regulation enhancement of building integrated photovoltaics*, Solar Energy, 2010, 84, pp. 1601-1612.

[11] Taqi Al.-Najjar H.M., Mahdi J.M.: *Novel mathematical modeling, performance analysis, and design charts for the typical hybrid photovoltaic/phase-change material (PV/PCM) system*, Applied Energy, 2022, 315, 119027.

[12] Zielenkiewicz W.: *Calorimetry,* Inst. of Phys. Chem. of Polish Acad. of Sciences. 2005.

[13] Shelby J.E.: *Thermal analysis of Glasses. Chapter 12 in Introduction to Glass Science and Technology*. The Royal Society of chemistry. 2005.

[14] Pielichowiska K., Pielichowski K.: *Różnicowa kalorymetria skaningowa z modulacja temperatury (MT-DSC)*, Laboratorium, 2007, 7-8, pp. 36-38.

[15] Hasan A., McCormack S.J., Huang M.J., Norton B.: *Characterization of phase change materials for thermal control of photovoltaics using Differential Scanning Calorimetry and Temperature History Method.* Energy Conversion and Management, 2014, 81, pp. 322-329.

[16] Sole A., Miro L., Barreneche C., Martorell I., Cabeza L.F.: *Review of the T-history method to determine thermophysical properties of phase change materials (PCM)*, Renew. Sustain. Energy Rev. 2013, 26, pp. 425-436.

[17] Domańska U.: *Thermophysical properties and thermodynamic phase behavior of ionic liquids,* Thermochim. Acta 2006, 448, pp. 19-30.

[18] Wróbel S., Marzec M.: *Różnicowa kalorymetria skaningowa*, Zakład Inżynierii Materiałów, s. 44.

[19] Yinping Z., Yi J., Yi J.: *A simple method, the T-history method, of determining the heat of fusion, specific heat and thermal conductivity of phase-change materials*. Meas. Sci. Technol. 1999, 10, 201.

[20] Yinping, Z., Yi J.: *A simple method, the T-history method, of determining the heat of fusion, specific heat and thermal conductivity of phase-change materials*; Meas Sci. Technol, 10 (3) (1999).

[21] Hong H., Kim S.K., Kim Y.S.: *Accuracy improvement of T-history method for measuring heat of fusion of various materials*. Int J Refrig, 2004, 27 (4), pp. 360-366.

[22] Marín J.M., Zalba B., Cabeza L.F., Mehling H.: *Determination of enthalpy-temperature curves of phase change materials with the temperature-history method: improvement to temperature dependent properties*; Meas Sci. Technol, 2003, 14 (2), pp. 184-189.

[23] Xie N., Huang Z., Luo Z., Gao X., Fang Y., Zhang Z.: *Inorganic salt hydrate for thermal energy storage,* Appl. Sci. 2017, 7, 1317.

[24] Rezvanpour M., Borooghani D., Torabi F., Pazoki M.: *Using $CaCl_2{\cdot}6H_2O$ as a phase change material for thermo-regulation and enhancing photovoltaic panels' conversion efficiency: Experimental study and TRNSYS validation*. Renewable Energy, 2020, 146, pp. 1907-1921.

[25] Ushak S., Gutierrez A., Galleguillos H., Fernandez A.G., Cabeza L.F., Grageda M.: *Thermophysical characterization of a by-product from the non-metallic industry as inorganic PCM*. Solar Energy Materials and Solar Cells, 2015, 132, pp. 385-391.

[26] Melcer A., Klugmann-Radziemska E., Lewandowski W.M.: *Materiały zmiennofazowe. Właściwości, klasyfikacja, zalety i wady*. Przem. Chem., 2012 7, pp. 1000-1011.

[27] Zwolińska M., Bogdan A.: *Związki zmiennofazowe w zastosowaniach techniczno-użytkowych i ergonomicznych*. Ergonomia, 2012, 4, pp. 22-25.

[28] Hussain S.I., Dinesh R., Roseline A.: *Enhanced thermal performance and study the influence of sub cooling on activated carbon dispersed eutectic PCM for cold storage applications*. Energy Build. 2017, 143, pp. 17-24.

[29] Pielichowska K., Pielichowski K.: *Phase change materials for thermal energy storage*. Prog. Mater. Sci. 2014, 65, pp. 67-123.

[30] Khan Z., Khan Z., Ghafoor A.: *A review of performance enhancement of PCM based latent heat storage system within the context of materials, thermal stability and compatibility*. Energy Convers. Manag. 2016, 115, pp. 132-158.

[31] Lorente S., Bejan A., Niu J.L.: *Construal design of latent thermal energy storage with vertical spiral heaters*. Int. J. Heat Mass Transf. 2015, 81, pp. 283-288.

[32] Li G., Zhang B., Li X., Zhou Y., Sun Q., Yun Q.: *The preparation, characterization and modification of a new phase change material: $CaCl_2{\cdot}6H_2O$–$MgCl_2{\cdot}6H_2O$ eutectic hydrate salt*. Sol. Energy Mater. Sol. Cells 2014, 126, pp. 51-55.

[33] Liu Y., Yang Y.: *Preparation and thermal properties od Na_2CO_3 $10H_2O$ $Na_2HPO_4 12H_2O$ eutectic hydrate salt as a novel phase change material for energy storage*. Applied Thermal Engineering 2006, 10, pp. 606-609.
[34] Xin W., Fang J. Jiang W., Ping L., Na L., Yanhan F., Wang L.: *Preparation and modification of novel phase change material Na_2SO_4 $10H_2O$ Na_2HPO_4 $12H_2O$ binary eutectic hydrate salt*. Energy Sources, Part A:Recovery, Utilization and Environmental Effects, 2019, pp. 1-12.
[35] Mohamed S.A., Al-Sulaiman F.A., Ibrahim N.I., Zahir M.H., Al-Ahmed A., Saidur R., Yılbaş B.S., Sahin A.Z.: *A review on current status and challenges of inorganic phase change materials for thermal energy storage systems*. Renew. Sustain. Energy Rev. 2017, 70, pp. 1072-1089.
[36] Dannemand M., Johansen J.B., Furbo S.: *Solidification behavior and thermal conductivity of bulk sodium acetate trihydrate composites with thickening agents and graphite*. Sol. Energy Mater. Sol. Cells 2016, 145, pp. 287-295.
[37] Shin H.K., Park M., Kim H.-Y., Park S.-J.: *Thermal property and latent heat energy storage behavior of sodium acetate trihydrate composites containing expanded graphite and carboxymethyl cellulose for phase change materials*. Appl. Therm. Eng. 2015, 75, pp. 978-983.
[38] Li Y., Yu S., Chen P., Rojas R., Hajian A., Berglund L.: *Cellulose nanofibers enable paraffin encapsulation and the formation of stable thermal regulation nanocomposites*. Nano Energy 2017, 34, pp. 541-548.
[39] Hu X. Huang Z., Yu X., Li B.: *Preparation and thermal energy storage of carboxymethyl cellulose-modified nanocapsules*. BioEnergy Res. 2013, 6, pp. 1135-1141.
[40] Jin X., Medina M.A., Zhang X., Zhang S.: *Phase-change characteristic analysis of partially melted sodium acetate trihydrate using DSC*. Int. J. Thermophys. 2014, 35, pp. 45-52.
[41] Gutierrez A., Ushak S., Galleguillos H., Fernandez A., Cabeza L.F., Grágeda M.: *Use of polyethylene glycol for the improvement of the cycling stability of bischofite as thermal energy storage material*. Appl. Energy 2015, 154, pp. 616-621.
[42] Kazemi Z., Mortazavi S.M.: *A new method of application of hydrated salts on textiles to achieve thermoregulating properties*, Thermochim. Acta 2014, 589, pp. 56-62.
[43] Duan Z.-J., Zhang H.-Z., Sun L.-X., Cao Z., Xu F., Zou Y.-J., Chu H.-L., Qiu S.-J., Xiang C.-L., Zhou H.-Y.: *$CaCl_2{\cdot}6H_2O$/expanded graphite composite as form-stable phase change materials for thermal energy storage,* J. Therm. Anal. Calorim. 2013, 115, pp. 111-117.
[44] Xu B., Li Z.: *Paraffin/diatomite composite phase change material incorporated cement-based composite for thermal energy storage*. Appl. Energy 2013, 105, pp. 229-237.
[45] Lasfargues M., Bell A., Ding Y.: *In Situ production of titanium dioxide nanoparticles in molten salt phase for thermal energy storage and heat-transfer fluid applications*, J. Nanopart. Res. 2016, 18, pp. 1-11.
[46] Tiagi V., Kaushik S.C.: *Development of phase change materials based microencapsulated technology for buildings: A review*. Renew. Sustain. Energy Rev. 2011, 15, pp. 1373-1391.
[47] Huang J., Wang T., Zhu P., Xiao J.: *Preparation, characterization, and thermal properties of the microencapsulation of a hydrated salt as phase change energy storage materials*. Thermochim. Acta 2013, 557, pp. 1-6.
[48] Korhammer K., Druske M.-M., Fopah-Lele A., Rammelberg H.U., Wegscheider N., Opel O., Osterland T., Ruck W.: *Sorption and thermal characterization of composite materials based on chlorides for thermal energy storage*, Appl. Energy 2016, 162, pp. 1462-1472.
[49] Huang Z., Luo Z., Gao X., Fang X., Fang Y., Zhang Z.: *Investigations on the thermal stability, long-term reliability of $LiNO_3$/KCl – Expanded graphite composite as industrial waste heat storage material and its corrosion properties with metals*. Appl. Energy 2017, 188, pp. 521-528.
[50] Cheng F., Wen R., Huang Z., Fang M., Liu Y.G., Wu X., Min X.: *Preparation and analysis of lightweight wall material with expanded graphite (EG)/paraffin composites for solar energy storage*, Appl. Therm. Eng. 2017, 120, pp. 107-114.
[51] Xu T., Li Y., Chen J., Liu J.: *Preparation and thermal energy storage properties of lino 3-kcl-nano 3/expanded graphite composite phase change material*, Sol. Energy Mater. Sol. Cells 2017, 169, pp. 215-221.
[52] Huang X., Alva G., Liu L., Fang G.: *Preparation, characterization and thermal properties of fatty acideutectics/ bentonite/expanded graphite composites as novel form–stable thermal energy storage materials*, Sol. Energy Mater. Sol. Cells 2017, 166, pp. 157-166.
[53] Cui W., Zhang H., Xia Y., Zou Y., Xiang C., Chu H., Qiu S., Xu F., Sun L.: *Preparation and thermophysical properties of a novel form-stable $CaCl_2{\cdot}6H_2O$/sepiolite composite phase change material for latent heat storage*, J. Therm. Anal. Calorim. 2017, 20, pp. 1-7.

ASSESSMENT OF THE POSSIBILITY OF USING CHALCEDONITE POWDER AS A COMPONENT OF MORTARS

OCENA MOŻLIWOŚCI ZASTOSOWANIA MĄCZKI CHALCEDONITOWEJ JAKO SKŁADNIKA ZAPRAW BUDOWLANYCH

Edyta Spychał, Anna Kotwa
Kielce University of Technology, Poland

Structure and Environment vol. 14, No. 4/2022, p. 119

DOI: 10.30540/sae-2022-014

Abstract

The article presents the results of the assessment of the possibility of using chalcedonite powder as a partial replacement for cement in mortars. Portland cement CEM I 42.5 R was used as a binder, which was replaced in the amount of 5%, 20%, 35% and 50% with chalcedonite powder. The experimental tests concerned the determination of the technological and mechanical properties of mortars: consistency, air content, compressive and bending strength, supplemented by X-ray diffraction analysis and calorimetric measurements of the pastes. The research results indicate that chalcedonite powder can be used in the production of mortars. The best mechanical properties of tested mortars were obtained in the case of replacing cement with the addition of powder in the amount of 5% and 20%.

Streszczenie

W artykule dokonano oceny możliwości wykorzystania mączki chalcedonitowej jako częściowego zamiennika cementu w zaprawach budowlanych. Jako spoiwo zastosowano cement portlandzki CEM I 42,5 R, który zastępowano w ilości 5%, 20%, 35% oraz 50% mączką chalcedonitową. Badania doświadczalne dotyczyły określenia właściwości technologicznych i mechanicznych zapraw: konsystencji, zawartości powietrza, wytrzymałości na ściskanie i zginanie, uzupełnionych o rentgenowską analizę dyfrakcyjną oraz badania kalorymetryczne zaczynów. Wyniki badań wskazują, że mączka chalcedonitowa może być stosowana do produkcji zapraw budowlanych. Najlepsze właściwości mechaniczne badanych zapraw uzyskano w przypadku zastąpienia cementu dodatkiem mączki w ilości 5% i 20%.

NUMERICAL INVESTIGATIONS OF THE THERMAL PROPERTIES OF WINDOW SYSTEMS: A REVIEW

PRZEGLĄD NUMERYCZNYCH METOD OKREŚLANIA WŁAŚCIWOŚCI CIEPLNYCH OKIEN

Karolina Sadko, Jerzy Zbigniew Piotrowski
Kielce University of Technology, Poland

Structure and Environment vol. 14, No. 4/2022, p. 126

DOI: 10.30540/sae-2022-015

Abstract

Windows are an essential part of building envelopes since they enhance the appearance of the building, allow daylight and solar heat to come in, and allow people to observe outside. However, conventional windows tend to have poor U-values, which cause significant heat losses during the winter season and undesired heat gain in summer. Modern glazing technologies are therefore required to improve thermal resistance and comfort of the occupants, whilst mitigating the energy consumption of buildings. In the present work, a comprehensive review of the numerical investigations of the thermal properties of window systems and glazed buildings partitions is presented. However, the proposed models to predict the thermal performance most often concern only specific cases of window systems related to geometry and used material solutions, focused on specific physical processes, thus they contain a lot of simplifications, such as omitting the influence of radiation, temperature changes or velocity profiles.

Streszczenie

Istotnymi elementami budynków są okna, które wpływają na ich wygląd, umożliwiają dostęp światła dziennego i ciepła pochodzącego z promieniowania słonecznego, a także pozwalają na obserwowanie otoczenia. Jednakże w porównaniu do pozostałych przegród budowlanych konwencjonalne okna charakteryzują się zwykle gorszymi wartościami współczynnika przenikania ciepła U, generując znaczne straty ciepła w sezonie zimowym i niepożądane zyski ciepła w lecie. W związku z tym konieczne jest poszukiwanie nowoczesnych rozwiązań w technologii okiennej, które poprawią opór cieplny i komfort mieszkańców, jednocześnie zmniejszając zużycie energii przez budynki. W niniejszej pracy przedstawiono przegląd numerycznych metod określania właściwości cieplnych okien i przeszklonych przegród budowlanych. Analiza literatury pokazuje, że proponowane modele dotyczą jednak najczęściej tylko konkretnych przypadków systemów okiennych, związanych z określoną geometrią i zastosowanymi rozwiązaniami materiałowymi, w których uwzględnia się jedynie wybrane procesy fizyczne. Skutkiem tego jest przyjmowanie podczas modelowania wymiany ciepła szeregu uproszczeń, takich jak pomijanie wpływu promieniowania czy nieuwzględnianie zmian temperatury i prędkości.

INFLUENCE OF ROAD TRAFFIC ON INDOOR AIR QUALITY

WPŁYW RUCHU DROGOWEGO NA JAKOŚĆ POWIETRZA WEWNĘTRZNEGO

Ewa Zender-Świercz, Michał Polański
Kielce University of Technology, Poland

Structure and Environment vol. 14, No. 4/2022, p. 142

DOI: 10.30540/sae-2022-016

Abstract

The quality of air that people breathe has become a very important parameter of quality of life. Pollution contributes to numerous diseases, problems with the absorption of knowledge, and also reduces work efficiency. The article attempts to find the relationship between road traffic and indoor air quality. The parameter used to assess air pollution was particulate matter (smog). The research was carried out in three localisations with different traffic volumes, in three places for each localisation, in the summer, autumn, and winter periods. It was found that in areas with heavy road traffic, this traffic causes an inflow of pollutants into the rooms. In low – traffic localisations, sources other than road traffic have a greater impact on the indoor air quality, especially in the cool periods (autumn, and winter).

Streszczenie

Jakość powietrza, jakim oddycha człowiek, stała się bardzo istotnym parametrem jakości życia. Zanieczyszczenia przyczyniają się do licznych zachorowań, problemów z przyswajaniem wiedzy, a także obniżają wydajność pracy. W artykule podjęto próbę odnalezienia zależności pomiędzy natężeniem ruchu drogowego i jakością powietrza wewnętrznego. Parametrem, który wykorzystano do oceny zanieczyszczenia powietrza, był pył zawieszony (smog). Badania przeprowadzono w trzech lokalizacjach o różnym natężeniu ruchu, w trzech miejscach dla każdej lokalizacji, w okresach lato, jesień i zima. Stwierdzono, że w lokalizacji o dużym natężeniu ruchu pojazdów ruch ten powoduje napływ zanieczyszczeń do pomieszczeń. W lokalizacjach o małym natężeniu ruchu większy wpływ na jakość powietrza wewnętrznego mają inne niż ruch drogowy źródła, szczególnie w okresach chłodnych (jesień, zima).

BEHAVIOR OF MAT FOUNDATION FOR A TEN-STORY BUILDING: FIXED BASE VS THREE-DIMENSIONAL SOIL MODEL

ZACHOWANIE SIĘ PODŁOŻA Z MATĄ DLA BUDYNKU DZIESIĘCIOPIĘTROWEGO: STAŁA BAZA A TRÓJWYMIAROWY MODEL GRUNTU

Farhaj Hasan, Nazmul Alam
University of Asia Pacific (UAP), Bangladesh
Al Amin
European University of Bangladesh (EUB), Bangladesh
Mahadi Hasan
Engineering & Research Associates (ERA), Bangladesh

Structure and Environment vol. 14, No. 4/2022, p. 153 DOI: 10.30540/sae-2022-017

Abstract

Soil is an anisotropic, heterogeneous, and inelastic complex material. It is difficult to represent the exact behavior of soil by numerical modelling in practice. Conventionally, soil is simplified to an idealized model where it is considered isotropic, homogeneous, and behaves elastically under loads. The idealization, in this case, is done using the proper elastic modulus, Poisson's ratio, and unit weight of soil depending upon the soil type. Although the exact soil behavior is simplified, using Finite Element Analysis (FEA) a more effective result can be obtained. A superstructure was modelled using ETABS using a fixed-base system and the base reaction forces were obtained. A mat and a soil element on which the mat was laid were modelled as a flexible-base system in Midas GTS NX. The base reactions obtained from ETABS were applied to the mat in the soil model to determine the settlements and, consequently, the spring stiffness. The superstructure was then modelled again, incorporating springs under the respective columns. Convergence in settlement, and base reactions were reached by iteration, and the final results from the flexible-base system were then compared with the fixed-base system. The center column settled the most, about 60 mm, and there was a decrease in settlement by 15% between the first model and the final iterated model. The base reaction for center columns decreased by 24% in the flexible base system compared to the fixed base system. However, an increase in base reaction was observed for both side and edge columns. There was an extremely erratic change in grade beams under a flexible base system, which shows that the superstructure elements are also affected by the change in the base system. It is

Streszczenie

Gleba jest materiałem złożonym anizotropowym, niejednorodnym i nieelastycznym. W praktyce trudno jest dokładnie odwzorować zachowanie gleby za pomocą modelowania numerycznego. Konwencjonalnie glebę upraszcza się do wyidealizowanego modelu, w którym uważa się ją za izotropową, jednorodną i zachowującą się elastycznie pod obciążeniem. Idealizacja w tym przypadku odbywa się za pomocą odpowiedniego modułu sprężystości, współczynnika Poissona i masy jednostkowej gruntu w zależności od rodzaju gruntu. Chociaż dokładne zachowanie gleby jest uproszczone, można uzyskać bardziej efektywne wyniki za pomocą analizy elementów skończonych (FEA). Konstrukcja nośna została wymodelowana za pomocą ETABS przy użyciu systemu stałej podstawy i uzyskano siły reakcji podstawy. Matę i element gruntu, na którym została położona, zamodelowano jako układ o elastycznej podstawie w programie Midas GTS NX. Reakcje bazowe uzyskane z ETABS naniesiono na matę w modelu gruntowym w celu określenia osiadań, a co za tym idzie sztywności sprężystej. Następnie ponownie wymodelowano konstrukcję nośną, włączając sprężyny pod odpowiednimi kolumnami. Zbieżność osiadania i reakcji bazowych została osiągnięta przez iterację, a końcowe wyniki z systemu o elastycznej podstawie zostały następnie porównane z systemem o stałej podstawie. Kolumna środkowa osiadła najbardziej, około 60 mm, a między pierwszym modelem a ostatecznym modelem iterowanym nastąpił spadek osiadania o 15%. Reakcja podstawy dla kolumn centralnych zmniejszyła się o 24% w systemie z podstawą elastyczną w porównaniu z systemem z podstawą stałą. Zaobserwowano jednak wzrost odczynu zasadowego zarówno dla kolumn bocznych, jak *recommended to use this approach, for the analysis of structures considering flexible base systems instead of fixed bases because it enhances the accuracy of analysis with feasible time consumption and less complex effort.*

i krawędziowych. Nastąpiła bardzo nieregularna zmiana belek niwelacyjnych pod elastycznym systemem bazowym, co pokazuje, że zmiany w systemie bazowym mają również wpływ na elementy konstrukcji nośnej. Zaleca się stosowanie tego podejścia do analizy konstrukcji z uwzględnieniem elastycznych systemów bazowych zamiast stałych baz, ponieważ zwiększa to dokładność analizy przy możliwej czasochłonności i mniejszym wysiłku.

INORGANIC SALT HYDRATES AS PHASE CHANGE MATERIALS (PCM) FOR THERMAL ENERGY STORAGE IN SOLAR INSTALLATIONS

NIEORGANICZNE HYDRATY SOLI JAKO MATERIAŁY ZMIENNOFAZOWE (PCM) DO MAGAZYNOWANIA ENERGII CIEPLNEJ W INSTALACJACH SŁONECZNYCH

Marta Styś-Maniara, Edyta Nartowska, Monika Metryka-Telka
Kielce University of Technology, Poland
Rafał Porowski
AGH University of Science and Technology, Poland

Structure and Environment vol. 14, No. 4/2022, p. 161 DOI: 10.30540/sae-2022-018

Abstract

The authors present a general idea of using inorganic salt hydrates in solar installations. A key role in this selection is played by thermophysical parameters, so the authors review their test methods and in turn characterize them for the most promising salt hydrates. Next, the authors describe the advantages and disadvantages of inorganic salt hydrates and indicate possibilities for their improvement. The use of salt hydrate converters in PV installations significantly improves the efficiency of photovoltaic modules. We show that at least 18 salt hydrates are promising for solar applications with the best ones being Sodium Hydrogen Phosphate Dodecahydrate, Sodium Carbonate Decahydrate and Calcium Chloride Hexahydrate. The selection of a test method for determining the thermophysical parameters of salt hydrates should be individual depending on the research objective. Comparing the methods presented, we believe that it is the DSC and DTA methods that provide the most accurate and repeatable results.

Streszczenie

Autorzy przedstawiają ogólną koncepcję wykorzystania nieorganicznych hydratów solnych w instalacjach solarnych. Kluczową rolę w tym doborze odgrywają parametry termofizyczne, dlatego autorzy dokonują przeglądu metod ich badania i kolejno charakteryzują je dla najbardziej obiecujących hydratów solnych i ich mieszanin. Następnie autorzy opisują zalety i wady nieorganicznych hydratów solnych oraz wskazują możliwości ich udoskonalenia. Zastosowanie konwerterów hydratów solnych w instalacjach PV znacząco poprawia sprawność modułów fotowoltaicznych. Wykazano, że co najmniej 18 hydratów soli i ich mieszanin jest obiecujących dla zastosowań solarnych ze względu na korzystne parametry termofizyczne, przy czym najlepsze z nich to dodekahydrat wodorofosforan sodu, dekahydrat węglanu sodu i heksadydrat chlorku wapnia. Z przeglądu literatury wynika, że wybór metody badawczej do określenia parametrów termofizycznych hydratów soli powinien być indywidualny w zależności od celu badań. Porównując przedstawione metody, stwierdzono, że to właśnie metody DSC i DTA dają najbardziej dokładne i powtarzalne wyniki.

Uniform requirements for manuscripts submitted to "Structure and Environment"

All manuscripts should be submitted in English.

Given name(s) and surname(s) of each author
Institutional affiliation(s)
Author's e-mail

Title

Format for the paper:
– Abstract
– Keywords
– Introduction
– Subsequent headings
– Summary
– References

The text should be single-spaced throughout. The font should be 11 pt Times New Roman. All paragraphs should be indented 0.5 cm.

Formulas, tables, figures and photographs should be numbered consecutively

Figures and photographs with a resolution of 300 dpi or higher must be submitted in *.TIFF, *.EPS, *.JPG, *.WMF format.

Figures, photographs and tables should be in English, but their captions should be given in English and Polish.

References: The paper submitted for publication must comply with copyright law provisions. Authors have to document sources of the photographs, figures, quotes and borrowings used in the article. References should be cited in square brackets through the text. The full list of references arranged in the citing order as they appear in the text should be placed at the end of the paper (with one language version only). The reference style is defined by the standard PN-ISO 690:2012 Information and documentation. Guidelines for bibliographic references and citations to information resources.

Examples

Whole books

[1] Author's surname followed by the initials: Title of the book. Place of publication: Publisher, Year of publication, ISBN number.

Edited books

[2] Surname and initials of the editor (Ed.): Title of the book. Place of publication: Publisher, Year of publication, ISBN number.

Chapters in edited books

[3] Author's surname followed by the initials: Title of the charter. (in): Title of the book. Place of publication: Publisher, Year of publication, page numbers (for example: pp. 10-20), ISBN number.

Journal articles

[4] Author's surname followed by the initials: Title of the article. "journal title" Year, Number, page numbers (for example: pp. 10-20), ISSN number

Web references

[5] Author's surname followed by the initials: Title of the work. [type of the source, for example: online]. [date when the reference was last Accessed: …]. Available online: web page

Podstawowe wymagania edytorskie dotyczące pisania artykułów do czasopisma „Structure and Environment”

Artykuł powinien być napisany w dwóch wersjach językowych: angielskiej oraz polskiej.

Imię i nazwisko autora
Nazwa uczelni
e-mail autora

Tytuł artykułu

Struktura artykułu:
– Streszczenie
– Słowa kluczowe
– Wprowadzenie
– Kolejne podtytuły
– Podsumowanie
– Bibliografia

Tekst artykułu powinien być napisany czcionką Times New Roman 11, interlinia pojedyncza, wcięcie akapitowe 0,5 cm.

Wzory, tabele, rysunki oraz zdjęcia powinny być ponumerowane zgodnie z kolejnością ich występowania w tekście.

Rysunki oraz zdjęcia o rozdzielczości 300 dpi lub wyższej, format *.TIFF, *.EPS, *.JPG, *.WMF.

Rysunki, zdjęcia oraz tabele zamieszczamy w wersji angielskiej, a ich tytuły podajemy zarówno w języku angielskim, jak i języku polskim.

Bibliografia: Artykuł przeznaczony do publikacji musi być przygotowany zgodnie z postanowieniami ustawy „Prawo autorskie”, które nakłada na autora obowiązek wykazania źródeł wykorzystanych zdjęć, rysunków cytowań, zapożyczeń. Źródła takie należy umieszczać w tekście w nawiasach kwadratowych. Zbiorcze zestawienie bibliografii umieszczamy na końcu artykułu w kolejności cytowania (tylko przy jednej wersji językowej).

Styl bibliograficzny definiuje norma: **PN-ISO 690:2012** *Informacja i dokumentacja. Wytyczne opracowania przypisów bibliograficznych i powołań na zasoby informacji*.

Przykłady

Pozycje książkowe
[1] Nazwisko i inicjały imion autora: *Tytuł: podtytuł*. Miejsce wydania: Wydawca, Rok, Numer ISBN.

Praca zbiorowa
[2] Nazwisko i inicjały imion redaktora (red): *Tytuł: podtytuł*. Miejsce wydania: Wydawca, Rok, Numer ISBN.

Rozdziały książek
[3] Nazwisko i inicjały imion autora: *Tytuł: podtytuł rozdziału*. [w]: *Tytuł publikacji*. Miejsce wydania: Wydawca, Rok, Strony (np. s. 10-20), Numer ISBN.

Artykuły w czasopismach
[4] Nazwisko i inicjały imion autora: *Tytuł artykułu.* „Tytuł czasopisma” Rok, Numer, Strony (np. s. 8-27), Numer ISSN.

Strony internetowe
[5] Nazwisko i inicjały imion autora: *Tytuł.* [typ nośnika (np. online)]. [data dostępu: ...]. Dostępny w internecie: Adres strony internetowej

THE REVIEW PROCESS

The following requirements need to be met by the paper:
– the title should reflect the content of the paper
– the content should be within the thematic scope of the journal
– the paper should be properly and clearly divided into paragraphs
– original elements need to be part of the paper
– the research method should be properly selected
– adequate references need to be cited
– interpretation and conclusions should match the presented test results
– the paper should not contain parts indicating commercial use